Free University of Berlin

Master Thesis

Program

MSc. Computational Sciences

$\boldsymbol{H}(\mathbf{div})$ - Conforming Finite Elements for the Stokes Equations

Student:
Cristina Melnic

Supervisor
Univ.-Prof. Dr. Volker John

Second Reviewer:
PD Dr. Alfonso Caiazzo

December 9, 2021

Statutory Declaration

I declare that I have developed and written the enclosed thesis completely by myself, and have not used sources or means without declaration in the text. Any thoughts from others or literal quotations are clearly marked.

The thesis was not used in the same or in a similar version to achieve an academic grading or is being published elsewhere.

Berlin (Germany), December 9, 2021

09.12.21 Melnic

Cristina Melnic

Acknowledgements

I would like to thank my supervisor, Univ.-Prof. Dr. Volker John, for his guidance and support in every stage of this work, as well as the expertise that allowed a more efficient problem-solving process.

I also want to acknowledge M.Sc. Derk Frerichs, for his patience of walking me through all the intricacies of the program package ParMooN [25] and the insightful discussions during the implementation stage. Moreover, I would like to thank Dr. Ulrich Wilbrandt for his first aid help in difficult situations involving both the theoretical and implementation parts.

I am grateful for having been a part of my supervisor's workgroup 'Numerical Mathematics and Scientific Computing' at the Weierstrass Institute, Berlin and learning research-related skills from its members in a stimulating environment.

Contents

List of Symbols

E edge of a mesh cell K. 32, 34–37

$H_{\mathbf{div}}$ space of divergence-free functions. 26

K mesh cell of $\mathcal{T}_h$. 22, 32–37

Q^h finite element pressure space. 22, 23, 26, 27, 32, 33, 35, 37

Q pressure space, $L_0^2(\Omega)$. 22, 27

$V_{\mathbf{div}}^h$ space of discretely divergence-free functions. 26, 27, 33

V^h finite element velocity space. 22, 23, 26, 28, 32–35, 37

$V_{\mathbf{div}}$ space of weakly divergence-free functions. 26–28, 33

V velocity space, $\boldsymbol{H}_0^1(\Omega)$. 22, 26, 27, 33

Ω domain. 22, 23, 26, 27, 32–35, 37–39, 44, 46

β continuous inf-sup constant. 27

$\boldsymbol{f}$ body force. 9–12, 15, 22, 35

$\boldsymbol{u}^h$ finite element velocity. 22, 23, 26, 27, 30, 35, 37, 41, 42, 44–46

$\boldsymbol{u}$ velocity. 11, 12, 15, 22–24, 26–31, 33, 34, 37–42

ϵ symmetry parameter of a_ϵ. 34–36

$\mathcal{E}_B^h$ set of domain boundary edges. 32, 34, 36

$\mathcal{E}_I^h$ set of interior edges. 32, 34, 36

$\mathcal{E}^h$ set of edges of $\mathcal{T}^h$. 32, 34–37

$\mathcal{T}^h$ triangulation of Ω. 22, 32–37, 43, 45

$\nabla\cdot_h$ discrete divergence operator. 23

ν kinematic viscosity. 26, 27, 35, 37, 38, 45

∂K boundary of a mesh cell K. 32–34

$\partial\Omega$ boundary of the domain. 12, 14, 15, 32–34, 38, 39

σ penalty parameter to ensure coercivity of a_ϵ. 6, 34–38, 40–43, 46

$a(\cdot,\cdot)$ velocity-velocity bilinear form. 12, 14, 22, 33

$a_\epsilon(\cdot,\cdot)$ DG velocity-velocity bilinear form. 33–35, 40, 46

$b(\cdot,\cdot)$ velocity-pressure bilinear form. 12, 14, 22, 23

$b^h(\cdot,\cdot)$ discrete velocity-pressure bilinear form. 23, 34

h_E diameter of an edge E. 34–37, 43, 44

h_K area of a mesh cell K. 35

h largest value of h_E for a given mesh $\mathcal{T}^h$. 27, 36, 37

p^h finite element pressure. 22, 26, 27, 30, 35, 37, 41, 42, 44–46

p pressure. 11, 15, 22, 26, 27, 34, 37–42

List of Figures

List of Tables

Chapter 1

Introduction

1.1 Motivation

The incompressible Navier-Stokes equations model the behavior of incompressible fluids using two fundamental physical laws — the conservation of linear momentum and the conservation of mass. They are of great interest in a range of fields such as weather forecasting, climate modelling, in medical simulations of blood vessels and in many other scientific and engineering applications.

Due to them being a constrained system of partial differential equations finding solutions is often challenging, and thus they are usually approximated by the means of numerical methods. To that end, the equations are discretized in space and time using methods appropriate to the problem at hand. In this work the stationary equations are discussed, so only the space discretization is of relevance, which is typically done using finite element methods.

The classical stable and convergent finite element methods, however, introduce a few problems, discussed in detail in [14], which this work will try to address. Firstly, the divergence constraint is usually satisfied only discretely, thus the approximated solutions are violating the law of conservation of mass, which can cause problems in many applications. In addition, the approximation of velocity gains a nonphysical dependence on pressure and viscosity, a phenomenon called lack of pressure-robustness, which causes erroneous results for problems where the pressure is much larger than velocity, or the viscosity is much smaller.

Whereas there exist methods to improve the results of the classical methods in relation to these limitations, $H(\mathrm{div})$-conforming finite element methods are known to eradicate them completely, which makes them an attractive topic of current research.

The goal of the thesis is to compare the properties of the $H(\mathrm{div})$-conforming finite element methods with the more traditionally used H^1-conforming finite element methods in approximating the solution to the Stokes equations. This is achieved by a short presentation of the analytical results from the literature for both methods, followed by the implementation of these methods for the Stokes equations in the program package ParMooN [25] and, ultimately, by using them to perform numerical studies. The latter aim to verify whether the theoretical predictions hold and to obtain a quantitative idea about the advantages and disadvantages of both methods in parallel.

The results of this work address the Stokes equations in particular, as a first step in analyzing the above-mentioned properties for the Navier-Stokes equations. The Stokes equations are an approximation to the Navier-Stokes equations in the special case of steady-state flow, which was considered in this work, and large viscosity of the fluid. The latter condition simplifies the problem from non-linear to linear, which reduces the number of technical details in the implementation process, without impacting the studied property. In addition, as mentioned in [14], it emphasizes that the above limitations originate in the discretization of the divergence operator, and not in the properties of nonlinearity or dominating convection of the full Navier-Stokes system.

1.2 Structure of the Thesis

The contents of this work are summarized in the following outline:

- In Chapter 2, a derivation of the incompressible Navier-Stokes equations from the physical point of view is presented. Then, the problem is reformulated via the non-dimensionalization procedure, such that it can be used in numerical analysis. Further, the variational formulation of the problem is presented and is identified with a linear saddle point problem. Then, the results for existence and uniqueness of a solution of such a problem are shown.

- Chapter 3 starts with an introduction to the theory of the finite element methods, where some fundamental theorems and concepts are presented. Then, the particularities of solving incompressible flow problems using finite element methods are discussed, followed by a presentation of inf-sup stable pairs of H^1-conforming spaces and their error estimates. Here, the limitations of these methods are discussed with respect to mass conservation and pressure robustness, as well as some methods to ameliorate them. In order to fully overcome these limitations, $H(\mathrm{div})$-conforming finite element methods are introduced and results for their error estimates are cited from literature.

- Chapter 4 contains numerical studies on the properties of $H(\mathrm{div})$-conforming finite element methods performed with the implemented discontinuous Galerkin formulation of Stokes equations in the program package ParMooN [25]. Namely, three different aspects are addressed: the choice of an optimal penalty parameter to ensure a well-conditioned problem, the convergence orders of the new method in comparison to the classical ones, and an illustration of the attained pressure-robustness property. Before presenting the studies themselves, examples of problems with prescribed solutions used for computations are introduced.

- Finally, Chapter 5 provides a summary of the obtained results, together with the conclusions that they point to, before closing with some comments on possible improvements and elaborations in future works.

Chapter 2

The Incompressible Navier-Stokes Equations

The goal of this chapter is to present the incompressible Navier-Stokes equations and their properties, along with the difficulties in solving them, which will then motivate the need of the methods from the subsequent chapters. The structure follows closely Chapters 2 and 3 from [13].

2.1 Physical background and derivation

The Navier-Stokes equations model the dynamics of fluids and come from two fundamental physical laws - conservation of mass and conservation of momentum. The physical quantities involved in these equations are the density of the fluid $\rho(t,\ \boldsymbol{x}):\ [\mathrm{kg/m^3}]$, the pressure $P(t,\ \boldsymbol{x}):[\mathrm{N/m^2}]$ and the velocity $\boldsymbol{v}(t,\ \boldsymbol{x}):[\mathrm{m/s}]$. These are assumed to be sufficiently smooth functions in the temporal and spatial domains $t\in[0,\ T]$ and $\boldsymbol{x}\in\Omega\subset\mathrm{R}^3$.

Let us consider an arbitrary open volume $\omega\in\Omega$ with smooth surface boundary $\partial\omega$, which is constant in time. The conservation of mass implies that the change of mass in the volume is equal to the flux of mass through the boundary and can be written as

$$\frac{d}{dt}m(t)=\frac{d}{dt}\int_\omega\rho(t,\boldsymbol{x})d\boldsymbol{x}=-\int_{\partial\omega}(\rho\boldsymbol{v})(t,\boldsymbol{s})\cdot\boldsymbol{n}(\boldsymbol{s})d\boldsymbol{s}.$$

Using the divergence theorem on the last integral term, yields

$$\int_\omega\nabla\cdot(\rho\boldsymbol{v})(t,\boldsymbol{x})d\boldsymbol{x}=\int_{\partial\omega}(\rho\boldsymbol{v})(t,\boldsymbol{s})\cdot\boldsymbol{n}(\boldsymbol{s})d\boldsymbol{s}.$$

Since the volume ω is arbitrary, the following relation is obtained,

$$\left(\partial_t\rho+\nabla\cdot(\rho\boldsymbol{v})\right)(t,\boldsymbol{x})=0\quad\forall t\in(0,T],\ \boldsymbol{x}\in\Omega. \tag{2.1}$$

This represents the first from the Navier-Stokes equations and is called the continuity equation. The derivation of the second equation originates in the Newton's second law. Confining the problem again to an arbitrary volume ω, the change of momentum in that volume is equal to the sum of integral of the net force density in the volume ω and the integral of the momentum flux across the boundary $\partial\omega$

$$\frac{d}{dt}\int_\omega\rho\boldsymbol{v}(t,\boldsymbol{x})d\boldsymbol{x}=\int_\omega f_{\mathrm{net}}\ (t,\boldsymbol{x})d\boldsymbol{x}-\int_{\partial\omega}(\rho\boldsymbol{v})(\boldsymbol{v}\cdot\boldsymbol{n})(t,\boldsymbol{s})d\boldsymbol{s}\ [\mathrm{N}].$$

Applying the divergence theorem on the surface integral and changing differentiation with respect to time, yields

$$\int_\omega\left(\partial_t(\rho\boldsymbol{v})+\nabla\cdot\left(\rho\boldsymbol{v}\boldsymbol{v}^T\right)\right)(t,\boldsymbol{x})d\boldsymbol{x}=\int_\omega\boldsymbol{f}_{\mathrm{net}}(t,\boldsymbol{x})d\boldsymbol{x}.$$

By applying the product rule, the previous relation becomes

$$\int_\omega\left(\partial_t\rho\boldsymbol{v}+\rho\partial_t\boldsymbol{v}+\ \boldsymbol{v}\boldsymbol{v}^T\nabla\rho+\rho(\nabla\cdot\boldsymbol{v})\boldsymbol{v}+\rho(\boldsymbol{v}\cdot\nabla)\boldsymbol{v}\right)(t,\boldsymbol{x})d\boldsymbol{x}\ \ =\int_\omega\boldsymbol{f}_{\mathrm{net}}(t,\boldsymbol{x})d\boldsymbol{x}.$$

Since for incompressible fluids the density ρ is constant and the velocity field has neither sinks nor sources $\nabla \cdot \boldsymbol{v} = 0$, the expression can be further simplified. Considering in addition that the volume ω is arbitrary, the final relation can be written as

$$\rho\left(\partial_t \boldsymbol{v} + (\boldsymbol{v} \cdot \nabla)\boldsymbol{v}\right) = \boldsymbol{f}_{\text{net}} \quad \forall t \in (0, T],\ \boldsymbol{x} \in \Omega. \tag{2.2}$$

The net force density is the result of superposition of external forces like gravity, electromagnetic force or buoyancy, and internal forces, which are forces that a fluid element exerts on the adjacent element. Examples of the latter are pressure and the viscous drag, and they represent contact forces, acting on the surface of the fluid element. Their net result on ω can be expressed as a surface integral of the product between the stress vector $\boldsymbol{t}$ $\left[\frac{\text{N}}{\text{m}^2}\right]$ and the surface element vector $d\boldsymbol{s}$. The conservation of momentum equation (2.2) with the force terms written explicitly becomes

$$\int_\omega \rho(t, \boldsymbol{x})\left(\partial_t \boldsymbol{v} + (\boldsymbol{v} \cdot \nabla)\boldsymbol{v}\right)(t, \boldsymbol{x}) d\boldsymbol{x} = \int_\omega \boldsymbol{f_{ext}}(t, \boldsymbol{x}) d\boldsymbol{x} + \int_{\partial\omega} \boldsymbol{t}(t, \boldsymbol{s}) d\boldsymbol{s}. \tag{2.3}$$

The Cauchy stress theorem (proof in [11], pages 50-52) states that the stress vector $\boldsymbol{t}$ denoting the state of stress at a point is uniquely determined by the stress tensor $\mathbb{S}$ $\left[\frac{\text{N}}{\text{m}^2}\right]$ and the unit normal to that point on the surface $\boldsymbol{n}$ through the relation $\mathbf{t} = \mathbb{S} \cdot \mathbf{n}$. Using the divergence theorem again, the limits of integration of the internal force term can be switched and a subsequent simplification of (2.3) is possible.

$$\int_{\partial\omega} \boldsymbol{t}(t, \boldsymbol{s}) d\boldsymbol{s} = \int_\omega \nabla \cdot \mathbb{S}(t, \boldsymbol{x}) d\boldsymbol{x},$$

$$\rho\left(\partial_t \boldsymbol{v} + (\boldsymbol{v} \cdot \nabla)\boldsymbol{v}\right) = \nabla \cdot \mathbb{S} + \boldsymbol{f}_{\text{ext}} \quad \forall t \in (0, T],\ \boldsymbol{x} \in \Omega. \tag{2.4}$$

Modelled in terms of the variables of the present problem, the stress tensor can be decomposed in two terms,

$$\mathbb{S} = \mathbb{V} - P\mathbb{I}. \tag{2.5}$$

The first term represents the viscous stress tensor $\mathbb{V}$ $\left[\frac{\text{N}}{\text{m}^2}\right]$, which contains the forces from the friction of fluid particles. Since friction can occur only when the particles have different velocities, the tensor is modelled in terms of a velocity gradient. Moreover, the condition of conservation of angular momentum results in the symmetry of the stress tensor $\mathbb{S}$ leaving only 6 unique components (proof in [13], pages 13-14). Therefore, the symmetry constraint imposes another dependence of $\mathbb{V}$ on the transpose of the velocity gradient. In case of small velocity gradients, the so-called Newtonian fluid, $\mathbb{V}$ is well approximated by the linear dependence on $\nabla \boldsymbol{v}$. With the additional incompressibility condition $\nabla \cdot \boldsymbol{v} = 0$, the viscous stress tensor $\mathbb{V}$ is only proportional to the velocity deformation tensor $\mathbb{D}(\boldsymbol{v})$ as in the expression below, μ $\left[\frac{\text{kg}}{\text{m s}}\right]$ being the first order viscosity constant

$$\mathbb{V} = 2\mu\mathbb{D}(\boldsymbol{v}) = \frac{\nabla \boldsymbol{v} + (\nabla \boldsymbol{v})^T}{2} \quad [1/\text{s}]. \tag{2.6}$$

The second term is the pressure P [Pa] from the forces acting on the surface of the fluid volume ω, with $\mathbb{I}$ - the identity tensor. The effect of the pressure only normal to the surface and directed inwards can be expressed as

$$-\int_{\partial\omega} P\boldsymbol{n} ds = -\int_\omega \nabla P d\boldsymbol{x} = -\int_\omega \nabla \cdot (P\mathbb{I}) d\boldsymbol{x}. \tag{2.7}$$

By substituting the terms (2.7), (2.6) making up the stress tensor in equation (2.4) and the incompressibility conditions in the continuity equation (2.1), the Navier-Stokes equations for incompressible fluids

$$\begin{aligned} \partial_t \boldsymbol{v} - 2\nu\nabla \cdot \mathbb{D}(\boldsymbol{v}) + (\boldsymbol{v} \cdot \nabla)\boldsymbol{v} + \nabla\frac{P}{\rho} &= \frac{\boldsymbol{f}_{\text{ext}}}{\rho} \text{ in } (0, T] \times \Omega, \\ \nabla \cdot \boldsymbol{v} &= 0 \quad \text{ in } (0, T] \times \Omega \end{aligned} \tag{2.8}$$

are obtained, where $\nu = \mu/\rho$ $\left[\frac{\text{m}^2}{\text{s}}\right]$ is the kinematic viscosity of the fluid.

2.2 The non-dimensionalization procedure

For the numerical analysis of the above equations, non-dimensionalization is required. This gives the means to quantitatively compare the terms in the equation to each other and better understand their influence on the overall dynamics. In this section, the procedure of getting to the non-dimensional version of the system is described.
Firstly, a change in notation is made by assigning a prime to quantities with dimensions from (2.8), t' and $\boldsymbol{x}'$. Subsequently, the conversion relations using the characteristic length L, velocity U and time T^* scales are established:

$$\boldsymbol{x} = \frac{\boldsymbol{x}'}{L}, \quad \boldsymbol{u} = \frac{\boldsymbol{v}}{U}, \quad t = \frac{t'}{T^*}.$$

Substituting these relations in (2.8), then multiplying by a factor of $\frac{1}{U^2}$ from both sides gives the following expressions in the non-dimensionalized time and space domains:

$$\begin{aligned} \frac{L}{UT^*}\partial_t \boldsymbol{u} - \frac{2\nu}{UL}\nabla \cdot \mathbb{D}(\boldsymbol{u}) + (\boldsymbol{u}\cdot\nabla)\boldsymbol{u} + \nabla\frac{P}{\rho U^2} &= \frac{L}{\rho U^2}\boldsymbol{f}_{\text{ext}} \quad \text{in } (0,T]\times\Omega, \\ \nabla\cdot\boldsymbol{u} &= 0 \quad \text{in } (0,T]\times\Omega. \end{aligned}$$

New variables using the obtained constants are defined in the following way

$$p = \frac{P}{\rho U^2}, \quad \text{Re} = \frac{UL}{v}, \quad \text{St} = \frac{L}{UT^*}, \quad \boldsymbol{f} = \frac{L}{\rho U^2}\boldsymbol{f}_{\text{ext}}.$$

Here, Re and St are the Reynolds and the Strouhal numbers, which allow the classification of different flow cases.
The Navier-Stokes equations in this notation and with an additional simplification using the characteristic timescale $T^* = L/U$ are the equations represented below, which are the basis for mathematical analysis and numerical simulations:

$$\partial_t \boldsymbol{u} - 2\nu\nabla\cdot\mathbb{D}(\boldsymbol{u}) + (\boldsymbol{u}\cdot\nabla)\boldsymbol{u} + \nabla p = \boldsymbol{f} \text{ in } (0,T]\times\Omega, \tag{2.9}$$

$$\nabla\cdot\boldsymbol{u} = 0 \text{ in } (0,T]\times\Omega. \tag{2.10}$$

There is, however, one more simplification to be done on the velocity deformation tensor $\mathbb{D}(\boldsymbol{u})$. Using the incompressibility property $\nabla\cdot\boldsymbol{v} = 0$ and the Schwarz theorem, the terms of the tensor can be re-written in the following way

$$\nabla\cdot(\nabla\boldsymbol{u}) = \Delta\boldsymbol{u}, \tag{2.11}$$

$$\nabla\cdot\left(\nabla\boldsymbol{u}^T\right) = \nabla\left(\nabla\cdot\boldsymbol{u}\right) = \boldsymbol{0}. \tag{2.12}$$

Applying these results to the term from (2.6) and substituting in the first equation from (2.10), yields

$$\partial_t \boldsymbol{u} - \nu\Delta\boldsymbol{u} + (\boldsymbol{u}\cdot\nabla)\boldsymbol{u} + \nabla p = \boldsymbol{f} \text{ in } (0,T]\times\Omega, \tag{2.13}$$

$$\nabla\cdot\boldsymbol{u} = 0 \text{ in } (0,T]\times\Omega. \tag{2.14}$$

In this study only the steady state incompressible Navier-Stokes equations will be considered, where the velocity and the pressure do not change with time. Therefore, the studied system (2.14) with $\partial_t\boldsymbol{u} = 0$ is rewritten as

$$\begin{aligned} -\nu\Delta\boldsymbol{u} + (\boldsymbol{u}\cdot\nabla)\boldsymbol{u} + \nabla p &= \boldsymbol{f} \text{ in } \Omega, \\ \nabla\cdot\boldsymbol{u} &= 0 \text{ in } \Omega. \end{aligned} \tag{2.15}$$

A necessary but not sufficient condition for a steady-state system is the time independence of $\boldsymbol{f}$ and of the boundary conditions.

The final non-dimensionalized form of equations (2.15) presents difficulties for the mathematical analysis. These are, namely, the coupling of velocity and pressure and the nonlinearity of the convective term. Additionally, for numerical simulations, difficulties appear in cases of a dominant convective term, or equivalently small viscosity. In the following subsections, the first steps of the analysis of the problem will be presented, with the goal of addressing some of these difficulties.

2.3 Variational formulation

Let us consider again the strong form of the incompressible Navier-Stokes equations (2.15) and specify homogeneous Dirichlet boundary conditions $\boldsymbol{u} = \mathbf{0}$ on the boundary $\partial\Omega$. The weak form is obtained by multiplying the respective system with test functions and integrating by parts over the domain Ω, thereby transferring the derivatives from the unknown functions to the test functions. The function spaces for velocity and pressure are the Hilbert spaces defined as

$$V = H_0^1(\Omega) = \left\{ \boldsymbol{v} : \boldsymbol{v} \in H^1(\Omega) \text{ with } \boldsymbol{v} = \mathbf{0} \text{ on } \partial\Omega \right\}, \tag{2.16}$$

where the value of $\boldsymbol{v}$ on the boundary is to be understood in the sense of traces,

$$Q = L_0^2(\Omega) = \left\{ q : q \in L^2(\Omega) \text{ with } \int_\Omega q(\boldsymbol{x}) d\boldsymbol{x} = 0 \right\}. \tag{2.17}$$

The inner product in V and the induced norm are given by

$$(\boldsymbol{v}, \boldsymbol{w}) = \int_\Omega (\nabla \boldsymbol{v} : \nabla \boldsymbol{w})(\boldsymbol{x}) d\boldsymbol{x}, \quad \|\boldsymbol{v}\|_V = \|\nabla \boldsymbol{v}\|_{L^2(\Omega)}. \tag{2.18}$$

Whereas the inner product and the induced norm in Q are given by

$$(q, r) = \int_\Omega (qr)(\boldsymbol{x}) d\boldsymbol{x}, \quad \|q\|_Q = \|q\|_{L^2(\Omega)}. \tag{2.19}$$

The dual space of V is $V' = H^{-1}(\Omega)$ and the dual of the pressure space is $Q' = Q$.
With the above definitions of $V = H_0^1(\Omega)$ and $Q = L_0^2(\Omega)$, the weak or variational problem of (2.15) can be formulated following the Remark 6.4 from [13]:
Given $\boldsymbol{f} \in H^{-1}(\Omega)$, find $(\boldsymbol{u}, p) \in V \times Q$ such that

$$\begin{aligned} (\nu \nabla \boldsymbol{u}, \nabla \boldsymbol{v}) + ((\boldsymbol{u} \cdot \nabla)\boldsymbol{u}, \boldsymbol{v}) - (\nabla \cdot \boldsymbol{v}, p) &= \langle \boldsymbol{f}, \boldsymbol{v} \rangle_{V',V}, \\ -(\nabla \cdot \boldsymbol{u}, q) &= 0, \end{aligned} \tag{2.20}$$

for all $(\boldsymbol{u}, p) \in V \times Q$.
An equivalent formulation is the following:

$$(\nu \nabla \boldsymbol{u}, \nabla \boldsymbol{v}) + ((\boldsymbol{u} \cdot \nabla)\boldsymbol{u}, \boldsymbol{v}) - (\nabla \cdot \boldsymbol{v}, p) + (\nabla \cdot \boldsymbol{u}, q) = \langle \boldsymbol{f}, \boldsymbol{v} \rangle_{V',V} \tag{2.21}$$

for all $(\boldsymbol{u}, p) \in V \times Q$.
The definitions of the function spaces imply that the terms in both formulations are well-defined. The weak form can be identified as an abstract saddle point problem, which is formally presented in the next section.

2.4 Linear saddle point problems

The abstract linear saddle point problem offers a context for studying the existence and uniqueness of solutions of incompressible flow problems. Its presentation here follows the Remarks 3.3, 3.7 and Theorems 3.18 and 3.46 from the Chapter 3 in [13].
Let V and Q be two real Hilbert spaces with inner products $(\cdot,\cdot)_V$ and $(\cdot,\cdot)_Q$ with their respective induced norms. Their dual spaces are given by V' and Q', with the dual pairings given by $\langle \cdot,\cdot \rangle_{V',V}$ and $\langle \cdot,\cdot \rangle_{Q',Q}$ and the induced norms.
Two continuous bilinear forms are considered $a(\cdot,\cdot) : V \times V \to \mathbb{R}$, $\quad b(\cdot,\cdot) : V \times Q \to \mathbb{R}$ with the usual definition of norms.
The abstract linear saddle point problem is the following: Find $(u, p) \in V \times Q$ such that for given $(f, r) \in V' \times Q'$

$$\begin{aligned} a(u, v) + b(v, p) &= \langle f, v \rangle_{V',V} \quad \forall v \in V, \\ b(u, q) &= \langle r, q \rangle_{Q',Q} \quad \forall q \in Q. \end{aligned} \tag{2.22}$$

Problem (2.22) can be equivalently formulated in terms of operators. The linear operators associated with the bilinear are the following

$$\begin{aligned} &A \in \mathcal{L}(V, V') \text{ defined by } \langle Au, v \rangle_{V',V} = a(u, v) \quad \forall u, v \in V, \\ &B \in \mathcal{L}(V, Q') \text{ defined by } \langle Bu, q \rangle_{Q',Q} = b(u, q) \quad \forall u \in V, \forall q \in Q. \end{aligned} \tag{2.23}$$

Let $B' \in \mathcal{L}(Q, V')$ be the adjoint (dual) operator of B defined by

$$\langle B'q, v\rangle_{V',V} = \langle Bv, q\rangle_{Q',Q} = b(v,q) \quad \forall v \in V, \forall q \in Q.$$

With these operators, problem (2.22) can be written in the equivalent form: Find $(u,p) \in V \times Q$ such that

$$\begin{aligned} Au + B'p &= f \text{ in } V', \\ Bu &= r \text{ in } Q'. \end{aligned} \tag{2.24}$$

Definition of the Well-posedness of (2.24).
The problem (2.24) is well-posed if the linear operator $\Phi(\cdot,\cdot)$ defined as

$$\Phi \in \mathcal{L}(V \times Q, V' \times Q') : \Phi(v,q) = (Av + B'q, Bv),$$

where $(\cdot,\cdot)$ stands for a vector with 2 components, is an isomorphism from $V \times Q$ onto $V' \times Q'$.

Definition of a bounded Bilinear Form.
Let $b(\cdot,\cdot) : V \times V \to \mathrm{R}$ be a bilinear form on the Banach space V. Then it is bounded if

$$|b(u,v)| \leq M||u||_V||v||_V, \ \forall u, v \in V, \ M > 0, \tag{2.25}$$

with the constant M independent of u and v.

Definition of a coercive Bilinear Form.
The bilinear form is coercive or $V-$elliptic if

$$b(u,u) \geq m||u||_V^2, \ \forall u \in V, m > 0, \tag{2.26}$$

where the constant m is independent of u.

In the case that the spaces V and Q are finite, with dimensions n_V and n_Q respectively, the operators can be represented with matrices, with $B' = B^T$, and the functions with vectors. So, the saddle point problem (2.24) becomes equivalent to the following linear system of equations

$$\begin{pmatrix} A & B^T \\ B & 0 \end{pmatrix} \begin{pmatrix} \underline{u} \\ \underline{p} \end{pmatrix} = \begin{pmatrix} \underline{f} \\ \underline{r} \end{pmatrix}, \quad \begin{pmatrix} A & B^T \\ B & 0 \end{pmatrix} \in \mathbb{R}^{(n_V+n_Q)\times(n_V+n_Q)}. \tag{2.27}$$

The well-posedness of the saddle-point problem is given by the invertibility of the system matrix, which equivalently insures a unique solution.
Considering the velocity and pressure separately, it is possible to solve the system (2.27) by solving the first equation and then inserting it in the second one as follows,

$$\underline{u} = A^{-1}\left(\underline{f} - B^T\underline{p}\right), \tag{2.28}$$

$$\left(BA^{-1}B^T\right)\underline{p} = BA^{-1}\underline{f} - \underline{r}. \tag{2.29}$$

If (2.29) has a unique solution $\underline{p}$, it can be inserted in (2.28), which will give a unique solution for $\underline{u}$ as well. In order to find the unique solutions, both A and $BA^{-1}B^T$ have to be non-singular. For the latter to be true, the condition $\ker\left(B^T\right) = \{\underline{0}\}$ has to hold, i.e., B must be injective on the range of $A^{-1}B^T$. Otherwise, if there is a non-zero $\underline{\tilde{p}} \in \ker\left(B^T\right)$, then also $\underline{p} + \underline{\tilde{p}}$ is a solution to (2.29) and $\underline{p}$ is no longer a unique solution.
When pressure and velocity are considered at once, the whole system matrix must be non-singular. This is given by the necessary condition $n_Q \leq n_V$. If A is non-singular, the system matrix is non-singular if and only if B has full rank. It will be shown that $\mathrm{rank}(B) = n_Q$ if and only if

$$\inf_{\underline{q}\in\mathbb{R}^{n_Q},\underline{q}\neq\underline{0}} \sup_{\underline{v}\in\mathbb{R}^{n_V},\underline{v}\neq\underline{0}} \frac{\underline{v}^T B^T \underline{q}}{\|\underline{v}\|_2\|\underline{q}\|_2} \geq \beta > 0. \tag{2.30}$$

Proof:
i) Let (2.30) be satisfied and $\mathrm{rank}(B) < n_Q$. In this case, there is a $\underline{q} \in \mathbb{R}^{n_Q}$, $\underline{q} \neq \underline{0}$, such that $\underline{q} \in \ker(B^T)$. Then, $\underline{v}^T B^T \underline{q} = \underline{0}$ for all $\underline{v} \in \mathbb{R}^{n_V}$, the supremum is zero and (2.30) cannot be

satisfied. This is a contradiction to the initial assumption, hence $\text{rank}(B) = n_Q$.
ii) Now let $\text{rank}(B) = n_Q$. For each $\underline{q} \in \mathbb{R}^{n_Q}$, $\underline{q} \neq \underline{0}$, $B^T\underline{q} \neq \underline{0}$ with $B^T \in \mathbb{R}^{n_V}$. Choosing $\underline{v} = B^T\underline{q}$ in (2.30) gives

$$\inf_{\underline{q}\in\mathbb{R}^n,\underline{q}\neq\underline{0}} \sup_{\underline{v}\in\mathbb{R}^{nv},\underline{v}\neq\underline{0}} \frac{\underline{v}^T B^T \underline{q}}{\|\underline{v}\|_2 \|\underline{q}\|_2} \geq \inf_{\underline{q}\in\mathbb{R}^n,\underline{q}\neq\underline{0}} \frac{\left\|B^T\underline{q}\right\|_2^2}{\left\|B^T\underline{q}\right\|_2 \|\underline{q}\|_2} \tag{2.31}$$

$$= \inf_{\underline{q}\in\mathbb{R}^n,\underline{q}\neq\underline{0}} \frac{\left\|B^T\underline{q}\right\|_2}{\|\underline{q}\|_2}. \tag{2.32}$$

The obtained relation takes the infimum over the Rayleigh quotient, which is identified as the smallest eigenvalue of BB^T and is expressed below

$$\inf_{q\in\mathbb{R}^n,q\neq\underline{0}} \frac{\underline{q}^T BB^T \underline{q}}{\underline{q}^T\underline{q}} = \lambda_{\min}\left(BB^T\right).$$

Since B was assumed to have full rank $\lambda_{\min}\left(BB^T\right) > 0$ and with (2.32), one gets the inequality (2.30) in terms of the minimal eigenvalue

$$\inf_{\underline{q}\in\mathbb{R}^n Q,\underline{q}\neq\underline{0}} \sup_{\underline{v}\in\mathbb{R}^{nV},\underline{v}\neq\underline{0}} \frac{\underline{v}^T B^T \underline{q}}{\|\underline{v}\|_2 \|\underline{q}\|_2} \geq \lambda_{\min}^{1/2}\left(BB^T\right) > 0.$$

■

In essence, the saddle point problem (2.27) has a unique solution if A is non-singular and B satisfies the inf-sup condition (2.30). This is formally stated in the next lemma:

Lemma on the Sufficient Condition on $a(\cdot,\cdot)$ for Well-posedness of (2.24) (Lemma 3.19 from [13])
With the assumption that the bilinear form $a(\cdot,\cdot)$ is V_0-elliptic (2.26), the problem (2.24) is well-posed if and only if the bilinear form $b(\cdot,\cdot)$ satisfies the following inf-sup condition

$$\exists\ \beta > 0,\ \text{s.t.} \inf_{q\in Q,q\neq 0} \sup_{v\in V,v\neq 0} \frac{b(v,q)}{||v||_V ||q||_Q} \geq \beta. \tag{2.33}$$

The proof can be found in [13] on pages 39 and 40. ■

2.5 Divergence-free vector spaces

For incompressible flow problems, one is interested in divergence-free and weakly divergence-free spaces. In this section, the definitions of such spaces will be presented.
The space of vector fields in L^2, with the divergence belonging to L^2 is defined as

$$H(\text{div},\Omega) = \{\boldsymbol{v} \in L^2(\Omega) : \nabla\cdot\boldsymbol{v} \in L^2(\Omega)\}. \tag{2.34}$$

A particular space of divergence-free functions used in numerical analysis is defined by

$$H_{div}(\Omega) = \{\boldsymbol{v} \in H(\text{div},\Omega) : \nabla\cdot\boldsymbol{v} = 0 \text{ and } \boldsymbol{v}\cdot\boldsymbol{n} = 0 \text{ on } \partial\Omega \text{ in the sense of traces}\}. \tag{2.35}$$

If for a vector field $\boldsymbol{v} \in L^1(\Omega)$ with $p \geq 1$ there exists a function $\theta \in L^1_{loc}(\Omega)$ such that

$$-\int_\Omega \nabla\psi\cdot\boldsymbol{v}d\boldsymbol{x} = \int_\Omega \psi\theta\ d\boldsymbol{x},\ \forall\psi \in C_0^\infty(\Omega),$$

then the function θ is the weak divergence of $\boldsymbol{v}$.
The weakly divergence-free spaces satisfy additionally the following condition

$$\int_\Omega \nabla\psi\cdot\boldsymbol{v}\ d\boldsymbol{x} = 0,\ \forall\psi \in C_0^\infty(\Omega).$$

The space of weakly divergence-free functions can be formally defined using the spaces V and Q from (2.16), (2.17) and represents the kernel of the operator B from the saddle point problem (2.24). This space is namely

$$V_0 = V_{\text{div}} = \{\boldsymbol{v} \in V : (\nabla \cdot \boldsymbol{v}, q) = 0 \ \forall \ q \in Q\}. \tag{2.36}$$

The divergence of the functions from V_{div} vanishes in the sense of L^2 almost everywhere in Ω. The regularity requirement for functions is thus weaker in H_{div} than in V_{div}.

2.6 Results for existence and uniqueness of a solution

In this section, the results for existence and uniqueness of a weak solution to (2.20) are presented. The existence of a weak solution always holds, whereas the uniqueness only in cases of sufficiently small external forces and small viscosity. If the solution is not unique, numerical simulations will yield time-dependent solutions. The full theorems are formulated as follows:

Theorem on the Existence of a Solution (Theorem 6.17 in [13])
Let $\Omega \subset \mathcal{R}^d$, $d \in 2, 3$ be a bounded domain with Lipschitz boundary, $\partial\Omega$ and let $\boldsymbol{f} \in H^{-1}(\Omega)$. Then there exists at least one solution of (2.20).

Theorem on the Existence and Uniqueness of a Solution for Small Data (Theorem 6.20 in [13])
Let the previous theorem on existence hold and let in addition

$$\frac{N_{div}||\boldsymbol{f}||_{H^{-1}(\Omega)}}{\nu^2} < 1 \tag{2.37}$$

then problem (2.21) has a unique solution $\boldsymbol{u} \in V_{div}$ and problem (2.20) has a unique solution $(\boldsymbol{u}, p) \in V \times Q$.

In the last theorem, N_{div} represents the norm of the convective term with basis functions belonging to the space V_{div}. It is defined as

$$N_{\text{div}} = \sup_{u,v,w \in V_{\text{div}} \setminus \{0\}} \frac{((\boldsymbol{u} \cdot \nabla)\boldsymbol{v}, \boldsymbol{w})}{\|\boldsymbol{u}\|_V \|\boldsymbol{v}\|_V \|\boldsymbol{w}\|_V}.$$

The proofs of the theorems can be found in reference [6].

Chapter 3

Finite Element Methods for the Incompressible Navier-Stokes Equations

This section aims to present fundamental results from the theory of finite element methods, following the lecture notes in [24] and the appendix B from the reference [13].

3.1 Brief Introduction into the Finite Element Method

3.1.1 The Ritz and Galerkin methods

The goal of the Finite Element Methods consists in computing an approximate solution to a differential equation by looking for it in a finite dimensional space V_h, with the basis $\{\phi_{1\leq i\leq N}\}$. The approximate solution has the form

$$u_h = \sum_{i=1}^{N} u_i \phi_i(x).$$

Given the function space V_h and the basis $\{\phi_i(x)\}$, the approximate solution u_h is completely determined by the coefficients u_i. The problem now consists in how to choose V_h and how to determine the coefficients u_i such that u_h is a good approximation to the solution u of the original problem.
The first idea, authored by Ritz in 1902, was to transform the boundary value problem into a minimization problem. This is rigorously captured by the Ritz representation theorem, given below. The Hilbert space V will be considered with the inner product $a(\cdot,\cdot) : V \times V \to R$ and the norm $||v||_V = a(v,v)^{1/2}$.

Representation theorem of Ritz.
Let $f \in V'$ be a continuous and linear functional, then there is a uniquely determined $u \in V$ with

$$a(u,v) = f(v),\ \forall v \in V. \tag{3.1}$$

In addition, u is the unique solution of the variational problem

$$F(v) = \frac{1}{2}a(v,v) - f(v) \to \min\ \forall v \in V. \tag{3.2}$$

Proof.

(i) Proving the existence of a solution u of a variational problem:
Since f is continuous, it holds that

$$|f(v)| \leq C||v||_V\ \forall v \in V,$$

from which follows

$$F(v) \geq \frac{1}{2}||v||_V^2 - C||v||_V \geq -\frac{1}{2}C^2,$$

where the result from the necessary criterion for a local minimum of $F(v)$ was used,

$$\frac{2}{2}||v||_V - C = 0 \iff ||v||_V = C.$$

Hence, the function $F(\cdot)$ is bounded from below and

$$\kappa = \inf_{v \in V} F(v)$$

exists.

Let $\{v_k\}_{k \in N}$ be a sequence with $F(v_k) \to k$ for $k \to \infty$. The parallelogram identity in a Hilbert space gives

$$||v_k - v_l||_V^2 + ||v_k + v_l||_V^2 = 2||v_k||_V^2 + 2||v_l||_V^2.$$

Using the linearity of $f(\cdot)$ and $\kappa \leq F(v)$ for all $v \in V$, one obtains

$$\begin{aligned} ||v_k - v_l||_V^2 = & \\ &= 2||v_k||_V^2 + 2||v_l||_V^2 - 4\left|\left|\frac{v_k + v_l}{2}\right|\right|_V^2 - 4f(v_k) - 4f(v_l) + 8f\left(\frac{v_k + v_l}{2}\right) \\ &= 4F(v_k) + 4F(v_l) + 4F\left(\frac{v_k + v_l}{2}\right) \\ &\leq 4F(v_k) + 4F(v_l) - 8\kappa \to 0, \text{ for } k,\ l \to \infty. \end{aligned}$$

Hence, $\{v_k\}_{k \in N}$ is a Cauchy sequence. Since V is a complete space, there exists a limit u of this sequence with $u \in V$. Because $F(\cdot)$ is continuous, it is $F(u) = \kappa$ and u is a solution of the variational problem.

(ii) Showing that each solution of the variational problem (3.2) is also a solution of (3.1):
For arbitrary $v \in V$, it holds that

$$\begin{aligned} \Phi(\epsilon) = F(u + \epsilon v) &= \frac{1}{2}a(u + \epsilon v, u + \epsilon v) - f(u + \epsilon v) \\ &= \frac{1}{2}a(u, u) + \epsilon a(u, v) + \frac{\epsilon^2}{2}a(v, v) - f(u) - \epsilon f(v) \end{aligned}$$

If u is a minimum of the variational problem, then the function $\Phi(\epsilon)$ has a minimum at $\epsilon = 0$. The necessary condition for a local minimum is then

$$0 = \Phi'(0) = a(u, v) - f(v),\ \forall v \in V.$$

(iii) Proving the uniqueness of the solution u:
To this end, proving the uniqueness of the solution of the equation (3.1) is sufficient. Otherwise, the existence of two solutions of the variational problem (3.2) would be a contradiction to the condition from the previous step. Let u_1 and u_2 be two solutions of the equation (3.1). The difference of both equations yields the following,

$$a(u_1 - u_2, v) = 0,\ \forall v \in V.$$

In particular, for $v = u_1 - u_2$, $||u_1 - u_2||_V = 0$, such that $u_1 = u_2$.

■

The Poisson problem with Dirichlet boundary conditions can be used as an example

$$-\Delta u = f. \text{ in } \Omega,\ u = 0,\ \text{on } \partial\Omega. \tag{3.3}$$

Its equivalent minimization problem can be formulated as follows,

$$\min_{u\in H_0^1(\Omega)} \left(\frac{1}{2}\int_\Omega |\nabla u(x)|^2 \mathrm{d}x - \int_\Omega f(x)u(x)\mathrm{d}x \right). \tag{3.4}$$

For the latter problem to be well-defined, the following Hilbert spaced, defined on a domain $\Omega \in \mathrm{R}^n$, are needed

$$H^1(\Omega) = \{u \in L^2(\Omega),\ \nabla u \in (L^2(\Omega))^d\},\quad H_0^1 = \{u \in H^1(\Omega),\ u = 0 \text{ on } \partial\Omega\} \tag{3.5}$$

The associated scalar product, the norm in $H^1(\Omega)$, the semi-norm in $H^1(\Omega)$ and the norm in $L^2(\Omega)$ are

$$\begin{aligned}
(u,v)_1 &= \int_\Omega \nabla u(x)\cdot\nabla v(x)\mathrm{d}x + \int_\Omega u(x)v(x)\mathrm{d}x,\\
||u||_{1,\Omega} &= \int_\Omega |\nabla u(x)|^2\mathrm{d}x + \int_\Omega u(x)^2\mathrm{d}x,\\
|u|_{1,\Omega} &= \int_\Omega |\nabla u(x)|^2\mathrm{d}x,\\
||u||_{0,\Omega} &= \int_\Omega u(x)^2\mathrm{d}x.
\end{aligned}$$

The standard minimization problem with a cost functional J defined on a Hilbert space V, of the form

$$\min_{u\in V} J[u]$$

consists in solving the associated Euler equation $J'[u] = 0$, by computing the Fréchet derivative. This approach results in the variational formulation which, in case of this problem, reads

$$\int_\Omega \nabla u(x)\cdot\nabla v(x)\mathrm{d}x = \int_\Omega f(x)v(x)\mathrm{d}x\ \forall v \in H_0^1(\Omega). \tag{3.6}$$

The Ritz - Galerkin method.
The principle of the Galerkin (or Ritz-Galerkin) method consists then in looking for a solution of the variational problem (3.2), in a finite dimensional space V_h of the space V where the exact solution of (3.1) is defined. In order to approximate this solution with a numerical method, it will be assumed that V has a countable orthonormal basis (Shauder basis). Then, there are finite-dimensional subspaces $V_1, V_2, ... \subset V$ with $\dim V_k = k$ with the property that for each $u \in V$ and each $\epsilon > 0$, there is a $K \in \mathrm{N}$ and a $u_k \in V_k$ with

$$||u - u_k||_V \leq \epsilon,\ \forall k \geq K. \tag{3.7}$$

An inclusion of the form $V_k \subset V_{k+1}$ is not required. The Ritz approximation of (3.1) and (3.2) is then given by the following problem:
Find $u_k \in V_k$ with

$$a(u_k, v_k) = f(v_k),\ \forall v_k \in V. \tag{3.8}$$

Best approximation property.
Additionally, the solution of (3.8) is the best approximation of u in V_k, which means that it satisfies

$$||u - u_k||_V = \inf_{v_k\in V_k} ||u - v_k||_V. \tag{3.9}$$

Proof.
Taking the difference between (3.3) and (3.8), one gets the following Galerkin orthogonality,

$$a(u - u_k, v_k) = 0,\ \forall v_k \in V_k. \tag{3.10}$$

Hence, $(u - u_k) \perp V_k$, meaning that u_k is the orthogonal projection of u onto V_k with respect to the inner product of V.
Taking $w_k \in V_k$ as an arbitrary element, using the Galerkin orthonormality (3.10) and the Cauchy-Schwarz inequality, it follows that

$$\begin{aligned}
||u - u_k||_V^2 &= a(u - u_k, u - u_k) = a(u - u_k, u - (u_k - w_k))\\
&= a(u - u_k, u - v_k) \leq ||u - u_k||_V ||u - v_k||_V.
\end{aligned}$$

Since $w_k \in V_k$ is arbitrary, $v_k \in V_k$ is arbitrary too, as $v_k = u_k - w_k$.

(i) For $||u-u_k||_V > 0$, division by $||u-u_k||_V$ gives the statement of the best approximation, namely, $||u-u_k||_V \leq ||u-v_k||, \forall v_k \in V_k$.

(ii) For $||u-u_k||_V = 0$, the statement is trivially true.

■

Convergence of the Ritz approximation.
It is also possible to prove that the Ritz approximation converges, i.e.

$$\lim_{k\to\infty} ||u-u_k||_V = 0.$$

Proof.
Using the best approximation property (3.9) and the property (3.7), one obtains

$$||u-u_k||_V = \inf_{v_k\in V_k} ||u-v_k||_V \leq \epsilon$$

for each $\epsilon < 0$ and $k \geq K(\epsilon)$. Hence, the convergence is proved. ■

Formulation as a linear system of equations.
In order to compute the solution u_k, the basis functions $\{\phi_{i=1}^k\}$ of V_k are used. The equation of the Ritz approximation (3.8) is satisfied for all v_k if and only if it satisfied for each basis functions ϕ_i. This follows from the linearity of the both sides of the equation with respect to the test function and from the representation of $v_k \in V_k$ as a linear combination of the basis functions, $v_k = \sum_{i=1}^k \alpha_i\phi_i$. Plugging the test function in this form into (3.8) gives

$$a(u_k, v_k) = \sum_{i=1}^k \alpha_i a(u_k, \phi_i) = \sum_{i=1}^k \alpha_i f(\phi_i) = f(v_k).$$

The equation is satisfied if $a(u_k, \phi_i) = f(\phi_i)$, $i = 1, .., k$. On the other hand, if (3.8) holds, then it holds for each basis function ϕ_i.
Now, writing the ansatz function as a linear combination of the basis functions $u_k = \sum_{j=1}^k u^j\phi_j$ and using the basis functions as test functions, one obtains the following

$$\sum_{j=1}^k a(u^j\phi_j, \phi_i) = \sum_{j=1}^k a(\phi_j, \phi_i)u^j = f(\phi_i),\ i = 1, ..., k.$$

The latter is equivalent to the linear system of equations $A\underline{u} = \underline{f}$, with the stiffness matrix $A = (a_{ij})_{i,j=1}^k = a(\phi_j, \phi_i)_{i,j=1}^{k=1}$ and the right-hand side $f_i = f(\phi_i)$, $i = 1, ..., k$.

Coming back to the example of the Poisson problem, one can write explicitly its variational problem in terms of the basis $(\phi_1, ..., \phi_k)$ that characterizes the space V_k. Using the latter ansatz and test functions, the variational form is expressed in the following way

$$\sum_{j=1}^k u^j \int_\Omega \nabla\phi_j(x) \cdot \nabla\phi_i(x)\mathrm{d}x = \int_\Omega f(x)\phi_i(x)\mathrm{d}x,\ i = 1, ..., k.$$

Where the matrix A is defined by the entries $\left(\int_\Omega \nabla\phi_i(x) \cdot \nabla\phi_j(x)\mathrm{d}x\right)_{1\leq i,j\leq k}$, the vector of unknown coefficients is $\underline{u} = (u^1, ..., u^k)^T$ and the right-hand side is $\underline{f} = \left(\int_\Omega f(x)\phi_1(x)\mathrm{d}x, ..., \int_\Omega f(x)\phi_N(x)\mathrm{d}x\right)^T$. Because the bilinear form $a(\cdot, \cdot)$ is an inner product, one can easily show that the matrix A is symmetric and positive definite, i.e.,

$$A = A^T \iff a(v, w) = a(w, v), \forall v, w \in V_k,$$
$$\underline{x}^T A\underline{x} > 0 \text{ for } \underline{x} \neq \underline{0} \iff a(v, v) > 0, \forall v \in V_k, v \neq 0.$$

□

In case the bilinear form is not an inner product, but is bounded (2.25) and coercive (2.26), it is possible to approximate the solution to (3.1) with the same idea as for the Ritz method, but which is called the Galerkin method. An equivalent to the Ritz Representation Theorem in this

case is the Lax-Milgram Theorem, whose statement and proof can be found in Appendix B1 of [13]. The discrete problem using the Galerkin method consists in finding $u_k \in V_k$ such that

$$b(u_k, v_k) = f(v_k), \ \forall v_k \in V_k. \tag{3.11}$$

The error estimate corresponding to this problem is given below.

Lemma of Cea.

Let $b : V \times V \to \mathrm{R}$ be a bounded and coercive bilinear form on the Hilbert space V and let $f \in V'$ be a bounded linear functional. Let u be a solution of (3.1) and u_k be a solution of (3.11), then the following error estimate holds

$$||u - u_k|| \leq \frac{M}{m} \inf_{v_k \in V_k} ||u - v_k||_V, \tag{3.12}$$

where the constants M and m are given in (2.25) and (2.26).

Proof.

The difference between (3.1) and (3.11) gives the error equation with the property of the Galerkin orthogonality,

$$b(u - u_k, v_k) = 0, \ \forall v_k \in V_k.$$

Using the Galerkin orthogonality, the coercivity (2.26) and boundedness (2.25) of the bilinear form, one obtains

$$||u - u_k||_V^2 \leq \frac{1}{m} b(u - u_k, u - u_k) = \frac{1}{m} b(u - u_k, u - v_k) \quad \leq \frac{M}{m} ||u - u_k||_V ||u - u_k||_V, \forall v_k \in V_k.$$

By dividing both sides by $||u - u_k|| \neq 0$, one obtains the statement of the lemma. ■

An important consideration for choosing the space V_h lies in its approximation properties. In the Lemma of Cea, the error is bounded by a multiple of the best approximation error, where the factor depends on the properties of the bilinear form. The study of the best approximation error will hence be of importance in the error analysis.

For efficiency purposes, basis functions with a small support are used. Since the products between basis functions vanish for most matrix components, sparse matrices are obtained, which can be optimally handled. To this end, the domain is decomposed into triangles/tetrahedra or quadrilaterals/hexahedra in 2D/3D and the basis functions are chosen to be low order polynomials, on each of the elements. The freedom to choose the shape of the elements of the mesh offers great flexibility to handle complicated geometries of the boundaries and contributes to the wide usability of the method.

3.1.2 Construction of a finite element space

This section will provide details on how the finite-dimensional space $V_k \subset V$ can be constructed in a practical way. It follows the sources [24] and [13].

Let (K, P, Σ) be a triple such that

(i) K is a closed subset of R^n of non-empty interior,

(ii) P is a finite dimensional vector space of functions defined on K,

(iii) Σ is a set of linear forms on P of finite cardinality N, $\Sigma = \sigma_{K,1}, ..., \sigma_{K,N}$.

Definition 1 The elements of Σ are called degrees of freedom of the finite element.

Definition 2 Σ is said to be P- unisolvent if for any N-tuple $\boldsymbol{\alpha} = (\alpha_1, ..., \alpha_N)$, there exists an unique element $p \in P$ such that $\sigma_{K,i}(p) = \alpha_i$ for $i = 1, ..., N$.

Definition 3 The triple (K, P, Σ) of R^n is called Finite Element if it satisfies (i), (ii) and (iii) and if Σ is P-unisolvent.

In the latter definition, K is the domain of definition of the finite element, P is the finite dimensional space of the approximation, and Σ uniquely defines a local basis of P for $\boldsymbol{\alpha}$ chosen from the set of Cartesian unit vectors. This triple builds the finite element matrices associated to

the variational formulation applied to functions in the approximation space P. The unisolvence property ensures that the elements of P characterized by the degrees of freedom form a local basis of P. This is given by the following conditions from Lemmas 1 and 2.

Lemma 1 The set Σ is P-unisolvent if and only if the two following properties are satisfied

(i) dim $P = |\Sigma|$=N,

(ii) If $\sigma_{K,j} = 0$ for $j = 1, ..., N$, then $p = 0$.

Lemma 2 The set Σ is P-unisolvent if and only if the two following properties are satisfied

(i) dim $P = |\Sigma|$=N,

(ii) There exist N linearly independent functions $p_i \in P$, $i = 1, ..., N$ such that $\sigma_{K,j}(p_i) = \delta_{ij}$.

Both lemmas check if the dimension equals the number of degrees of freedom and then check the injectivity or the surjectivity, which both imply bijectivity given the correct dimension, of the mapping $P \to \mathrm{R}^N$, $p \mapsto (\sigma_{K,1}(p), ..., \sigma_{K,N}(p))$.

The Global Functionals.
Let the global functionals $\sigma_1, ..., \sigma_N : \mathrm{C}^s(\overline{\Omega}) \to \mathrm{R}$ be continuous linear functionals of the same type as in the set of linear form Σ. The restriction of functionals to $C^s(K)$ defines a set of local functionals $\sigma_{K,1}, ..., \sigma_{K,N}$, where it is assumed that the local functionals are unisolvent on $P(K)$. □

The Finite Element Space.
A basis function defined on Ω with $v|_K \in P(K)$ for all $K \in \mathcal{T}^h$ is called continuous with respect to the functional $\sigma_i : \Omega \to \mathrm{R}$ if

$$\sigma_i(v|_{K_1}) = \sigma_j(v|_{K_2}), \quad \forall K_1, K_2 \in \omega_i,$$

where ω_i is the union of all mesh cells K_j, for which there is a $p \in P(K_j)$ with $\sigma_i(p) \neq 0$.
The space below is defined as the finite element space:

$$S = \{v \in L^\infty(\Omega) : v|_K \in P(K) \text{ and } v \text{ is continuous with respect to } \sigma_i, \ i = 1, ..., N\}.$$

The global basis $\{\phi_j\}_{j=1}^N$ of S is defined by the condition

$$\phi_j \in S, \quad \sigma_i(\phi) = \delta_{ij}, \quad i, j = 1, ..., N.$$

A global basis function coincides with a local basis function on each cell, which implies the uniqueness of the global basis function.
The continuity of the global functionals $\{\sigma_i\}_{i=1}^N$ does not always imply the continuity of the finite element functions. This depends on the definition of the functionals that determine the finite element space. □

3.2 H^1-Conforming Methods

This section presents the formalism of the classical methods used to solve the Stokes equations and explains the origin of the problems with their approximated solutions, which this thesis aims to address, namely violation of mass conservation and lack of pressure robustness. To that end, the Stokes finite element problem is presented, together with the necessary conditions for solvability. Further, pairs of finite element spaces for these methods will be introduced, as well as error estimates with their convergence rates. The structure and content of the section follows closely Section 3 from [14] and Chapter 4.2 from [13], to which it is referred for certain proofs and further details.

3.2.1 The Galerkin finite element method

The variational formulation of the incompressible Navier-Stokes equations from Chapter 2.3 (2.20) restricted to the Stokes case, i.e., steady-state flow with large viscosity, has the following form: Find the weak solution $(\boldsymbol{u}, p) \in V \times Q := \boldsymbol{H}_0^1(\Omega) \cap L_0^2(\Omega)$, which satisfies the system below

$$a(\boldsymbol{u}, \boldsymbol{v}) + b(\boldsymbol{v}, p) = (\boldsymbol{f}, \boldsymbol{v}) \quad \forall \boldsymbol{v} \in V, \tag{3.13}$$

$$b(\boldsymbol{u}, q) = (g, q) \quad \forall q \in Q, \tag{3.14}$$

with $a(\boldsymbol{u}, \boldsymbol{v}) = \nu(\nabla \boldsymbol{u}, \nabla \boldsymbol{v})$ and $b(\boldsymbol{v}, q) = -(\nabla \cdot \boldsymbol{v}, q)$.
The finite element method aims to approximate the solution above using finite-dimensional spaces of piecewise polynomials $V^h \times Q^h \subset V \times Q$ on a triangulation of the domain Ω, with mesh cells $K \in \mathcal{T}^h$. The Galerkin finite element method to solve the Stokes equations has the following form: Find the solution $(\boldsymbol{u}^h, p^h) \in V^h \times Q^h$ to the system

$$a(\boldsymbol{u}^h, \boldsymbol{v}^h) + b(\boldsymbol{v}^h, p^h) = (\boldsymbol{f}, \boldsymbol{v}^h) \quad \forall \boldsymbol{v}^h \in V^h, \tag{3.15}$$

$$b(\boldsymbol{u}^h, q^h) = (g, q^h) \quad \forall q^h \in Q^h. \tag{3.16}$$

Since the last lemma of Chapter 2.4 implies that solving the Stokes problem (3.13) - (3.14) requires the coercivity of the $a(\cdot, \cdot)$ bilinear form and a $b(\cdot, \cdot)$ bilinear form that satisfies the inf-sup condition (2.33), similar requirements will have to be imposed on the finite element problem (3.15) - (3.16). This will ensure existence and uniqueness of the approximated solution, as well as convergence to the analytical solution, as the mesh width becomes smaller. To this end, the finite element spaces V^h and Q^h must satisfy the discrete inf-sup condition below from the Remark 3.51 of [13].

The discrete inf-sup condition.(Remark 3.51 from [13])
The combination of spaces V^h and Q^h is inf-sup stable if it holds that

$$\inf_{q^h \in Q^h \setminus \{0\}} \sup_{\boldsymbol{v}^h \in V^h \setminus \{\boldsymbol{0}\}} \frac{b^h(\boldsymbol{v}^h, q^h)}{||\boldsymbol{v}^h||_{V^h} ||q^h||_{Q^h}} \geq \beta_{is}^h > 0 \tag{3.17}$$

or equivalently if there is a $\beta_{is}^h > 0$ such that

$$\sup_{\boldsymbol{v}^h \in V^h \setminus \{\boldsymbol{0}\}} \frac{b^h(\boldsymbol{v}^h, q^h)}{||\boldsymbol{v}^h||_{V^h}} \geq \beta_{is}^h \, ||q^h||_{Q^h}, \ \forall q^h \in Q^h. \tag{3.18}$$

Here, the bilinear form $b^h : V^h \times Q^h \to \mathrm{R}$ is defined by

$$b^h(\boldsymbol{v}^h, q^h) = -\sum_{K \in \mathcal{T}^h} (\nabla \cdot \boldsymbol{v}^h, q^h)_K. \tag{3.19}$$

The norms in the denominator are defined as follows

$$||\boldsymbol{v}^h||_{V^h} = \left(\sum_{K \in \mathcal{T}^h} (\nabla \boldsymbol{v}^h, \nabla \boldsymbol{v}^h)_K \right)^{1/2}, \quad ||q^h||_{Q^h} = ||q^h||_{L^2(\Omega)}. \tag{3.20}$$

□

Since the finite element spaces is this chapter are conforming, i.e., $V^h \subset V$ and $Q^h \subset Q$, the

bilinear form $b^h(\cdot,\cdot)$ is identical to $b(\cdot,\cdot)$ and can be expressed with an integral over the domain Ω. Additionally, the velocity norm is $||\boldsymbol{v}^h||_{V^h} = ||\nabla \boldsymbol{v}^h||_{L^2(\Omega)}$. This, however, will not be the case for the $H(\text{div})$-conforming finite elements, discussed in Chapter 3.3, where the generality of the definitions above will be of use.
Spaces that satisfy this condition are presented in Section 3.2.2, from which the Taylor-Hood pairs P_k/P_{k-1}, $k \geq 2$ and the MINI element $P_1 \oplus V^h_{\text{bub}}/P_1$ will be used for comparison with $H(\text{div})$-conforming spaces in the numerical studies from Chapter 4.
Computations with the (discretely) inf-sup stable pairs, however, do not ensure even a weakly divergence-free (2.5) approximation $\boldsymbol{u}^h$ to the pointwise divergence-free (2.34) solution $\boldsymbol{u}$. The reason lies in the fact that the discrete inf-sup condition only implies that the discrete divergence operator (3.21) is surjective from V^h to Q^h.

The discrete divergence operator
The operator $\nabla\cdot_h : V^h \to Q^h$ is called discrete divergence and is defined as

$$(\nabla \cdot_h \boldsymbol{v}^h, q^h) = (\nabla \cdot \boldsymbol{v}^h, q^h) \quad \forall q^h \in Q^h. \tag{3.21}$$

□

Hence, the divergence-free condition is enforced only locally and the discretely inf-sup stable pairs of spaces satisfy the condition $\nabla\cdot_h\, V^h = Q^h$, but the global divergence-free property does not hold, i.e., $\nabla \cdot V^h \not\subset Q^h$. This causes the limitations of the violation of mass and lack of pressure-robustness, in a way which becomes clear upon analyzing the error estimates, as done in section 3.2.3.

3.2.2 Inf-sup stable pairs of finite element spaces

This section will present pairs of finite element spaces that satisfy the (discrete) inf-sup condition, based on Chapter 3.6 from [13].

1. **The MINI Element.**
   This element is defined on simplicial meshes and is given by

   $$V^h = P_1 \oplus V^h_{\text{bub}}, \quad Q^h = P_1, \tag{3.22}$$

   with V^h_{bub} - the space of local bubble functions

   $$V^h_{\text{bub}} = \{v^h_{\text{bub}} : \text{supp}(v^h_{\text{bub}}) = K,\ v^h_{bub}|_K = \alpha \prod_{i=1}^{d+1} \lambda_i,\ K \in \mathcal{T}^h, \alpha \in \mathrm{R}\},$$

   where λ_i are the barycentric coordinates of the simplex K. It follows that

   $$v^h_{\text{bub}}|_K \in P_{d+1}(K) \cap H^1_0(K).$$

   This pair was first introduced in [2] and it is the lowest order conforming inf-sup stable pair of finite element spaces. Its construction relies on the idea of enriching the standard finite element space for velocity such that the discrete inf-sup condition (3.17) is satisfied. The proof of the latter can be found in Theorem 3.121. of [13].

2. **The Family of Taylor-Hood Finite Element Spaces.**
   This family on triangular and tetrahedral grids is given by $P_k/P_{k-1}, k \geq 2$, and on quadrilateral and hexahedral grids by $Q_k/Q_{k-1}, k \geq 2$. Therefore, the pressure is approximated by a continuous function, so $b^h(\cdot,\cdot) = b(\cdot,\cdot)$ and $||\cdot||_{V^h} = ||\cdot||_V$.
   The proof that the pair $P_k/P_{k-1}, k \geq 2$ satisfies the discrete inf-sup condition (3.17) in two and three dimensions can be found in Theorems 3.128 and 3.129 of [13]. And the proof of the latter for the pair $Q_k/Q_{k-1}, k \geq 2$ in two and three dimensions can be found in [19] and [20] respectively.
   The pairs from the Taylor-Hood finite element family are among the most popular ones used, especially the pairs with $k = 2$, because of the simplicity of their implementation.

3. **Spaces on Simplicial Meshes with Discontinuous Pressure.**
   These spaces are of interest due to the fact that they satisfy a property that is called in the

literature local mass conservation. An illustration of the latter follows from the Remark 4.32. in [13]:
Let us consider meshes with affinely mapped grid cells. Since the piecewise constant functions are a subspace of a discontinuous pressure finite element space, one can make the following changes in the discrete continuity equation

$$0 = \sum_{K\in\mathcal{T}^h} \int_K (\nabla \cdot \boldsymbol{u}^h) q(\boldsymbol{x}) d\boldsymbol{x} = \sum_{K\in\mathcal{T}^h} q^h \int_K (\nabla \cdot \boldsymbol{u}^h)(\boldsymbol{x}) d\boldsymbol{x} \quad \forall q^h \in P_0 \text{ or } q^h \in Q_0. \tag{3.23}$$

Considering an arbitrary mesh cell K_1 and another arbitrary mesh cell $K_2 \neq K_1$, one can choose the following

$$q^h = \begin{cases} 1, & \text{in } K_1, \\ -\frac{|K_1|}{|K_2|}, & \text{in } K_2, \\ 0, & \text{else,} \end{cases} \qquad q^h \in L_0^2(\Omega).$$

Substituting q^h in (3.23), one obtains

$$\int_{K_2} \nabla \cdot \boldsymbol{u}^h(\boldsymbol{x}) d\boldsymbol{x} = \frac{|K_2|}{|K_1|} \int_{K_1} \nabla \cdot \boldsymbol{u}^h(\boldsymbol{x}) d\boldsymbol{x} \quad \forall K_2 \in \mathcal{T}^h.$$

It follows that

$$\begin{aligned} \int_\Omega \nabla \cdot \boldsymbol{u}^h(\boldsymbol{x}) d\boldsymbol{x} &= \sum_{K\in\mathcal{T}^h} \int_K \nabla \cdot \boldsymbol{u}^h(\boldsymbol{x}) d\boldsymbol{x} = \sum_{K\in\mathcal{T}^h} \frac{|K|}{|K_1|} \int_{K_1} \nabla \cdot \boldsymbol{u}^h(\boldsymbol{x}) d\boldsymbol{x} \\ &= \frac{1}{|K_1|} \int_{K_1} \nabla \cdot \boldsymbol{u}^h(\boldsymbol{x}) d\boldsymbol{x} \sum_{K\in\mathcal{T}^h} |K| \\ &= \frac{|\Omega|}{|K_1|} \int_{K_1} \nabla \cdot \boldsymbol{u}(\boldsymbol{x}) d\boldsymbol{x}. \end{aligned} \tag{3.24}$$

Using integration by parts, the result below is obtained

$$\int_\Omega \nabla \cdot \boldsymbol{u}^h(\boldsymbol{x}) d\boldsymbol{x} = \int_{\partial\Omega} \boldsymbol{u}^h \cdot \boldsymbol{n}(\boldsymbol{s}) d\boldsymbol{s} = 0.$$

Therefore, the last term on the right-hand side of (3.24) vanishes and since the cell K_1 was chosen to be arbitrary, the local mass conservation equation is obtained

$$\int_K \nabla \cdot \boldsymbol{u}^h(\boldsymbol{x}) d\boldsymbol{x} = 0 \quad \forall K \in \mathcal{T}^h. \tag{3.25}$$

However, it is shown in Fig. 4.4. of [13] that the magnitude of the error $||\nabla \cdot \boldsymbol{u}^h||_{L^2(\Omega)}$ is the same for both discretizations with continuous and certain discretizations with discontinuous pressure finite element space despite the local mass conservation property of the latter. □

Examples of spaces with discontinuous pressure are presented below.

(i) **The Scott-Vogelius Pair.**
This pair is given by $P_k/P_{k-1}^{\text{disc}}$, $k \geq 2$. It has the property of being weakly divergence-free, i.e.,

$$\nabla \cdot V^h = \nabla \cdot P_k = P_{k-1}^{\text{disc}} = Q^h.$$

It is shown in Example 3.73. from [13] that the Scott-Vogelius finite element does not generally satisfy the discrete inf-sup condition (3.17). However, it can be proved that it satisfies the discrete inf-sup condition (3.17) on special meshes.
In two dimensions, it is proved in [23] that the discrete inf-sup condition (3.17) is fulfilled for $k \geq 4$ if there is no singular vertex in the mesh. A vertex is singular if the edges that meet at the vertex fall onto two straight lines. For this purpose, barycentric-refined grids are used, where from an admissible triangular mesh, new edges are introduced by connecting all the vertices of the mesh cell with its barycenter (an example is Fig. 3.9. from [13]). A proof for the fulfilment of the discrete inf-sup condition (3.17) for $P_k/P_{k-1}^{\text{disc}}$

with $k \in \{2, 3\}$ on barycentric-refined meshes can be found in [12].
In three dimensions, it is proved in [22] that the condition is fulfilled for $k \geq 3$ on barycentric-refined meshes, where it avoids singular vertices and edges.

(ii) **The $P_2^{\text{bubble}}/P_1^{\text{disc}}$ and $P_3^{\text{bubble}}/P_2^{\text{disc}}$ Pairs.**
These pairs were proposed in [5] with the goal of obtaining an inf-sup stable pair of finite element spaces with a piecewise linear and discontinuous pressure on arbitrary simplicial grids by enriching the velocity space using bubble functions.
In two-dimensions, mesh cell bubble functions are added. For each triangular mesh cell, the cell bubble function is given by the product of the barycentric coordinates $\lambda_1\lambda_2\lambda_3$. In three dimensions, it is proposed in [5] that the space is enriched with all the mesh cell bubble functions and all the face bubble functions. For a mesh cell K with barycentric coordinates $\lambda_1, ..., \lambda_4$, the mesh cell bubble functions are in this case $\lambda_1\lambda_2\lambda_3\lambda_4$ and the four face bubble functions are the product of three mutually distinct barycentric coordinates.
In practice, one has to note that the bubble functions are higher order degree polynomials and require higher order quadrature rules. In [8] the choice $P_2^{\text{bubble}}/P_1^{\text{disc}}$ is considered to be optimal. An example of a higher order inf-sup stable pair by enrichment with bubble functions is $P_3^{\text{bubble}}/P_2^{\text{disc}}$ given in [5].

(iii) **The Bernardi-Raugel Element.**
The Bernandi-Raugel finite element of first order P_1^{BR}/P_0 is constructed by enriching the space $P_1(K)$ with vector-valued basis functions. Using the barycentric coordinates $\lambda_i,\ i = 1, ..., d+1$, face (or in two dimensions edge) bubble functions are defined by

$$\boldsymbol{v}_{\text{bub},i}^h = \prod_{j=1, j\neq i}^{d+1} \lambda_j \boldsymbol{n}_i, \qquad i = 1, ..., d+1,$$

where $\boldsymbol{n}_i$ is the unit normal pointing outward on the face E_i, which is opposite to the vertex $\boldsymbol{a}_i$. The local finite element space is given by

$$P_1^{\text{BR}}(K) = P_1(K) \oplus \text{span}\left\{\boldsymbol{v}_{\text{bub},i}^h,\ i = 1, ..., d+1\right\}.$$

The degrees of freedom are the values at the vertices $\boldsymbol{v}^h(\boldsymbol{a_i}),\ i = 1, ..., d+1$, and the fluxes through the faces $\boldsymbol{v} \cdot \boldsymbol{n}_i,\ i = 1, ..., d+1$.
The combination of the basis functions and local functionals leads to continuous functions in the global velocity space (Remark 3.138. in [13]).
The proof of discrete inf-sup stability of the global space is based on the construction of the Fortin operator (presented in Lemma 3.78. of [13]). The properties of the Fortin operator are proved in Lemma II.4 of [3].
According to [3], the construction of the velocity space and the proof of the inf-sup condition can be extended to regular families of triangulations made of quadrilaterals. Similarly, in three-dimensions, the Bernardi-Raugel element of order two $P_2^{\text{BR}}/P_1^{\text{disc}}$ is defined (details in Remark 3.140 of [13]).

4. **Spaces on Quadrilateral and Hexahedral Meshes with Discontinuous Pressure.**
The most common pairs of spaces of this type are $Q_k/P_{k-1}^{\text{disc}}$ with $k \geq 2$. In Example 3.71. of [13] it is shown that the pair of spaces $Q_1/P_0 = Q_1/Q_0$ is in general not inf-sup stable. For $k \geq 2$ there are two types of $Q_k/P_{k-1}^{\text{disc}}$ spaces - mapped and unmapped.
For the unmapped type, the local space Q_k is defined by a mapping from a reference cell $\hat{K}$ while the space $P_{k-1}^{\text{disc}}(K)$ is defined on the mesh cell K. The mapped type is defined entirely with the reference transformation. This transformation from a quadrilateral or hexahedral reference cell is in general a bilinear or trilinear mapping. Therefore, it gives rise to mesh cells with curved boundaries (Remark 3.141. from [13]) and, in general, does not preserve the type of mapped functions, i.e., the images of polynomials are generally not polynomials. Hence, the mapped and unmapped pairs of spaces are in general different.
Proofs of the fulfilment of the discrete inf-sup condition (3.17) for the unmapped pairs of spaces $Q_k/P_{k-1}^{\text{disc}}$ in two dimensions can be found in the Chapter II, Theorem 3. of [7] and in case of the mapped pairs of spaces $Q_k/P_{k-1}^{\text{disc}}$ for d dimensions can be found in [18].

3.2.3 Error estimates for the Galerkin method

The derivation of error estimates for the above inf-sup stable pairs with the property that $\nabla \cdot V^h \not\subset Q^h$ requires the definition of the space of discretely divergence-free functions V^h_{div} below

$$V^h_{\text{div}} = \{\boldsymbol{v}^h \in V^h : \; b^h(\boldsymbol{v}^h, q^h) = 0, \quad \forall q^h \in Q^h\}, \tag{3.26}$$

which is the kernel of the discrete divergence operator (3.21). The functions of this space, as mentioned above, are not generally divergence-free (2.35) nor weakly divergence-free, i.e., $V^h_{\text{div}} \not\subset H_{\text{div}}$ and $V^h_{\text{div}} \not\subset V_{\text{div}}$. Nevertheless, they can be used as test functions both in the continuous problem (3.13)-(3.14) and the finite element problem (3.15)-(3.16) as $V^h_{\text{div}} \subset V^h \subset V$ holds.

Error estimate for the gradient of velocity. (based on Sect. 3 [14] and Ch. 4.2 [13])
By choosing such test functions, $q^h = 0$ and taking the difference, the following relation is obtained

$$a(\boldsymbol{u} - \boldsymbol{u}^h, \boldsymbol{v}^h) + b(\boldsymbol{v}^h, p - p^h) = 0 \quad \forall \boldsymbol{v}^h \in V^h_{\text{div}}. \tag{3.27}$$

Because of the local divergence-free property $b(\boldsymbol{v}^h, p^h) = 0$ and the error equation reduces to

$$a(\boldsymbol{u} - \boldsymbol{u}^h, \boldsymbol{v}^h) + b(\boldsymbol{v}^h, p) = 0 \quad \forall \boldsymbol{v}^h \in V^h_{\text{div}}.$$

But since globally, the test function isn't divergence-free, the dependence on pressure cannot be removed from the error estimate for velocity. To bring (3.27) to a more suggestive form, a term $b(\boldsymbol{v}^h, q^h) = 0$ for arbitrary $q^h \in Q^h$ is added on the left-hand side. Moreover, the following decomposition for the error is substituted in (3.27)

$$\boldsymbol{u} - \boldsymbol{u}^h = (\boldsymbol{u} - \tilde{\boldsymbol{u}}^h) - (\boldsymbol{u}^h - \tilde{\boldsymbol{u}}^h) =: \boldsymbol{\eta} - \boldsymbol{\phi}^h, \quad \text{for arbitrary } \tilde{\boldsymbol{u}}^h \in V^h_{\text{div}},$$

alongside with choosing $\boldsymbol{v}^h = \boldsymbol{\phi}^h$. These changes lead to the expression

$$\nu ||\nabla \boldsymbol{\phi}^h||^2_{L^2(\Omega)} = \nu(\nabla \boldsymbol{\eta}, \nabla \boldsymbol{\phi}^h) - (\nabla \cdot \boldsymbol{\phi}^h, p - q^h), \quad \forall q^h \in Q^h. \tag{3.28}$$

Applying the Cauchy-Schwarz inequality to the first term on the right-hand side, yields

$$|(\nabla \boldsymbol{\eta}, \nabla \boldsymbol{\phi}^h)| \leq ||\nabla \boldsymbol{\eta}||_{L^2(\Omega)} ||\nabla \boldsymbol{\phi}^h||_{L^2(\Omega)}.$$

Similarly, applying the Cauchy-Schwarz inequality to the second term on the right-hand side, together with the estimate $||\nabla \cdot \boldsymbol{\phi}^h||_{L^2(\Omega)} \leq ||\nabla \boldsymbol{\phi}^h||_{L^2(\Omega)}$ (Lemma 3.179 in [13]), gives

$$\begin{aligned} |-(\nabla \cdot \boldsymbol{\phi}^h, p - q^h)| &\leq ||p - q^h||_{L^2(\Omega)} ||\nabla \cdot \boldsymbol{\phi}^h||_{L^2(\Omega)} \\ &\leq ||p - q^h||_{L^2(\Omega)} ||\nabla \boldsymbol{\phi}^h||_{L^2(\Omega)}. \end{aligned}$$

By further using the two inequalities above in equation (3.28) and dividing it by $\nu ||\nabla \boldsymbol{\phi}^h||_{L^2(\Omega)} \neq 0$ the relation below is obtained

$$||\nabla \boldsymbol{\phi}^h||_{L^2(\Omega)} \leq ||\nabla \boldsymbol{\eta}||_{L^2(\Omega)} - \nu^{-1} ||p - q^h||_{L^2(\Omega)}, \quad \forall q^h \in Q^h.$$

For the case $||\nabla \boldsymbol{\phi}^h||_{L^2(\Omega)} = 0$, the relation trivially holds, and the case $\nu = 0$ is excluded since it is not physically relevant. Ultimately, combining it with the triangle inequality of the gradient of the error decomposition, gives

$$\begin{aligned} ||\nabla(\boldsymbol{u} - \boldsymbol{u}^h)||_{L^2(\Omega)} &\leq ||\nabla \boldsymbol{\phi}^h||_{L^2(\Omega)} + ||\nabla \boldsymbol{\eta}||_{L^2(\Omega)} \\ &\leq 2||\nabla \boldsymbol{\phi}^h||_{L^2(\Omega)} + \nu^{-1} ||p - q^h||_{L^2(\Omega)}. \end{aligned}$$

The resulting estimate in terms of the best approximation errors is then given by

$$||\nabla(\boldsymbol{u} - \boldsymbol{u}^h)||_{L^2(\Omega)} \leq 2 \inf_{\tilde{\boldsymbol{u}}^h \in V^h_{\text{div}}} ||\nabla(\boldsymbol{u} - \tilde{\boldsymbol{u}}^h)||_{L^2(\Omega)} + \nu^{-1} \inf_{q^h \in Q^h} ||p - q^h||_{L^2(\Omega)}. \tag{3.29}$$

■

Error estimate for the divergence of velocity. (based on Sect.3 [14] and Ch. 4.2 [13])
The error in the divergence is bounded by the same estimate (3.29), since from Lemma 3.179 [13]

$$||\nabla \cdot \boldsymbol{v}||_{L^2(\Omega)} \leq ||\nabla \boldsymbol{v}||_{L^2(\Omega)} \quad \forall \boldsymbol{v} \in H^1_0(\Omega), \tag{3.30}$$

so it holds that

$$||\nabla \cdot (\boldsymbol{u} - \boldsymbol{u}^h)||_{L^2(\Omega)} \leq ||\nabla(\boldsymbol{u} - \boldsymbol{u}^h)||_{L^2(\Omega)}.$$

Moreover, since $\nabla \cdot \boldsymbol{u} = 0$, $||\nabla \cdot (\boldsymbol{u} - \boldsymbol{u}^h)||_{L^2(\Omega)} = ||\nabla \cdot \boldsymbol{u}^h||_{L^2(\Omega)}$ and the divergence error estimate can be written as

$$||\nabla \cdot \boldsymbol{u}^h||_{L^2(\Omega)} \leq 2 \inf_{\tilde{\boldsymbol{u}}^h \in V^h_{\text{div}}} ||\nabla(\boldsymbol{u} - \tilde{\boldsymbol{u}}^h)||_{L^2(\Omega)} + \nu^{-1} \inf_{q^h \in Q^h} ||p - q^h||_{L^2(\Omega)}. \tag{3.31}$$

■

Using the estimate (3.29) together with similar tools to the ones used in its derivation above, errors in terms of the best approximations can be derived for pressure and velocity. In case of the former, the inf-sup condition is also used and in case of the latter — a formulation of a dual problem introduced in (3.33). Here only the results are presented, with a reference to proofs of Theorems 4.25 and 4.28 in [13] for the full derivation.

Error estimate for pressure. (Theorem 4.25 in [13])

$$||p - p^h||_{L^2(\Omega)} \leq \frac{2\nu}{\beta} \inf_{\boldsymbol{v}^h \in V^h_{\text{div}}} ||\nabla(\boldsymbol{u} - \boldsymbol{v}^h)||_{L^2(\Omega)} + \left(1 + \frac{2}{\beta}\right) \inf_{q^h \in Q^h} ||p - q^h||_{L^2(\Omega)} \tag{3.32}$$

□

Error estimate for velocity. (Theorem 4.28 in [13])
Let $(\boldsymbol{\phi}_{\hat{\boldsymbol{f}}}, \xi_{\hat{\boldsymbol{f}}})$ be the solution of the dual Stokes problem for a velocity in V_{div}: For a given $\hat{\boldsymbol{f}} \in L^2(\Omega)$, find $(\boldsymbol{\phi}_{\hat{\boldsymbol{f}}}, \xi_{\hat{\boldsymbol{f}}}) \in V \times Q$ such that

$$\begin{aligned} -\nu \Delta \boldsymbol{\phi}_{\hat{\boldsymbol{f}}} - \nabla \xi_{\hat{\boldsymbol{f}}} &= \hat{\boldsymbol{f}} \quad \text{in } \Omega, \\ \nabla \cdot \boldsymbol{\phi}_{\hat{\boldsymbol{f}}} &= 0 \quad \text{in } \Omega. \end{aligned} \tag{3.33}$$

Then the following error estimate for velocity holds

$$\begin{aligned} ||\boldsymbol{u} - \boldsymbol{u}^h||_{L^2(\Omega)} \leq &\left(||\nabla(\boldsymbol{u} - \boldsymbol{u}^h)||_{L^2(\Omega)} + \nu^{-1} \inf_{q^h \in Q^h} ||p - q^h||_{L^2(\Omega)} \right) \\ &\times \sup_{\hat{\boldsymbol{f}} \in L^2(\Omega) \setminus \{\boldsymbol{0}\}} \frac{1}{||\hat{\boldsymbol{f}}||_{L^2(\Omega)}} \left[\inf_{\boldsymbol{\phi}^h \in V^h_{\text{div}}} ||\nabla(\boldsymbol{\phi}_{\hat{\boldsymbol{f}}} - \boldsymbol{\phi}^h)||_{L^2(\Omega)} + \inf_{r^h \in Q^h} ||\xi_{\hat{\boldsymbol{f}}} - r^h||_{L^2(\Omega)} \right]. \end{aligned} \tag{3.34}$$

□

Using interpolation errors to estimate the best approximation errors, the expressions (3.29)-(3.32) and (3.34) can be transformed to include convergence orders. The results are presented below.

Error expressions with interpolation estimates.(Corollary 4.30 in [13])
Let $(\boldsymbol{u}, p)$ be the solution to the Stokes equations with $\boldsymbol{u} \in H^{k+1}(\Omega) \cap V$ and $p \in H^k(\Omega) \cap Q$. Then, the error estimates (3.35)-(3.38) hold for the following inf-sup stable pairs of finite element spaces

(i) The MINI element P_1^{bubble}/P_1;

(ii) The Taylor-Hood element P_k/P_{k-1}, $k \geq 2$;

(iii) The elements $P_2^{\text{bubble}}/P_1^{\text{disc}}$, $P_3^{\text{bubble}}/P_2^{\text{disc}}$, $P_2^{\text{BR}}/P_1^{\text{disc}}$ and $Q_k/P_{k-1}^{\text{disc}}$ for $k \leq 2$.

$$||\nabla(\boldsymbol{u} - \boldsymbol{u}^h)||_{L^2(\Omega)} \leq Ch^k(||\boldsymbol{u}||_{H^{k+1}(\Omega)} + \nu^{-1}||p||_{H^k(\Omega)}), \tag{3.35}$$

$$||\nabla \cdot \boldsymbol{u}^h||_{L^2(\Omega)} \leq Ch^k(||\boldsymbol{u}||_{H^{k+1}(\Omega)} + \nu^{-1}||p||_{H^k(\Omega)}), \tag{3.36}$$

$$||p - p^h||_{L^2(\Omega)} \leq Ch^k(\nu||\boldsymbol{u}||_{H^{k+1}(\Omega)} + ||p||_{H^k(\Omega)}), \tag{3.37}$$

$$||\boldsymbol{u} - \boldsymbol{u}^h||_{L^2(\Omega)} \leq Ch^{k+1}(||\boldsymbol{u}||_{H^{k+1}(\Omega)} + \nu^{-1}||p||_{H^k(\Omega)}), \tag{3.38}$$

with the constant C being dependent on the inverse of the inf-sup constant β.
The estimate (3.38) requires in addition a regular solution to the Stokes dual problem (3.33). The meaning of regular in this context is defined in Remark 4.27 of [13], but for the purpose of this work it will be assumed given, as the two-dimensional domain from the numerical studies in Ch.

4 is bounded, convex and polyhedral. □

The error estimates (3.35), (3.36) and (3.38) show a scaling of the velocity errors with pressure and the inverse of viscosity. Therefore, in problems where the values of either pressure and/or viscosity are much larger than velocity, the second term in the error estimate dominates and the value of obtained velocity scales the same way as pressure and/or inversely proportional to viscosity. This phenomenon is identified as lack of pressure robustness and is closely linked to the fact that the functions in the finite element space are not weakly divergence-free $V^h \not\subset V_{\text{div}}$, i.e., conservation of mass is not ensured. If this were not the case, i.e., if $V^h \subset V_{\text{div}}$, the second term on the right hand-side in (3.28) would vanish and the error estimate (3.29) would not contain the best approximation of the pressure. As a result, the best approximation of pressure would have not been inherited by expressions (3.35), (3.36) and (3.38), so the velocity errors would not contain the pressure term, making the method pressure robust.

3.3 Techniques for reducing the violation of mass conservation

The presentation in this section is based on Chapter 4.6 from [13].

1. **The Grad-Div Stabilization**
   This method consists in adding a penalty term with user-chosen parameters. These parameters depend on the mesh size and on the problem at hand, and they have to be carefully chosen to yield the optimal order of convergence. Based on the weak form of the Stokes problem (3.13) and (3.14) with $g = 0$, the grad-div stabilization method in case of conforming finite element spaces is: Find $(\boldsymbol{u}^h, p^h) \in V^h \times Q^h$ such that

$$\begin{aligned} \nu(\nabla \boldsymbol{u}^h, \nabla \boldsymbol{v}^h) - (\nabla \cdot \boldsymbol{v}^h, p^h) + \sum_{K \in \mathcal{T}^h} \mu_K (\nabla \cdot \boldsymbol{u}^h, \nabla \cdot \boldsymbol{v}^h)_K &= (\boldsymbol{f}, \boldsymbol{v}^h) \quad \forall \boldsymbol{v}^h \in V^h, \\ -(\nabla \cdot \boldsymbol{u}^h, p^h) &= 0 \quad \forall q^h \in Q^h, \end{aligned} \tag{3.39}$$

   with the stabilization parameters $\{\mu_K\}$, $\mu_K \geq 0$.
   The bilinear form $a^h(\cdot, \cdot)$ is defined in the expression below

$$a^h(\boldsymbol{u}^h, \boldsymbol{v}^h) = \nu(\nabla \cdot \boldsymbol{u}^h, \nabla \cdot \boldsymbol{v}^h) + \sum_{K \in \mathcal{T}^h} \mu_K (\nabla \cdot \boldsymbol{u}^h, \nabla \cdot \boldsymbol{v}^h)_K \quad \forall \boldsymbol{u}^h, \boldsymbol{v}^h \in V^h.$$

   Since the first term is symmetric and positive definite and the second is symmetric and positive semi-definite, the bilinear form $a^h(\cdot, \cdot)$ is $V^h -$ elliptic and, in particular, $V^h_{\text{div}} -$ elliptic. So, the existence and uniqueness of a solution for pairs of the finite element spaces that satisfy the discrete inf-sup condition (3.17) is ensured. In practice, a good choice of stabilization parameters is determined by optimal error estimates with respect to some norm. Ultimately, the dependence of the error bound (3.41) on the parameter μ is determined by whether the sequence of divergence-free subspaces of the velocity space has the so-called optimal approximation property (3.40) defined below.

   Optimal Approximation Property of a Sequence of Divergence-free Subspaces.
   Let us consider a quasi-uniform family of triangulations $\{\mathcal{T}^h\}_{h>0}$ with characteristic mesh size h. If for all $\boldsymbol{v} \in V_{\text{div}} \cap H^{k+1}(\Omega)$ there exists a sequence $\{\boldsymbol{v}^h\} \in V^h_{\text{div,div}}$, where $V^h_{\text{div,div}} = V_{\text{div}} \cap V^h_{\text{div}}$, with

$$||\nabla(\boldsymbol{v} - \boldsymbol{v}^h)||_{L^2(\Omega)} \leq C_{\text{div}} h^k ||\boldsymbol{v}||_{H^{k+1}(\Omega)} \tag{3.40}$$

   and C_{div} independent of h, then the sequence of spaces $V^h_{\text{div,div}}$ possesses the optimal approximation property with respect to the space V_{div}. □

   The pair of inf-sup stable finite element spaces and the triangulation of the domain influence whether the optimal approximation property holds. Special cases exist such as Taylor-Hood

pairs of spaces P_k/P_{k-1} with $k \geq d$ on barycentric-refined simplicial grids or the MINI element on Union Jack grids. In the general case, however, sequences with such a property are not expected to exist.

Finite Element Error Estimate for the $L^2(\Omega)$ Norm of the Gradient of Velocity
Given the assumptions of the Theorem 4.21 from [13], let $(\boldsymbol{u}, p)$ be the solution of (3.13)-(3.14) and let $(\boldsymbol{u}^h, p^h)$ be the solution of (3.39). Then, the error in the $L^2(\Omega)$ norm of the gradient of velocity is bounded by

$$\begin{aligned} ||\nabla(\boldsymbol{u} - \boldsymbol{u}^h)||^2_{L^2(\Omega)} \leq \inf_{\boldsymbol{v}^h \in V^h_{\text{div}}} \left(4||\nabla(\boldsymbol{u} - \boldsymbol{v}^h)||^2_{L^2(\Omega)} + 2\frac{\mu}{\nu}||\nabla \cdot \boldsymbol{v}^h||^2_{L^2(\Omega)}\right) \\ + \frac{2}{\mu\nu} \inf_{q^h \in Q^h} ||p - q^h||^2_{L^2(\Omega)}. \end{aligned} \tag{3.41}$$

The proof can be found in [13] on pages 222 and 223. □

When determining the error bounds in cases of Taylor-Hood pairs or the MINI element, a-priori estimates of (3.41) can be computed for cases in which $\{V^h_{\text{div,div}}\}$ possesses the optimal approximation property or not (the estimates and the proofs can be found in Corollaries 4.124 and 4.126 from [13]). By choosing the optimal parameters in all cases (Remarks 4.125 and 4.127 in [13]), one can see to what extent the violation of conservation of mass is reduced using this technique. Overall, in comparison to the Galerkin discretization, the impact of the inverse of the viscosity and of the pressure on the error bounds is reduced. Nevertheless, it does not remove these problems nor lead to weakly divergence-free discrete solutions. Still, it is a popular stabilization method for incompressible flow problems due to its simplicity.

2. **Choosing Appropriate Test Functions**
The goal of this technique is to obtain a finite element velocity error estimate $||\boldsymbol{u} - \boldsymbol{u}^h||_{V^h}$ that is independent of pressure and viscosity. i.e., achieve pressure robustness. In that context, the analysis of the Stokes equations for the Crouzeix-Raviart finite element P_1^{nc}/P_0 will be discussed.

Error Estimate for the V^h Norm of the Velocity.
Let $\Omega \subset \mathrm{R}^d$, $d \in \{2, 3\}$, be a bounded domain with polyhedral and Lipschitz continuous boundary and let $(\boldsymbol{u}, p)$ be a unique and sufficiently smooth solution of the Stokes problem. Consider a quasi-uniform family of triangulations and let $(\boldsymbol{u}^h, p^h) \in P_1^{nc} \times P_0$ be the unique solution of the Stokes finite element problem, then the following error estimate holds

$$||\boldsymbol{u} - \boldsymbol{u}^h||_{V^h} \leq Ch(|\boldsymbol{u}|_{H^2(\Omega)} + ||\nabla p||_{L^2(\Omega)}), \tag{3.42}$$

with the constant Ω depending on the regularity of the family of triangulations.
Proof.
The expression (3.42) is found by substituting the Best Approximation Error Estimate for V^h_{div} (Lemma 4.53, page 167 in [13])

$$\inf_{\boldsymbol{v}^h \in V^h_{\text{div}}} ||\boldsymbol{u} - \boldsymbol{v}^h|| \leq Ch|\boldsymbol{u}|_{H^2(\Omega)}, \tag{3.43}$$

and the Consistency Error Estimate (Lemma 4.55, page 168 in [13])

$$|a^h(\boldsymbol{u}, \boldsymbol{v}) - (\boldsymbol{f}, \boldsymbol{v})| \leq Ch(|\boldsymbol{u}|_{H^2(\Omega)} + ||\nabla p||_{L^2(\Omega)})||\boldsymbol{v}||_{V^h}, \tag{3.44}$$

in the Abstract Error Estimate or Second Lemma of Strang (Lemma 4.51, page 167 in [13])

$$||\boldsymbol{u} - \boldsymbol{u}^h||_{V^h} \leq 2 \inf_{\boldsymbol{v}^h \in V^h_{\text{div}}} ||\boldsymbol{u} - \boldsymbol{v}^h||_{V^h} + \inf_{\boldsymbol{v}^h \in V^h_{\text{div}}, ||\boldsymbol{v}^h||_{V^h}=1} |a^h(\boldsymbol{u}, \boldsymbol{v}^h) - (\boldsymbol{f}, \boldsymbol{v}^h)|. \tag{3.45}$$

■

Upon a detailed inspection of the proof of the Consistency Error Estimate (Lemma 4.55, page 168 in [13]), one can see that the pressure term does not vanish because a term coming from $(\boldsymbol{f}, \boldsymbol{v})_K$ does not become zero for functions $\boldsymbol{v} \in V^h_{div}$. If the function $\boldsymbol{v}$ is chosen from

an appropriate space, this term vanishes and a pressure robust method is obtained. In particular, $\boldsymbol{v} \in V_{\text{div}} \oplus V^h_{\text{Hdiv}}$, where V^h_{Hdiv} is the appropriate space, a subspace of $H_{div}(\Omega)$, and moreover a subspace of $H(\text{div}, \Omega)$. In the first presentation of the method in the literature [1], it was proposed to use on the right-hand side of the Stokes equations a test function from the Raviart-Thomas space of the lowest order RT_0, which is an appropriate projection of the Crouzeix-Raviart test function. The following modified problem is therefore obtained:

The modified problem.
Find $(\boldsymbol{u}^h, p^h) \in V^h \times Q^h = P_1^{nc} \times P_0$ such that

$$\begin{aligned} \nu a^h(\boldsymbol{u}^h, \boldsymbol{v}^h) + b^h(\boldsymbol{v}^h, p^h) &= (\boldsymbol{f}, P_{E,RT_0}\boldsymbol{v}^h), \quad \forall \boldsymbol{v}^h \in V^h, \\ b^h(\boldsymbol{u}^h, q^h) &= 0, \quad \forall q^h \in Q^h, \end{aligned} \tag{3.46}$$

with the bilinear forms

$$a^h(\boldsymbol{u}^h, \boldsymbol{w}^h) = \sum_{K \in \mathcal{T}^h} (\nabla \boldsymbol{v}^h, \nabla \boldsymbol{w}^h)_K \text{ and } b^h(\boldsymbol{v}^h, q^h) = -\sum_{K \in \mathcal{T}^h} (\nabla \cdot \boldsymbol{v}^h, q^h)_K,$$

and the interpolation operator given by $P^h_{E,RT_0} : V \cup V^h \to RT_0$,

$$(P^h_{E,RT_0}\boldsymbol{v} \cdot \boldsymbol{n}_E)(\boldsymbol{m}_E) = \begin{cases} \frac{1}{|E|}\int_E \boldsymbol{v} \cdot \boldsymbol{n}_E d\boldsymbol{s}, & \text{if } E \in \mathcal{E}^h, \\ 0, & \text{if } E \in \overline{\mathcal{E}}^h \backslash \mathcal{E}^h, \end{cases}$$

with constant values for the normal component on each face E. □

Indeed, the analysis of the modified problem yields a consistency error estimate (3.47) with no terms involving pressure, which then leads to a velocity error estimate (3.48) with the same property.

Lemma: Consistency Error Estimate in Case of the Modified Problem.
Let $(\boldsymbol{u}, p)$ be a sufficiently smooth solution of the Stokes equations with $\boldsymbol{u} \in C^1(\overline{\Omega}) \cap V$, $p \in C(\overline{\Omega}) \cap Q$. Consider a family of quasi-uniform triangulations, then it holds for all $\boldsymbol{v} \in V_{\text{div}} \oplus V^h_{\text{div}}$

$$|\nu a^h(\boldsymbol{u}, \boldsymbol{v}) - (\boldsymbol{f}, P^h_{E,RT_0}\boldsymbol{v})| \leq C\nu h |\boldsymbol{u}|_{H^2(\Omega)} ||\boldsymbol{v}||_{V^h}. \tag{3.47}$$

The proof can be found in [13] at Lemma 4.136, page 232. □

Theorem: Error Estimate for the V^h Norm of the Velocity in Case of the Modified Problem.
Assuming the domain Ω and the pair $(\boldsymbol{u}, p)$ defined for the estimate (3.42), consider a quasi-uniform family of triangulations and let $(\boldsymbol{u}^h, p^h) \in P_1^{nc} \times P_0$ be the unique solution of the finite element problem (3.46) with modified test function on the right-hand side. Then the following error estimate is valid

$$||\boldsymbol{u} - \boldsymbol{u}^h||_{V^h} \leq Ch|\boldsymbol{u}|_{H^2(\Omega)}. \tag{3.48}$$

Proof.
By inserting the best approximation error estimate (3.43) and the consistency error estimate of the modified problem (3.47) into the abstract error estimate (2nd Lemma of Strang) (3.45), one obtains the expression (3.48). ■

It must be noted that the velocity solution $\boldsymbol{u}^h$ of (3.46) is not divergence free in the sense of $H_{\text{div}(\Omega)}$ since it is a function from V^h_{div}. It becomes so only after applying as post-processing the operator P^H_{E,RT_0} (for details, see (4.175) in [13]).

3. Constructing Divergence-Free and Inf-Sup Stable Pairs of Finite Element Spaces

In this section, approaches for constructing pairs of finite elements that satisfy the inf-sup

condition, and lead to weakly divergence-free velocities, i.e., $||\nabla \cdot \boldsymbol{u}^h||_{L^2(\Omega)} = 0$, are presented. The latter property is achieved if $\nabla \cdot V^h \subset Q^h$ holds. Namely, by taking the test function $q^h = \nabla \cdot \boldsymbol{u}^h$ in the discrete continuity equation one can obtain

$$(\nabla \cdot \boldsymbol{u}^h, \nabla \cdot \boldsymbol{u}^h) = ||\nabla \cdot \boldsymbol{u}^h||^2_{L^2(\Omega)} = 0.$$

□

The Smooth de Rham Complex or Stokes Complex in Two Dimensions.
A de Rham complex is a sequence of mappings and the one needed for the Stokes problem is called the smooth de Rham complex and is given by

$$\mathrm{R} \to H^2(\Omega) \xrightarrow{\mathbf{curl}} H^1(\Omega) \xrightarrow{\mathrm{div}} L^2(\Omega) \to 0. \tag{3.49}$$

A de Rham complex is called to be exact if the range of each operator is the kernel of the succeeding operator. The exactness of the de Rham complex (3.49) implies:

(i) If $w \in H^2(\Omega)$ is curl-free, then w is a constant function;

(ii) If $\boldsymbol{v} \in H^1(\Omega)$ is divergence-free then, $\boldsymbol{v} = \mathbf{curl}\ w$ for some $w \in H^2(\Omega)$;

(iii) The map div : $H^1(\Omega) \to L^2(\Omega)$ is surjective, since the kernel of the last operator is $L^2(\Omega)$.

It can be shown that the smooth de Rham complex (3.49) is exact on bounded, simply connected domains $\Omega \subset \mathrm{R}^2$ with Lipschitz boundary. □

A Finite Element Subcomplex.
A finite element subcomplex of (3.49) with finite element spaces $W^h \subset H^2(\Omega)$, $V^h \subset H^1(\Omega)$, and $Q^h \subset L^2(\Omega)$ is given by

$$\mathrm{R} \to H^2(\Omega) \xrightarrow{\mathbf{curl}} V^h(\Omega) \xrightarrow{\mathrm{div}} Q^h(\Omega) \to 0. \tag{3.50}$$

If the finite element subcomplex (3.50) is exact, it implies the following properties:

(i) The pair of finite element spaces V^h/Q^h satisfies the discrete inf-sup condition (3.18) given that the mapping div has a right inverse that is bounded independently of the mesh width;

(ii) Computations with the finite element spaces V^h/Q^h give weakly divergence-free velocity fields, since it holds that div $V^h = Q^h$.

□

An example of such a sub-complex of finite elements is the Scott-Vogelius SV_k family. For instance, the pair in two dimensions P_2/P_1^{disc} satisfies the inf-sup condition on special grids like the barycentric-refined grids (Example 4.144 in [13]). Other pairs of spaces for the Stokes equations can be constructed with different $H^2(\Omega)$ conforming finite element spaces. However, they are of little importance in practice since they involve high order polynomial degrees of basis functions or degrees of freedom that aren't convenient to implement.

Weakly Divergence-free Velocity Solutions with Lower Order Spaces.
It turns out that there are no lower order pairs of conforming spaces that can be used in practice, so the conformity of the finite element velocity space has to be abandoned, i.e. $V^h \not\subset H^1(\Omega)$. Since the desired property remains $||\nabla \cdot \boldsymbol{u}^h||_{L^2(\Omega)} = 0$, the divergence of the velocity space still has to be in $L^2(\Omega)$. The latter property is given for $V^h \subset H(\mathrm{div}, \Omega)$. The simplest choice of such a space on simplicial meshes is $V^h = RT_0$, the Raviart-Thomas space of the lowest order, which in combination with P_0 can be shown to satisfy a discrete inf-sup condition (Section 7.1.2. in [4]). However, the non-conformity of V^h requires a piecewise definition of the problem, which yields a large consistency error for RT_0/P_0 and the solutions do not converge. To achieve convergence, modifications of the method are required, which will be examined in Chapter 3.4. □

3.4 H(div)-Conforming Methods

This section introduces $H(\text{div})$-conforming spaces as inf-sup stable and divergence-free finite element spaces, which ensure properties like conservation of mass and pressure robustness for the approximated velocity solution, with the disadvantage of non-conformity to the H^1 space. The reasons and implications of these properties are here elaborated upon, and examples of such spaces are provided. Ultimately, error estimates are presented and discussed. The structure of this section follows closely the contents in section 4.4 of [14] and the proofs from chapters 1, 2, 6 in [21].

3.4.1 H(div)-conforming inf-sup stable pairs of spaces

The finite element method is defined on the triangulation $\mathcal{T}^h$ of the domain Ω, with $K \in \mathcal{T}^h$ being the set of mesh cells and $\mathcal{E}^h \in \partial K$ — the set of facets (edges in 2d and faces in 3d, for simplicity it will further be referred to the 2d case). The set of boundary and interior edges are denoted by $\mathcal{E}^h_B \in \mathcal{E}^h$, with the property that $\forall E \in \mathcal{E}^h_B,\ E \cap \partial\Omega \neq \emptyset$, and $\mathcal{E}^h_I := \mathcal{E}^h \backslash \mathcal{E}^h_B$, respectively.
The finite element spaces V^h and Q^h, discussed in this section, contain functions that are discontinuous across interior edges from the set $\mathcal{E}^h_I$. If two mesh cells K_1 and K_2 are neighbors and share one common side E, there are two traces of the function $\boldsymbol{v}^h \in V^h$ along E. Using the values from both sides, the average and a jump functions for $\boldsymbol{v}^h$ are defined, assuming that the normal vector to the edge $\boldsymbol{n}_E$ is oriented from K_1 to K_2:

$$\{\boldsymbol{v}^h\} = \frac{1}{2}(\boldsymbol{v}^h|_{K_1}) + \frac{1}{2}(\boldsymbol{v}^h|_{K_2}), \quad [\boldsymbol{v}^h] = (\boldsymbol{v}^h|_{K_1}) - (\boldsymbol{v}^h|_{K_2}) \quad \forall E = \partial K_1 \cap \partial K_2.$$

The extension of the definition above to the boundary edges $E \in \mathcal{E}^h_B$ is given by

$$\{\boldsymbol{v}^h\} = [\boldsymbol{v}^h] = (\boldsymbol{v}^h|_{K_1}) \quad \forall e = \partial K_1 \cap \mathcal{E}^h_B.$$

Lemma 3.66 of [13] presented below gives a criterion for ensuring that the finite element space is a subspace of $H(\text{div}, \Omega)$, namely that a function from a $H(\text{div}, \Omega)$ space is continuous with respect to its normal component across the interior edges $\mathcal{E}^h_I$.

Sufficient and Necessary Condition for a Finite Element Function to be in $H(\text{div}, \Omega)$. A finite element function $\boldsymbol{v}^h \in L^2(\Omega)$ belongs to $H(\text{div}, \Omega)$ (2.34), if and only if $\boldsymbol{v}^h \cdot \boldsymbol{n}_E$ is continuous across all edges $E \in \mathcal{E}^h_I$ of the triangulation.
Proof.
By definition, $\nabla \cdot \boldsymbol{v}^h \in L^2(\Omega)$ if and only if there exists a function $w \in L^2(\Omega)$ such that

$$-\int_\Omega \boldsymbol{v}^h(\boldsymbol{x}) \cdot \nabla\phi(\boldsymbol{x}) d\boldsymbol{x} = \int_\Omega w(\boldsymbol{x})\phi(\boldsymbol{x}) d\boldsymbol{x}, \quad \forall \phi \in C_0^\infty(\Omega). \tag{3.51}$$

Using integration by parts

$$\begin{aligned}
-\int_\Omega \boldsymbol{v}^h(\boldsymbol{x}) \cdot \nabla\phi(\boldsymbol{x}) d\boldsymbol{x} &= -\sum_{K\in\mathcal{T}^h} \int_K \boldsymbol{v}^h(\boldsymbol{x}) \cdot \nabla\phi(\boldsymbol{x}) d\boldsymbol{x} \\
&= \sum_{K\in\mathcal{T}^h} \left(\int_K \nabla \cdot \boldsymbol{v}^h(\boldsymbol{x})\phi(\boldsymbol{x}) d\boldsymbol{x} - \int_{\partial K} \phi(\boldsymbol{s}) \boldsymbol{v}^h(\boldsymbol{s}) \cdot \boldsymbol{n}_{\partial K} d\boldsymbol{s} \right) \\
&= \sum_{K\in\mathcal{T}^h} \int_K \nabla \cdot \boldsymbol{v}^h(\boldsymbol{x})\phi(\boldsymbol{x}) d\boldsymbol{x} - \sum_{K\in\mathcal{T}^h} \sum_{E\in\partial K} \int_E \phi(\boldsymbol{s}) \boldsymbol{v}^h(\boldsymbol{s}) \cdot \boldsymbol{n}_E d\boldsymbol{s} \\
&= \int_\Omega \nabla \cdot \boldsymbol{v}^h(\boldsymbol{x})\phi(\boldsymbol{x}) d\boldsymbol{x} - \sum_{E\in\mathcal{E}^h_I} \int_E \phi(\boldsymbol{s}) [\boldsymbol{v}^h \cdot \boldsymbol{n}_E]_E(\boldsymbol{s}) d\boldsymbol{s} \\
&\quad - \sum_{E\in\mathcal{E}^h_B} \int_E \phi(\boldsymbol{s}) \boldsymbol{v}^h(\boldsymbol{s}) \cdot \boldsymbol{n}_E d\boldsymbol{s}, \quad \forall \phi \in C_0^\infty(\Omega).
\end{aligned}$$

The last term vanishes since the test functions are zero on the boundary of Ω. Then, (3.51) is satisfied if and only if all the integrals on the interior edges vanish for all test functions. Therefore, the jumps $[\boldsymbol{v}^h \cdot \boldsymbol{n}_E]_E$ are zero, which is equivalent to the normal component of $\boldsymbol{v}^h$ being continuous

across all interior edges. ■

Examples of spaces that satisfy this condition and will be used in numerical studies are the Raviart-Thomas space of order $k \geq 0$

$$RT_k := \{\boldsymbol{v}^h \in H_0(\mathrm{div}, \Omega) : \ \boldsymbol{v}^h|_T \in RT_k(T), \quad \forall T \in \mathcal{T}^h\}, \tag{3.52}$$

where the local Raviart-Thomas space is defined as

$$RT_k(T) := \boldsymbol{P}_k(T) + \boldsymbol{x}P_k(T), \quad \forall T \in \mathcal{T}^h, \tag{3.53}$$

and the Brezzi-Douglas-Marini space of degree $k \geq 1$

$$BDM_k := \{\boldsymbol{v}^h \in H_0(\mathrm{div}, \Omega) : \ \boldsymbol{v}^h|_T \in \boldsymbol{P}_k(T), \quad \forall T \in \mathcal{T}^h\}. \tag{3.54}$$

Here, the following definition for $H_0(\mathrm{div}, \Omega)$ holds

$$H_0(\mathrm{div}, \Omega) = \{\boldsymbol{v}^h \in H(\mathrm{div}, \Omega) : \ \boldsymbol{v} \cdot \boldsymbol{n}|_{\partial\Omega} = 0\}.$$

These spaces form inf-sup stable pairs with the discontinuous piecewise polynomial spaces with vanishing mean — $Q^h = P_k^{disc}$ for $V^h = RT_k$ and $Q^h = P_{k-1}^{disc}$ for $V^h = BDM_k$, i.e., the condition (3.17) holds in the following form

$$\inf_{q^h \in Q^h \setminus \{0\}} \sup_{\boldsymbol{v}^h \in V^h \setminus \{\boldsymbol{0}\}} \frac{\int_\Omega (\nabla \cdot \boldsymbol{v}^h) q^h d\boldsymbol{x}}{||\boldsymbol{v}^h||_{H(\mathrm{div},\Omega)} ||q^h||_{L^2(\Omega)}} \geq \beta^h > 0. \tag{3.55}$$

From their definition it is clear that the relation $\nabla \cdot V^h \subseteq Q^h$ is satisfied, thus making the approximated solution globally divergence-free. So, in this case the discretely divergence-free functions are also weakly divergence-free, i.e., $V^h_{\mathrm{div}} \subset V_{\mathrm{div}}$.

However, these pairs of spaces cannot be used directly in the Stokes finite element problem (3.15)-(3.16) since the resulting system is not well-defined. The reason is that the spaces $V^h = BDM_k$ or RT_k are non-conforming, i.e., $V^h \not\subset V = H_0^1$ and the gradient of functions does not exist globally. Even if a piecewise gradient is defined, the method would not be consistent with the continuous Stokes problem (3.13)-(3.14), i.e., for $\boldsymbol{u} \in H^2(\Omega) \cap H_0^1(\Omega)$ and $\boldsymbol{v}^h \in V^h$

$$-\int_\Omega \Delta \boldsymbol{u} \cdot \boldsymbol{v}^h d\boldsymbol{x} \neq a(\boldsymbol{u}, \boldsymbol{v}^h),$$

and the solution would not converge. To fix these problems, two modifications can be made — either change the bilinear forms in (3.15)-(3.16) using techniques from discontinuous Galerkin (DG) methods or impose continuity of the tangential components in a weak sense. Here only the former method in 2d will be discussed and implemented, the latter being referred to pages 519-521 of [14] for further details.

3.4.2 DG formulation of the Stokes problem

Using interior-penalty methods of the discontinous Galerkin formulation, the bilinear form $a(\cdot, \cdot)$ in (3.15) is modified to ensure consistency with the Laplace operator.

Derivation of the DG bilinear form $a_\epsilon(\cdot, \cdot)$.(based on Section 4.4 in [14] and Chapter 1.2 of [21])
The first step consists in multiplying the Laplacian term from the continuous problem (2.15) by a test function from one of the above defined discontinuous finite element spaces $\boldsymbol{v}^h \in V^h \subset H_0(div, \Omega)$ and integrating over a mesh cell K. From the Green's theorem, it follows that $\forall \boldsymbol{v}^h \in V^h$

$$-\int_K \Delta \boldsymbol{u} \cdot \boldsymbol{v}^h d\boldsymbol{x} = \int_K \nabla \boldsymbol{u} : \nabla \boldsymbol{v}^h \ - \int_{\partial K} \nabla \boldsymbol{u} \boldsymbol{n}_K \cdot \boldsymbol{v}^h ds.$$

Further, by summing over all the mesh cells K in the triangulation $\mathcal{T}^h$ of the domain Ω the following expression is obtained

$$-\int_\Omega \Delta \boldsymbol{u} \cdot \boldsymbol{v}^h d\boldsymbol{x} = \int_\Omega \nabla_h \boldsymbol{u} : \nabla_h \boldsymbol{v}^h \ - \sum_{K \in \mathcal{T}^h} \int_{\partial K} \nabla \boldsymbol{u} \boldsymbol{n}_K \cdot \boldsymbol{v}^h ds,$$

where ∇_h is the piecewise gradient operator. The sum over the mesh cells K in the last term can be substituted with the sum over the line integrals along edges $E \in \mathcal{E}^h$ and the piecewise continuity of $\boldsymbol{v}^h$ requires a formulation involving the jump function

$$-\int_\Omega \Delta \boldsymbol{u} \cdot \boldsymbol{v}^h d\boldsymbol{x} = \int_\Omega \nabla_h \boldsymbol{u} : \nabla_h \boldsymbol{v}^h \; - \sum_{E \in \mathcal{E}^h} \int_E [\nabla \boldsymbol{u} \boldsymbol{n}_K \cdot \boldsymbol{v}^h] ds.$$

The following identity can be applied to the last term:

$$[\nabla \boldsymbol{u} \boldsymbol{n}_K \cdot \boldsymbol{v}^h] = \{\nabla \boldsymbol{u} \boldsymbol{n}_K\}[\boldsymbol{v}^h] + \{\boldsymbol{v}^h\}[\nabla \boldsymbol{u} \boldsymbol{n}_K].$$

Since $\boldsymbol{u}$ is twice continuously differentiable, the jump vanishes across all edges and the last term is zero. The resulting equality below can be used to construct a DG bilinear form for the finite element method, which is consistent with the Laplace operator:

$$-\int_\Omega \Delta \boldsymbol{u} \cdot \boldsymbol{v}^h d\boldsymbol{x} = \int_\Omega \nabla_h \boldsymbol{u} : \nabla_h \boldsymbol{v}^h \; - \sum_{E \in \mathcal{E}^h} \int_E \{\nabla \boldsymbol{u} \boldsymbol{n}_K\}[\boldsymbol{v}^h] ds \quad \forall \boldsymbol{v}^h \in V^h.$$

Such a bilinear form, while consistent, would lack the properties of symmetry and coercivity that the continuous equation possesses. To compensate for this lack, two trivial terms are added to the above relation that take advantage of the continuity of $\boldsymbol{u}$: a transposed expression of the second term to ensure symmetry and a so-called penalty term to ensure coercivity

$$\begin{aligned} a_\epsilon(\boldsymbol{u}, \boldsymbol{v}^h) :&= \int_\Omega \nabla_h \boldsymbol{u} : \nabla_h \boldsymbol{v}^h \; - \sum_{E \in \mathcal{E}^h} \int_E \{\nabla \boldsymbol{u} \boldsymbol{n}_E\}[\boldsymbol{v}^h] - \epsilon \sum_{E \in \mathcal{E}^h} \int_E \{\nabla \boldsymbol{v}^h \boldsymbol{n}_E\}[\boldsymbol{u}] ds + \sum_{E \in \mathcal{E}^h} \frac{\sigma}{h_E} \int_E [\boldsymbol{v}^h][\boldsymbol{u}] \\ &= -\int_\Omega \Delta \boldsymbol{u} \cdot \boldsymbol{v}^h d\boldsymbol{x} \qquad \forall \boldsymbol{v}^h \in V^h \subset H_0(\mathrm{div}, \Omega). \end{aligned} \tag{3.56}$$

The additional parameters serve to control the type of desired symmetry, $\epsilon = \{-1, 1, 0\}$ for an antisymmetric, symmetric or incomplete bilinear form, ensure coercivity of $a_\epsilon(\cdot, \cdot)$ (2.26), via an appropriate choice of σ and the scaling factor h_E is the diameter of the edge E. ■

Derivation of $b^h(\cdot, \cdot)$ for the DG case. (based on the contents in Chapter 6.3 from [21])
Using a similar procedure on the pressure term in the Stokes approximation of momentum equation from (2.15), an expression for the DG velocity-pressure bilinear form can be derived. To that end, the pressure term is multiplied by the test function $\boldsymbol{v}^h \in V^h \subset H_0(div, \Omega)$, then integrated over the mesh cell K and the Green's theorem is applied, resulting in

$$\int_K \nabla p \cdot \boldsymbol{v}^h = -\int_K p \nabla \cdot \boldsymbol{v}^h + \int_{\partial K} p \boldsymbol{v}^h \cdot \boldsymbol{n}_K.$$

Summing over all the mesh cells K, or equivalently over mesh edges $\mathcal{E}^h$, and expressing the discontinuous terms with the help of the jump function gives

$$\sum_{K \in \mathcal{T}^h} \int_K \nabla p \cdot \boldsymbol{v}^h = -\sum_{K \in \mathcal{T}^h} \int_K p \nabla \cdot \boldsymbol{v}^h + \sum_{E \in \mathcal{E}_B^h \cup \mathcal{E}_I^h} \int_E [p \boldsymbol{v}^h \cdot \boldsymbol{n}_E].$$

Next, the jump function in the last term can be rewritten using the identity below

$$[p \boldsymbol{v}^h \cdot \boldsymbol{n}_E] = [p]\{\boldsymbol{v}^h \cdot \boldsymbol{n}_E\} + \{p\}[\boldsymbol{v}^h \cdot \boldsymbol{n}_E].$$

The term $[\boldsymbol{v}^h \cdot \boldsymbol{n}_E]$ vanishes on the interior edges $\mathcal{E}_I^h$, because of the normal continuity of the functions in the $H(\mathrm{div}, \Omega)$ space and on the boundary edges $\mathcal{E}_B^h$, because the test functions are from the space $H_0(\mathrm{div}, \Omega)$ with the property $\boldsymbol{v}^h \cdot \boldsymbol{n}_E|_{\partial\Omega} = 0$. Moreover, the pressure solution to the Stokes equations is continuous, so $[p] = 0$, making the first term vanish as well.
As a result, the DG velocity-pressure bilinear form can be defined as follows

$$b_h(\boldsymbol{v}^h, p) := -\sum_{K \in \mathcal{T}^h} \int_K p \nabla \cdot \boldsymbol{v}^h = \sum_{K \in \mathcal{T}^h} \int_K \nabla p \cdot \boldsymbol{v}^h \quad \forall \boldsymbol{v}^h \in V^h \subset H_0(\mathrm{div}, \Omega). \tag{3.57}$$

■

The DG Stokes finite element problem.
The discontinuous Galerkin finite element method that approximates the solution to the Stokes problem is then formulated using (3.56) and (3.57) in the following way:
Find the pair $(\boldsymbol{u}^h, p^h) \in V^h \times Q^h$, where $V^h \subset H_0(\text{div}, \Omega)$ and Q^h is chosen such that the discrete inf-sup stability (3.17) is satisfied, that is the solution to the system

$$\nu a_\epsilon(\boldsymbol{u}^h, \boldsymbol{v}^h) + b_h(\boldsymbol{v}^h, p^h) = (\boldsymbol{f}, \boldsymbol{v}^h), \quad \forall \boldsymbol{v}^h \in V^h, \tag{3.58}$$

$$b_h(\boldsymbol{u}^h, q^h) = 0, \qquad \forall q^h \in Q^h. \tag{3.59}$$

□

As a result, the obtained finite element method is consistent with the continuous Stokes problem (3.13)-(3.14) and satisfies the requirement of inf-sup stability for well-posedness through the choice of pair of finite element spaces. The additional requirement of coercivity (2.26) of $a_\epsilon(\cdot,\cdot)$ is not automatically ensured, but depends on the choice of parameter σ for the symmetry type of $a_\epsilon(\cdot,\cdot)$, specified by the parameter $\epsilon = \{-1, 1, 0\}$.

Conditions for coercivity of the bilinear form $a_\epsilon(\cdot,\cdot)$. (based on Chapter 2.7 in [21])
Applying the definition (2.26) to the DG problem (3.58)-(3.59), the bilinear form $a_\epsilon(\cdot,\cdot)$ is coercive if there exists a positive constant $m > 0$, such that

$$m||\boldsymbol{v}^h||^2_{\mathcal{E}} \leq a_\epsilon(\boldsymbol{v}^h, \boldsymbol{v}^h), \quad \forall \boldsymbol{v}^h \in V^h \subset H_0(\text{div}, \Omega), \tag{3.60}$$

where the energy norm $||\cdot||_{\mathcal{E}}$ is defined in following expression with $\sigma > 0$

$$\begin{aligned} ||\boldsymbol{v}^h||^2_{\mathcal{E}} :&= \sum_{K\in\mathcal{T}^h} \int_K \nabla \boldsymbol{v}^h : \nabla \boldsymbol{v}^h + \sum_{E\in\mathcal{E}^h} \frac{\sigma}{h_E} \int_E [\boldsymbol{v}^h] \cdot [\boldsymbol{v}^h] \\ &= \sum_{K\in\mathcal{T}^h} ||\nabla \boldsymbol{v}^h||^2_{L^2(K)} + \sum_{E\in\mathcal{E}^h} \frac{\sigma}{h_E} ||[\boldsymbol{v}^h]||^2_{L^2(E)}. \end{aligned} \tag{3.61}$$

In what follows, values of σ for which (3.60) holds true will be determined for each symmetry type of $a_\epsilon(\cdot,\cdot)$.

(i) In the case of an antisymmetric bilinear form for $\epsilon = -1$, i.e., $a_{-1}(\boldsymbol{u}^h, \boldsymbol{v}^h) = -a_{-1}(\boldsymbol{v}^h, \boldsymbol{u}^h)$, the bilinear form becomes

$$a_{-1}(\boldsymbol{v}^h, \boldsymbol{v}^h) := \int_\Omega \nabla_h \boldsymbol{v}^h : \nabla_h \boldsymbol{v}^h \; - \sum_{E\in\mathcal{E}^h} \int_E \{\nabla \boldsymbol{v}^h \boldsymbol{n}_E\}[\boldsymbol{v}^h] + \{\nabla \boldsymbol{v}^h \boldsymbol{n}_E\}[\boldsymbol{v}^h] ds + \sum_{E\in\mathcal{E}^h} \frac{\sigma}{h_E} \int_E [\boldsymbol{v}^h][\boldsymbol{v}^h].$$

The two middle terms vanish and the coercivity property (3.60) holds for $m = 1$, namely,

$$||\boldsymbol{v}^h||^2_{\mathcal{E}} = a_{-1}(\boldsymbol{v}^h, \boldsymbol{v}^h) \quad \forall \boldsymbol{v}^h \in V^h \subset H_0(\text{div}, \Omega). \tag{3.62}$$

(ii) The case of the symmetric bilinear form with $\epsilon = 1$, i.e., $a_1(\boldsymbol{u}^h, \boldsymbol{v}^h) = a_1(\boldsymbol{v}^h, \boldsymbol{u}^h)$, or the incomplete bilinear form a_0 with $\epsilon = 0$:
Using Cauchy-Schwarz's inequality, an upper bound of the term $\sum_{E\in\mathcal{E}^h} \int_E \{\nabla \boldsymbol{v}^h \boldsymbol{n}_E\} \cdot [\boldsymbol{v}^h]$ can be found:

$$\begin{aligned} \sum_{E\in\mathcal{E}^h} \int_E \{\nabla \boldsymbol{v}^h \boldsymbol{n}_E\}\, [\boldsymbol{v}^h] &\leq \sum_{E\in\mathcal{E}^h} ||\{\nabla \boldsymbol{v}^h \boldsymbol{n}_E\}||_{L^2(E)} ||[\boldsymbol{v}^h]||_{L^2(E)} \\ &\leq \sum_{E\in\mathcal{E}^h} ||\{\nabla \boldsymbol{v}^h \boldsymbol{n}_E\}||_{L^2(E)}\; ||[\boldsymbol{v}^h]||_{L^2(E)} \left(\frac{1}{{h_E}^{\beta_0}}\right)^{1/2-1/2}. \end{aligned} \tag{3.63}$$

For an interior edge E shared by two mesh cells K_1 and K_2, the triangle inequality gives the following relation:

$$||\{\nabla \boldsymbol{v}^h \boldsymbol{n}_E\}||_{L_2(E)} \leq \frac{1}{2}||(\nabla \boldsymbol{v}^h)|_{K_1} \boldsymbol{n}_E||_{L_2(E)} + \frac{1}{2}||(\nabla \boldsymbol{v}^h)|_{K_2} \boldsymbol{n}_E||_{L_2(E)}.$$

By using the trace inequality below (Chapter 2.1.4 in [21])

$$||\nabla v \cdot \boldsymbol{n}_E||_{L^2(E)} \leq C_t {h_K}^{-1/2} ||\nabla v||_{L^2(K)}, \quad \forall v \in P_k(K), \tag{3.64}$$

with C_t being dependent on the polynomial degree k, applied to vectors of higher dimension, the expression below is obtained

$$||\{\nabla \boldsymbol{v}^h \boldsymbol{n}_E\}||_{L_2(E)} \leq \frac{C_t}{2} h_{K_1}^{-1/2} ||\nabla \boldsymbol{v}^h||_{L_2(K_1)} + \frac{C_t}{2} h_{K_2}^{-1/2} ||\nabla \boldsymbol{v}^h||_{L_2(K_2)}. \tag{3.65}$$

Since h_E is the length of an edge in 2d ($d = 2$) and the area of a face in $3d$ ($d = 3$), the following relation holds

$$h_E \leq {h_E}^{d-1} \leq h^{d-1}, \tag{3.66}$$

where h is the largest h_E in the mesh $\mathcal{T}^h$.
By combining the relation (3.63) with the estimate (3.65) and using (3.66) one obtains the following relation

$$\begin{aligned}
\int_E \{\nabla \boldsymbol{v}^h \boldsymbol{n}_E\} \cdot [\boldsymbol{v}^h] &\leq \frac{C_t {h_E}^{\beta_0/2}}{2} \left(h_{K_1}^{-1/2} ||\nabla \boldsymbol{v}^h||_{L^2(K_1)} + h_{K_2}^{-1/2} ||\nabla \boldsymbol{v}^h||_{L^2(K_2)} \right) \left(\frac{1}{{h_E}^{\beta_0}} \right)^{1/2} |||[\boldsymbol{v}^h]|||_{L^2(E)} \\
&\leq \frac{C_t}{2} \left(h_{K_1}^{\frac{\beta_0}{2}(d-1)-\frac{1}{2}} + h_{K_2}^{\frac{\beta_0}{2}(d-1)-\frac{1}{2}} \right) \left(||\nabla \boldsymbol{v}^h||^2_{L^2(K_1)} + ||\nabla \boldsymbol{v}^h||^2_{L^2(K_2)} \right)^{1/2} \\
&\qquad \times \left(\frac{1}{{h_E}^{\beta_0}} \right)^{1/2} |||[\boldsymbol{v}^h]|||_{L^2(E)} \\
&\leq C_t \left(||\nabla \boldsymbol{v}^h||^2_{L^2(K_1)} + ||\nabla \boldsymbol{v}^h||^2_{L^2(K_2)} \right)^{1/2} \left(\frac{1}{{h_E}^{\beta_0}} \right)^{1/2} |||[\boldsymbol{v}^h]|||_{L^2(E)},
\end{aligned}$$

if β_0 satisfies the condition $\beta_0(d-1) \geq 1$ and if it is assumed, without loss of generality, that $h \leq 1$. A similar bound is obtained for E being a boundary edge. In that case, the value of the average reduces to $\{\nabla \boldsymbol{v}^h\} = \nabla \boldsymbol{v}^h$. Let n_0 denote the maximum number of neighbors an element can have. So, for a conforming mesh, $n_0 = 3$ for a triangle and $n_0 = 4$ for a quadrilateral or tetrahedron. By summing the estimate above over all edges, one obtains the following expression

$$\begin{aligned}
\sum_{E \in \mathcal{E}^h} \int_E \{\nabla \boldsymbol{v}^h \boldsymbol{n}_E\} \cdot [\boldsymbol{v}^h] &\leq C_t \left(\sum_{E \in \mathcal{E}^h} \frac{1}{{h_E}^{\beta_0}} |||[\boldsymbol{v}^h]|||^2_{L^2(E)} \right)^{1/2} \\
&\qquad \times \left(\sum_{E \in \mathcal{E}_I^h} (||\nabla \boldsymbol{v}^h||^2_{L^2(K_1)} + ||\nabla \boldsymbol{v}^h||^2_{L^2(K_2)}) + \sum_{E \in \mathcal{E}_B^h} ||\nabla \boldsymbol{v}^h||^2_{L^2(K_1)} \right)^{1/2} \\
&\leq C_t \sqrt{n_0} \left(\sum_{E \in \mathcal{E}^h} \frac{1}{|e|^{\beta_0}} |||[\boldsymbol{v}^h]|||^2_{L^2(E)} \right)^{1/2} \left(\sum_{K \in \mathcal{T}^h} ||\nabla \boldsymbol{v}^h||^2_{L^2(K)} \right)^{1/2}.
\end{aligned}$$

Using Young's inequality with $\delta > 0$ gives

$$\sum_{E \in \mathcal{E}^h} \int_E \{\nabla \boldsymbol{v}^h \boldsymbol{n}_E\} \cdot [\boldsymbol{v}^h] \leq \frac{\delta}{2} \sum_{K \in \mathcal{T}^h} ||\nabla \boldsymbol{v}^h||^2_{L^2(K)} + \frac{C_t^2 n_0}{2\delta} \sum_{E \in \mathcal{E}^h} \frac{1}{{h_E}^{\beta_0}} |||[\boldsymbol{v}^h]|||^2_{L^2(E)}.$$

So, the following lower bound for $a_\epsilon(\boldsymbol{v}^h, \boldsymbol{v}^h)$ is obtained

$$a_\epsilon(\boldsymbol{v}^h, \boldsymbol{v}^h) \geq \left(1 - \frac{\delta}{2}|1+\epsilon| \right) \sum_{K \in \mathcal{T}^h} ||\nabla \boldsymbol{v}^h||^2_{L^2(K)} + \sum_{E \in \mathcal{E}^h} \frac{\sigma - \frac{C_t^2 n_0}{2\delta}|1+\epsilon|}{{h_E}^{\beta_0}} |||[\boldsymbol{v}^h]|||^2_{L^2(E)}.$$

By choosing $\delta = 1$ if $\epsilon = 0$ and $\delta = 1/2$ if $\epsilon = 1$ and choosing σ large enough (for instance, $\sigma \geq C_t^2 n_0$ if $\epsilon = 0$ and $\sigma \geq 4C_t^2 n_0$ if $\epsilon = 1$), the coercivity property (3.60) holds with $m = 1/2$

$$a_\epsilon(\boldsymbol{v}^h, \boldsymbol{v}^h) \geq \frac{1}{2} ||\boldsymbol{v}^h||^2_{\mathcal{E}}. \tag{3.67}$$

A summary of the above results with their classification in literature is presented below:

(i) The antisymmetric bilinear form a_{-1} is coercive for any choice of $\sigma > 0$ and the method is called nonsymmetric interior penalty Galerkin (NIPG);

(ii) For the symmetric a_1 and incomplete a_0 bilinear forms, coercivity is ensured if $\beta_0(d-1) \geq 1$ and if σ is bounded below by a large enough constant and the methods are called symmetric interior penalty Galerkin (SIPG) and incomplete interior penalty Galerkin (IIPG), respectively.

■

Further, error estimates will be presented for the case of the symmetric interior penalty Galerkin (SIPG), as this is the method for which the numerical studies in Chapter 4 are performed.

Error estimates for the SIPG method. (based on contents from Section 4.4 of [14])
Using the approximation properties of the finite element spaces (3.52), (3.54) and the weakly divergence-free property of the $H_0(\mathrm{div}, \Omega)$ space in the derivation of error estimates of the solutions approximating $\boldsymbol{u} \in \boldsymbol{H}^s(\Omega)$ and $p \in H^r(\Omega)$, leads to the following results:

$$||\boldsymbol{u} - \boldsymbol{u}^h||_{1,h} \leq C \inf_{\boldsymbol{v}^h \in V^h} ||\boldsymbol{u} - \boldsymbol{v}^h||_{1,h} \leq C h^{l-1} ||\boldsymbol{u}||_{H^l(\Omega)}, \tag{3.68}$$

$$\begin{aligned} ||p - p^h||_{L^2(\Omega)} &\leq C \left(\inf_{q^h \in Q^h} ||p - q^h||_{L^2(\Omega)} + \nu ||\boldsymbol{u} - \boldsymbol{v}^h||_{1,h} \right) \\ &\leq C \left(h^m ||p||_{H^m(\Omega)} + \nu h^{l-1} ||\boldsymbol{u}||_{H^l(\Omega)} \right), \end{aligned} \tag{3.69}$$

where $l = \min\{s, k+1\}$. If $V^h \times Q^h$ is the Raviart-Thomas pair, then $m = \min\{r, k+1\}$ and if it is the BDM pair, then $m = \min\{r, k\}$.
The discrete H^1-norm is defined as

$$||\boldsymbol{v}^h||_{1,h}^2 := \sum_{K \in \mathcal{T}^h} ||\nabla \boldsymbol{v}^h||_{L^2(K)}^2 + \sum_{E \in \mathcal{E}^h} h_E ||\{\nabla \boldsymbol{v}^h \boldsymbol{n}_E\}||_{L^2(E)} + \sum_{E \mathcal{E}^h} {h_E}^{-1} ||[\boldsymbol{v}^h]||_{L^2(E)}.$$

□

Alternative theorem for RT_k/P_k (Theorems 5.2.6 and 5.3.8 from [16])
For the Raviart-Thomas pair RT_k/P_k, $k \geq 1$, it holds that

$$||\boldsymbol{u} - \boldsymbol{u}^h||_{1,h} \leq h^k |\boldsymbol{u}|_{k+1}, \tag{3.70}$$

$$||p - p^h||_{L^2(\Omega)} \leq h^k (|\boldsymbol{u}|_{k+1} + |p|_k), \tag{3.71}$$

$$\nabla \cdot \boldsymbol{u}^h = 0. \tag{3.72}$$

The L^2-norm of the velocity error requires, similarly to the estimate for the Galerkin discretization (3.38), a regular solution to the dual Stokes problem (3.33) and is given in the expression below

$$||\boldsymbol{u} - \boldsymbol{u}^h||_{L^2(\Omega)} \leq C h^{k+1} |\boldsymbol{u}|_{k+1}. \tag{3.73}$$

□

The pressure-robust and mass conserving properties of the $H(\mathrm{div})$-conforming methods can be seen in the velocity error estimates (3.68), (3.70), (3.73). Thus, they are the by-product of vanishing dependence of the velocity error on pressure and viscosity observed in estimates of the H^1-conforming methods (3.35), (3.36), (3.38).

Chapter 4

Numerical Studies

In this chapter, the properties of the implemented $H(\mathrm{div})$-conforming finite element methods for the Stokes equations are discussed. This includes comparisons of their results with both the analytical convergence orders (section 4.3), and with the results from the H^1-conforming elements (sections 4.3, 4.4), as well as a study of an appropriate penalty parameter choice to ensure a well-conditioned problem (section 4.2).
To this end, the DG interior-penalty method for Stokes equations (3.58)-(3.59) was implemented in the program package ParMooN [25]. Then, computations for concrete examples of problems with analytical solutions (introduced in section 4.1) were performed. With the given boundary conditions and the right hand-side values determined by the problem of choice, the linear system of equations was assembled using degrees of freedom determined by the $H(\mathrm{div})$- or H^1- conforming pairs of velocity/pressure finite element spaces, and solved with a direct solver from the UMFPACK library, for various values of viscosity ν, penalty parameters σ, and refinement levels. Ultimately, relevant quantities like the condition number and errors in respective norms were obtained indirectly or directly from the data given in output by the program. All of the figures in this work were created using the package Matplotlib [9], unless indicated otherwise.

4.1 Examples

4.1.1 Harmonic solution

This example was taken from the program package ParMooN [25] as a prescribed solution for testing two-dimensional steady-state Navier Stokes equations. The domain of definition is the unit square $\Omega = (0,1)^2$ with homogeneous Dirichlet boundary conditions $\boldsymbol{u} = \mathbf{0}$ on $\partial\Omega$. The velocity field is given by

$$\boldsymbol{u} = \begin{pmatrix} \sin(\pi x) \\ -\pi y \cos(\pi x) \end{pmatrix}. \tag{4.1}$$

It is easy to verify that the velocity field is divergence-free

$$\nabla \cdot \boldsymbol{u} = \partial_x u_1 + \partial_y u_2 = \pi \cos(\pi x) - \pi \cos(\pi x) = 0.$$

The pressure is in $L^2_0(\Omega)$ and is chosen to be the following expression

$$p = \sin(\pi x)\cos(\pi y). \tag{4.2}$$

The plotted functions in Mathematica [10] can be seen in figure 4.1.

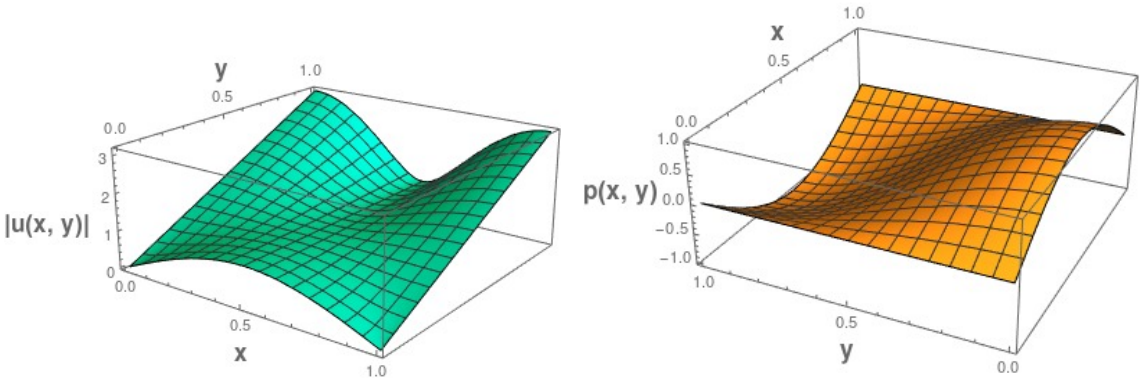

(a) $|\boldsymbol{u}(x,y)|$ (b) $p(x,y)$

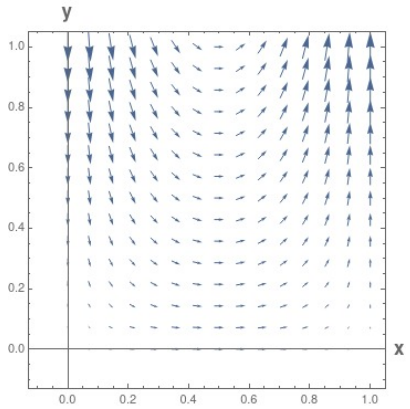

(c) $\boldsymbol{u}(x,y)$

Figure 4.1: Plots of the 'Harmonic solution' example using [10]

4.1.2 Polynomial solution

This two-dimensional, steady-state example is introduced as Example D.3 in [13] and can also be found in the package ParMooN [25]. It is defined on the unit square domain $\Omega = (0,1)^2$ with homogeneous Dirichlet boundary conditions $\boldsymbol{u} = \boldsymbol{0}$ on $\partial\Omega$. The velocity field is defined using the stream function

$$\phi = 1000x^2(1-x)^4y^3(1-y)^2,$$

and is given by

$$\boldsymbol{u} = \begin{pmatrix} \partial_y\phi \\ -\partial_x\phi \end{pmatrix} = 1000 \begin{pmatrix} x^2(1-x)^4y^2(1-y)(3-5y) \\ -2x(1-x)^3(1-3x)y^3(1-y)^2 \end{pmatrix}. \tag{4.3}$$

Using the Theorem of Schwarz, one can verify that this velocity is divergence-free:

$$\nabla \cdot \boldsymbol{u} = \partial_x u_1 + \partial_y u_2 = \partial_{xy}\phi - \partial_{yx}\phi = \partial_{xy}\phi - \partial_{xy}\phi = 0.$$

The boundary conditions require the pressure to be in $L_0^2(\Omega)$. In this case, it was chosen

$$p = \pi^2(xy^3\cos(2\pi x^2y) - x^2y\sin(2\pi xy)) + \frac{1}{8}. \tag{4.4}$$

The plotted vector field of velocity in figure 4.2 shows that it has a profile of a vortex.

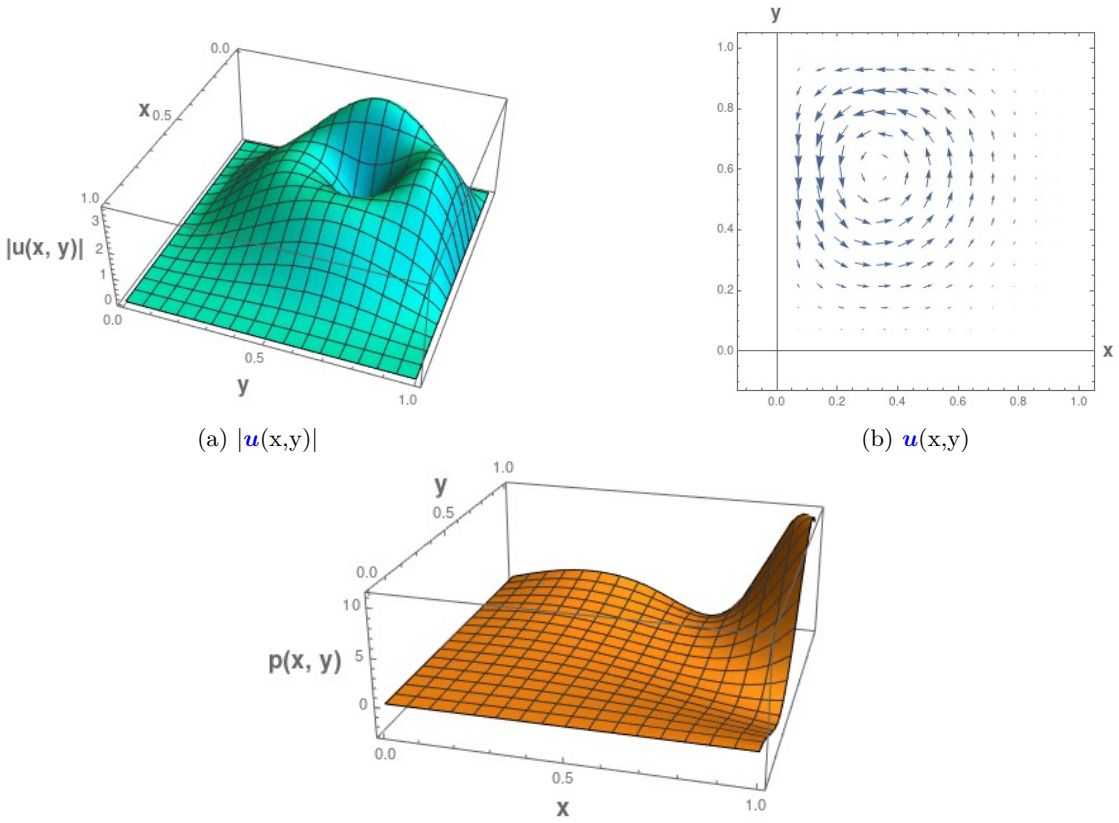

(a) $|\boldsymbol{u}(x,y)|$ (b) $\boldsymbol{u}(x,y)$

(c) $p(x,y)$

Figure 4.2: Plots of the 'Polynomial solution' example using [10]

4.2 Condition number dependence on σ

This study has the goal of testing the numerical robustness of the symmetric formulation of the implemented DG interior-penalty method for Stokes equations with the $H(\text{div})$-conforming finite element spaces BDM_1 and RT_1.

Contrary to the analytic prediction of a stable and accurate method for a sufficiently large penalty parameter σ (equation (3.67)), a dependence of the convergence of the solver on σ was observed. This phenomenon has been studied by Wang et al. in the article [15], where a linear dependence of the condition number on σ was concluded, whereas no major differences in errors were noted after a sufficiently large value of σ.

A similar study to the one in [15] is performed in this section to determine an appropriate choice of σ for the subsequent calculations, since for meaningful conclusions a converging approximation to the solution is required. The difficulty inherent to the problem is that the penalty parameter must not be too small in order to guarantee coercivity of $a_\epsilon(\cdot,\cdot)$, and at the same time not too large, to avoid a large condition number of the whole matrix and, thereby, an ill-conditioned problem.

To that end, computations were performed on the grid with the 3^{rd} refinement level, using the 'Polynomial solution' example. The quantities of interest were the errors in the L^2 norm and the H^1 semi-norm, obtained from the program ParMooN [25] in the output, and the condition number of the matrix of the linear system computed in MATLAB [17] using the *cond*() command.

The search for an appropriate σ interval was done by first considering a rather extended range of values for computations $\sigma \in [10^{-7}, 10^{7}]$ (tables 4.1 and 4.2), and determining intervals within those ranges, where the quantities reach optimal approximation properties. Upon a close examination of the tables, it is clear that the first optimal range is between $\sigma = 10$ and $\sigma = 100$, because there the error values reach their minima. The refined studies in this range from tables 4.3 and

4.4 show that the condition numbers and the errors are smaller for the first values of σ. This is why, even more detailed results are considered for values of σ between 5 and 35 (tables 4.5 and 4.6). Here one can see that the best overall properties are reached in the case of the RT_1 space for $\sigma = [5, 10]$, and in the case of BDM_1 for the range $\sigma = [1, 15]$. For simplicity, the value $\sigma = 10$ will be used in further computations, for both types of spaces.

This type of studies show that having to ensure fitting values for the additional parameter σ can be laborious and is a disadvantage of the SIPG methods for Stokes equations. Moreover, the values of the condition numbers are rather high, which indicates a risk of the problem being ill-conditioned and therefore giving non-converging results. However, it will be seen in following sections that once the parameters are determined, the use of $H(\mathrm{div})$-conforming space will result in considerable advantages of mass conservation and pressure robustness.

σ	condition	$\|\|\boldsymbol{u} - \boldsymbol{u}^h\|\|_{L^2}$	$\|\|\nabla \cdot \boldsymbol{u}^h\|\|_{L^2}$	$\|\boldsymbol{u} - \boldsymbol{u}^h\|_{H^1}$	$\|\|p - p^h\|\|_{L^2}$	$\|p - p^h\|_{H^1}$
1.0e-07	1.21e+19	1.63e+01	2.95e-14	2.67e+02	1.06e+01	1.57e+01
1.0e-06	7.08e+20	1.63e+01	2.58e-14	2.67e+02	1.06e+01	1.57e+01
1.0e-05	1.06e+19	1.63e+01	2.82e-14	2.67e+02	1.06e+01	1.57e+01
1.0e-04	3.56e+19	1.62e+01	2.66e-14	2.65e+02	1.05e+01	1.57e+01
1.0e-03	4.32e+19	1.53e+01	2.18e-14	2.49e+02	9.91e+00	1.57e+01
1.0e-02	6.54e+19	1.11e+01	2.07e-14	1.73e+02	6.84e+00	1.57e+01
1.0e-01	4.94e+19	9.86e+00	1.58e-14	1.92e+02	7.96e+00	1.57e+01
1.0e+00	3.70e+19	3.43e+00	4.66e-15	8.21e+01	1.55e+00	1.57e+01
1.0e+01	3.94e+20	3.23e-01	2.05e-15	6.54e+00	8.09e-01	1.57e+01
1.0e+02	9.55e+21	8.60e-01	1.02e-15	8.94e+00	3.16e+00	1.57e+01
1.0e+03	2.21e+22	1.35e+00	4.57e-16	1.26e+01	6.41e+00	1.57e+01
1.0e+04	4.33e+23	1.48e+00	4.22e-16	1.36e+01	7.39e+00	1.57e+01
1.0e+05	7.20e+24	1.49e+00	4.21e-16	1.37e+01	7.52e+00	1.57e+01
1.0e+06	3.90e+24	1.50e+00	4.72e-16	1.37e+01	7.53e+00	1.57e+01
1.0e+07	6.98e+24	1.50e+00	4.75e-16	1.37e+01	7.53e+00	1.57e+01

Table 4.1: First search of optimal σ for BDM_1

σ	condition	$\|\|\boldsymbol{u} - \boldsymbol{u}^h\|\|_{L^2}$	$\|\|\nabla \cdot \boldsymbol{u}^h\|\|_{L^2}$	$\|\boldsymbol{u} - \boldsymbol{u}^h\|_{H^1}$	$\|\|p - p^h\|\|_{L^2}$	$\|p - p^h\|_{H^1}$
1.0e-07	1.57e+20	1.63e+01	2.03e-13	2.67e+02	2.66e+01	9.55e+02
1.0e-06	7.04e+18	1.63e+01	1.87e-13	2.67e+02	2.66e+01	9.55e+02
1.0e-05	2.81e+19	1.63e+01	2.00e-13	2.67e+02	2.66e+01	9.54e+02
1.0e-04	3.58e+19	1.62e+01	1.98e-13	2.65e+02	2.64e+01	9.48e+02
1.0e-03	1.55e+19	1.53e+01	1.83e-13	2.49e+02	2.48e+01	8.92e+02
1.0e-02	2.33e+19	1.11e+01	1.37e-13	1.73e+02	1.76e+01	6.51e+02
1.0e-01	5.50e+19	9.86e+00	1.25e-13	1.92e+02	1.56e+01	5.13e+02
1.0e+00	2.46e+19	3.43e+00	3.15e-14	8.21e+01	4.08e+00	1.50e+02
1.0e+01	1.25e+20	3.23e-01	1.48e-14	6.54e+00	6.67e-01	1.14e+01
1.0e+02	7.59e+22	8.60e-01	8.13e-15	8.94e+00	3.16e+00	2.22e+01
1.0e+03	2.13e+22	1.35e+00	1.78e-15	1.26e+01	6.46e+00	4.09e+01
1.0e+04	4.89e+23	1.48e+00	4.99e-16	1.36e+01	7.46e+00	4.77e+01
1.0e+05	5.07e+24	1.49e+00	4.59e-16	1.37e+01	7.58e+00	4.86e+01
1.0e+06	3.58e+25	1.50e+00	4.63e-16	1.37e+01	7.59e+00	4.87e+01
1.0e+07	1.99e+27	1.50e+00	4.87e-16	1.37e+01	7.60e+00	4.87e+01

Table 4.2: First search of optimal σ for RT_1

σ	condition	$\|\|\boldsymbol{u}-\boldsymbol{u}^h\|\|_{L^2}$	$\|\|\nabla\cdot\boldsymbol{u}^h\|\|_{L^2}$	$\|\boldsymbol{u}-\boldsymbol{u}^h\|_{H^1}$	$\|\|p-p^h\|\|_{L^2}$	$\|p-p^h\|_{H^1}$
1.0e+01	3.94e+20	3.23e-01	2.05e-15	6.54e+00	8.09e-01	1.57e+01
2.0e+01	2.50e+20	4.55e-01	2.00e-15	6.84e+00	1.22e+00	1.57e+01
3.0e+01	1.51e+21	5.45e-01	1.82e-15	7.19e+00	1.58e+00	1.57e+01
4.0e+01	3.31e+21	6.14e-01	1.43e-15	7.52e+00	1.89e+00	1.57e+01
5.0e+01	2.80e+21	6.71e-01	1.29e-15	7.81e+00	2.16e+00	1.57e+01
6.0e+01	1.76e+22	7.20e-01	1.27e-15	8.08e+00	2.40e+00	1.57e+01
7.0e+01	9.09e+20	7.62e-01	1.13e-15	8.33e+00	2.62e+00	1.57e+01
8.0e+01	1.14e+22	7.98e-01	9.83e-16	8.55e+00	2.81e+00	1.57e+01
9.0e+01	3.64e+21	8.31e-01	9.86e-16	8.75e+00	2.99e+00	1.57e+01
1.0e+02	9.55e+21	8.60e-01	1.02e-15	8.94e+00	3.16e+00	1.57e+01

Table 4.3: Second search of optimal σ for BDM_1

σ	condition	$\|\|\boldsymbol{u}-\boldsymbol{u}^h\|\|_{L^2}$	$\|\|\nabla\cdot\boldsymbol{u}^h\|\|_{L^2}$	$\|\boldsymbol{u}-\boldsymbol{u}^h\|_{H^1}$	$\|\|p-p^h\|\|_{L^2}$	$\|p-p^h\|_{H^1}$
1.0e+01	1.25e+20	3.23e-01	1.48e-14	6.54e+00	6.67e-01	1.14e+01
2.0e+01	2.76e+20	4.55e-01	1.32e-14	6.84e+00	1.15e+00	1.41e+01
3.0e+01	1.07e+21	5.45e-01	1.32e-14	7.19e+00	1.53e+00	1.56e+01
4.0e+01	8.03e+20	6.14e-01	1.26e-14	7.52e+00	1.86e+00	1.68e+01
5.0e+01	2.70e+20	6.71e-01	1.15e-14	7.81e+00	2.14e+00	1.79e+01
6.0e+01	1.50e+21	7.20e-01	9.96e-15	8.08e+00	2.39e+00	1.88e+01
7.0e+01	1.67e+21	7.62e-01	9.87e-15	8.33e+00	2.61e+00	1.98e+01
8.0e+01	2.21e+21	7.98e-01	8.71e-15	8.55e+00	2.81e+00	2.06e+01
9.0e+01	1.11e+21	8.31e-01	8.24e-15	8.75e+00	2.99e+00	2.14e+01
1.0e+02	7.59e+22	8.60e-01	8.13e-15	8.94e+00	3.16e+00	2.22e+01

Table 4.4: Second search of optimal σ for RT_1

σ	condition	$\|\|\boldsymbol{u}-\boldsymbol{u}^h\|\|_{L^2}$	$\|\|\nabla\cdot\boldsymbol{u}^h\|\|_{L^2}$	$\|\boldsymbol{u}-\boldsymbol{u}^h\|_{H^1}$	$\|\|p-p^h\|\|_{L^2}$	$\|p-p^h\|_{H^1}$
5.0e+00	1.20e+20	2.17e-01	2.63e-15	6.82e+00	6.17e-01	1.57e+01
1.0e+01	3.94e+20	3.23e-01	2.05e-15	6.54e+00	8.09e-01	1.57e+01
1.5e+01	4.13e+20	3.97e-01	1.91e-15	6.67e+00	1.02e+00	1.57e+01
2.0e+01	2.50e+20	4.55e-01	2.00e-15	6.84e+00	1.22e+00	1.57e+01
2.5e+01	4.10e+20	5.03e-01	1.76e-15	7.02e+00	1.40e+00	1.57e+01
3.0e+01	1.51e+21	5.45e-01	1.82e-15	7.19e+00	1.58e+00	1.57e+01
3.5e+01	1.14e+21	5.81e-01	1.67e-15	7.36e+00	1.74e+00	1.57e+01

Table 4.5: Third search of optimal σ for BDM_1

σ	condition	$\|\|\boldsymbol{u}-\boldsymbol{u}^h\|\|_{L^2}$	$\|\|\nabla\cdot\boldsymbol{u}^h\|\|_{L^2}$	$\|\boldsymbol{u}-\boldsymbol{u}^h\|_{H^1}$	$\|\|p-p^h\|\|_{L^2}$	$\|p-p^h\|_{H^1}$
5.0e+00	3.55e+19	2.17e-01	1.73e-14	6.82e+00	3.72e-01	8.09e+00
1.0e+01	1.25e+20	3.23e-01	1.48e-14	6.54e+00	6.67e-01	1.14e+01
1.5e+01	5.25e+20	3.97e-01	1.35e-14	6.67e+00	9.21e-01	1.30e+01
2.0e+01	2.76e+20	4.55e-01	1.32e-14	6.84e+00	1.15e+00	1.41e+01
2.5e+01	1.90e+21	5.03e-01	1.38e-14	7.02e+00	1.35e+00	1.49e+01
3.0e+01	1.07e+21	5.45e-01	1.32e-14	7.19e+00	1.53e+00	1.56e+01
3.5e+01	2.17e+21	5.81e-01	1.25e-14	7.36e+00	1.70e+00	1.62e+01

Table 4.6: Third search of optimal σ for RT_1

4.3 Convergence order

In this section, the convergence histories of the approximated solutions for velocity, pressure, and divergence of velocity to problems with analytical solutions are discussed. The results can be found in Appendix A.1. The Reynolds number was chosen $Re = 10$ and the penalty parameter $\sigma = 10$, the latter being a result of the study of the previous section 4.2. Then, computations are performed with the $H(\text{div})$-conforming finite element spaces BDM_k and RT_k, $k = 1, 2$ and 3 on a grid $\mathcal{T}^h$ with triangular mesh cells at various refinement levels of the grid, i.e., mesh width h_E. The respective errors in the L_2 norm were given in the output of the ParMooN [25] program package, as the analytical solutions were prescribed.
The study aims to verify whether the analytical predictions of convergence orders from the error estimates in Chapter 3.4 are met. Moreover, a comparison of the error estimates and convergence orders of the widely used H^1-conforming elements is done using similar computations with the $MINI$ and TH_k finite element spaces and a Galerkin discretization of the Stokes equation from the ParMooN [25] package. This allows for a determination of the advantages and limitations of the newly implemented DG method.

The detailed results from Appendix A.1 are summarized in table 4.7. In the cases of BDM_k, RT_k with $k = 1, 2$, the analytical convergence orders given by (3.73), (3.71) are met and there is little difference in comparison to the H^1-conforming spaces $MINI$ and TH_2 of the same order (figures A.1 and A.4). For the case $k = 3$ however, some irregularities are observed in the convergence histories A.1e, A.1f, A.4e and A.4f, which seem to be indicating that the system is ill-conditioned. Moreover, the results of computations with RT_0 don't converge and have large errors (figures A.2a, A.2b, A.5a, A.2b).
The Scott-Vogelius element SV_k with $k > 2$ has unstable results with large errors. However, this behavior is expected from the theory (Chapter 3.2), since the grid used in the simulation is not barycentric-refined, so the element is not inf-sup stable.

Space	L^2 **error**	**Theory**	**Harmonic sol.**	**Polynomial sol.**
RT0	u	-	<h^2 (large error)	no convergence
	p	-	no convergence	<h^1 (large error)
MINI	u	h^2	h^2	h^2
	p	h^1	>h^1	>h^1
RT1	u	h^2	h^2	h^2
	p	h^1	h^1	h^1
BDM1	u		h^2	h^2
	p		h^1	h^1
TH2	u	h^3	h^3	h^3
	p	h^2	h^2	h^2
RT2	u	h^3	h^3	h^3
	p	h^2	h^2	h^2
BDM2	u		h^3	h^3
	p		h^2	h^2
SV2	u	-	~h^3 (ill-conditioned)	<h^3
	p	-	missing (nan result)	missing (nan result)
TH3	u	h^4	<h^4	<h^4
	p	h^3	<h^3	<h^3
RT3	u	h^4	~h^4 (ill-conditioned)	~h^4 (ill-conditioned)
	p	h^3	~h^3 (ill-conditioned)	~h^3 (ill-conditioned)
BDM3	u		~h^4 (ill-conditioned)	~h^4 (ill-conditioned)
	p		~h^3 (ill-conditioned)	~h^3 (ill-conditioned)
SV3	u	-	~h^4 (large error)	<<h^4 (ill-conditioned)
	p	-	~h^3 (large error)	~h^3 (large error)
SV4	u	-	~h^4 (large error)	~h^4 (ill-conditioned)
	p	-	~h^3 (large error)	~h^3 (large error)

Table 4.7: Overview of convergence orders for all finite element pairs

Furthermore, it can be seen in figures A.3 and A.6 that computations with $H(\text{div})$-conforming finite element spaces provide great improvement to the $||\nabla \cdot \boldsymbol{u}^h||_{L^2(\Omega)}$ values with H^1-conforming spaces. These errors for computations with RT_k and BDM_k are essentially zero and, therefore, the property of mass conservation is ensured, as expected. It may seem problematic that the trend of convergence for RT_k and BDM_k is reversed, i.e., the values $||\nabla \cdot \boldsymbol{u}^h||_{L^2(\Omega)}$ become larger with finer h_E, but even at their maximum they reach values of order 10^{-10} (figures A.3e and A.6e), which are too small to impact the results in any significant way and can be attributed to round-off errors.
The computations with the Scott-Vogelius SV_k element give mixed results (figures A.3d, A.3f, A.6d and A.6f) with regard to the convergence of the errors $||\nabla \cdot \boldsymbol{u}^h||_{L^2(\Omega)}$ (with the mesh not being barycentric-refined). For $k = 2$, they behave mostly similarly to RT_k and BDM_k, whereas for $k = 3$ and 4, they are similar to TH_3. In all cases, however, these results are rather irregular and large values of errors for SV_3 and SV_4 can be observed.

Therefore, one can conclude that for $k = 1$ and 2, the $H(\text{div})$-conforming spaces RT_k and BDM_k are an improvement to the classical H^1-conforming $MINI$ and TH_k elements, since the convergence orders and magnitudes of errors for $\boldsymbol{u}^h$ and p^h are the same, with the advantage that the divergence-free property of velocity $\boldsymbol{u}^h$ is satisfied exactly.
In the cases of $k > 2$ and RT_0, further investigations are needed to determine whether they can improve the classical methods, since a seemingly ill-conditioned problem for the former and a lack of convergence for the latter were observed. Moreover, it was verified that, as expected, the locally divergence-free element SV_k, $k > 2$ cannot be used to solve the Stokes finite element problem if the grid is not barycentric-refined. Hence, its theoretical advantages have restricted use in practice.

4.4 Pressure robustness

In this section, numerical studies that verify the pressure robustness of the $H(\mathrm{div})$ finite element methods are discussed. The extensive results of the simulations can be found in Appendix A.2.

Computations that approximate solutions to both examples were performed on a mesh $\mathcal{T}^h$ that contains triangles, using H^1-conforming and $H(\mathrm{div})$-conforming finite element methods, with the Galerkin and the SIPG discontinuous Galerkin discretizations of the Stokes equations, respectively, for different values of the Reynolds number Re ($Re \propto \nu^{-1}$) and different refinement levels.

The finite element theory from chapters 3.2 and 3.4 predicts that for H^1-conforming methods, the errors of velocity are proportional (or inversely proportional) to the values of pressure (or viscosity) as observed from (3.36) and (3.38). On the other hand, for $H(\mathrm{div})$-conforming methods, this effect vanishes due to the property (3.72), i.e, a divergence-free velocity field is obtained and the error no longer has the dependence on pressure or viscosity (3.68).

These effects can indeed be observed in practice for both examples in figures A.7, A.8, A.10 and A.11. The results for the $MINI$ and TH_k elements, with $k = 2$ and 3, show a lack of pressure robustness in that the error for the divergence of velocity $\boldsymbol{u}^h$ increases proportionally to Re, and in this way reaches unacceptable values, as, for example, of order 10^4. The results for BDM_k and RT_k spaces ($k = 1, 2, 3$) are presented in parallel to the $MINI$ and TH_k elements to show how efficiently these methods solve this problem. It is clear that for both BDM_k and RT_k, $k = 1, 2$ and 3, the results are equally pressure robust, with whatever existing differences being attributed to round-off errors.

Even the results for the space RT_0, having errors for $\boldsymbol{u}^h$ and p^h that failed to converge in section 4.3, can be seen in figures A.9a and A.12a to be pressure robust. The results for the space SV_2 show a tendency towards pressure robustness, but the errors are too large to be useful (figures A.9b and A.12b). SV_3, on the other hand, is not pressure robust at all (figures A.9c and A.12c), but again, one must bear in mind that the theory predicts accurate results for these elements only on barycentric-refined grids, which is not the case here.

It can be concluded that all $H(\mathrm{div})$-conforming spaces from this study are pressure robust, thus eradicating the unphysical effects of pressure and viscosity on the velocity approximation observed in H^1-conforming methods. Moreover, it was confirmed that with respect to this property as well, the Scott-Vogelius element SV_k, $k = 2$ and 3 does not yield reliable results on grids that are not barycentric-refined.

Chapter 5

Conclusion and Outlook

This thesis aimed to study the properties that $H(\text{div})$-conforming spaces have in solving the finite element Stokes problem. To that end, the discontinuous Galerkin formulation of the Stokes equations was implemented in the program package ParMooN [25] and computations for solutions of the examples from chapter 4.1 were performed using the Brezzi-Douglas-Marini BDM_k and Raviart-Thomas RT_k finite element spaces with $k = 1, 2$ and 3. Similar computations were done with the classical H^1-conforming spaces like the $MINI$ P_1^{bub}/P_1 and Taylor-Hood TH_k, which are neither pressure-robust or mass conserving, and with Scott-Vogelius SV_k spaces, which posses the property of local mass conservation.

In Chapter 3.4 it is stated that the discontinuous Galerkin formulation for the Stokes equations (3.56)-(3.57) introduced a parameter σ that, at least for the symmetric case (SIPG), must be large enough to ensure the coercivity of the bilinear form $a_\epsilon(\cdot,\cdot)$. However, the study of an appropriate value for this parameter from Chapter 4.2 noted that the condition number, as well as error values, increase with larger σ and optimal results were found in the range of $\sigma = [5, 15]$. The need for such prior investigations can represent a disadvantage in practice.

The orders of convergence for pressure and velocity computed using BDM_k and RT_k spaces for $k = 1$ and 2, and the magnitude of their errors were similar to the $MINI$ and TH_2 elements, with the supplementary advantage of exactly vanishing error $||\nabla \cdot \boldsymbol{u}^h||_{L^2(\Omega)}$, which is also the property that ensures mass conservation. The $H(\text{div})$-conforming spaces for $k = 3$ showed a behavior which seemed characteristic to an ill-conditioned system, and therefore needs further investigation with respect to the choice of the solver of the linear system of equations. The computations of $\boldsymbol{u}^h$ and p^h using the TH_0 finite element space also presented limitations, as the errors are either too large or they do not converge. The reasons for such behavior could originate in the theory of $H(\text{div})$-conforming spaces for the Stokes equations, since in Theorems 5.2.6 and 5.3.8 from [16], which give an upper bound for errors in the L^2 norm, only the RT_k with $k > 1$ are explicitly stated.

With regard to pressure robustness however, all computations with $H(\text{div})$-conforming spaces in this study showed optimal results, thereby eradicating the non-physical dependence of velocity on both pressure and viscosity in H^1-conforming methods.

The computations with SV_k spaces for $k = 2, 3$ and 4 for a regular mesh made of triangles showed irregularities and large errors. This behavior is not excluded by theory and is just a confirmation of the fact that the SV_k element is not inf-sup stable on general meshes. A further study on barycentric-refined grids for both SV_k and $H(\text{div})$-conforming spaces would be of interest, as it would determine which method has a better-conditioned problem on special grids and, thus, which method would be more advantageous.

Aside from the above suggested investigations, similar studies could be done on rectangular mesh cells, as here only triangular mesh cells were considered. Also, a natural continuation of the study would be to implement the full steady-state incompressible Navier-Stokes equations by adding the DG discretization of the convective term. Furthermore, an extension of the equations to 3-dimensional domains would allow for studies of more complex phenomena, such as turbulence.

Appendix A

Numerical Results

A.1 Convergence histories

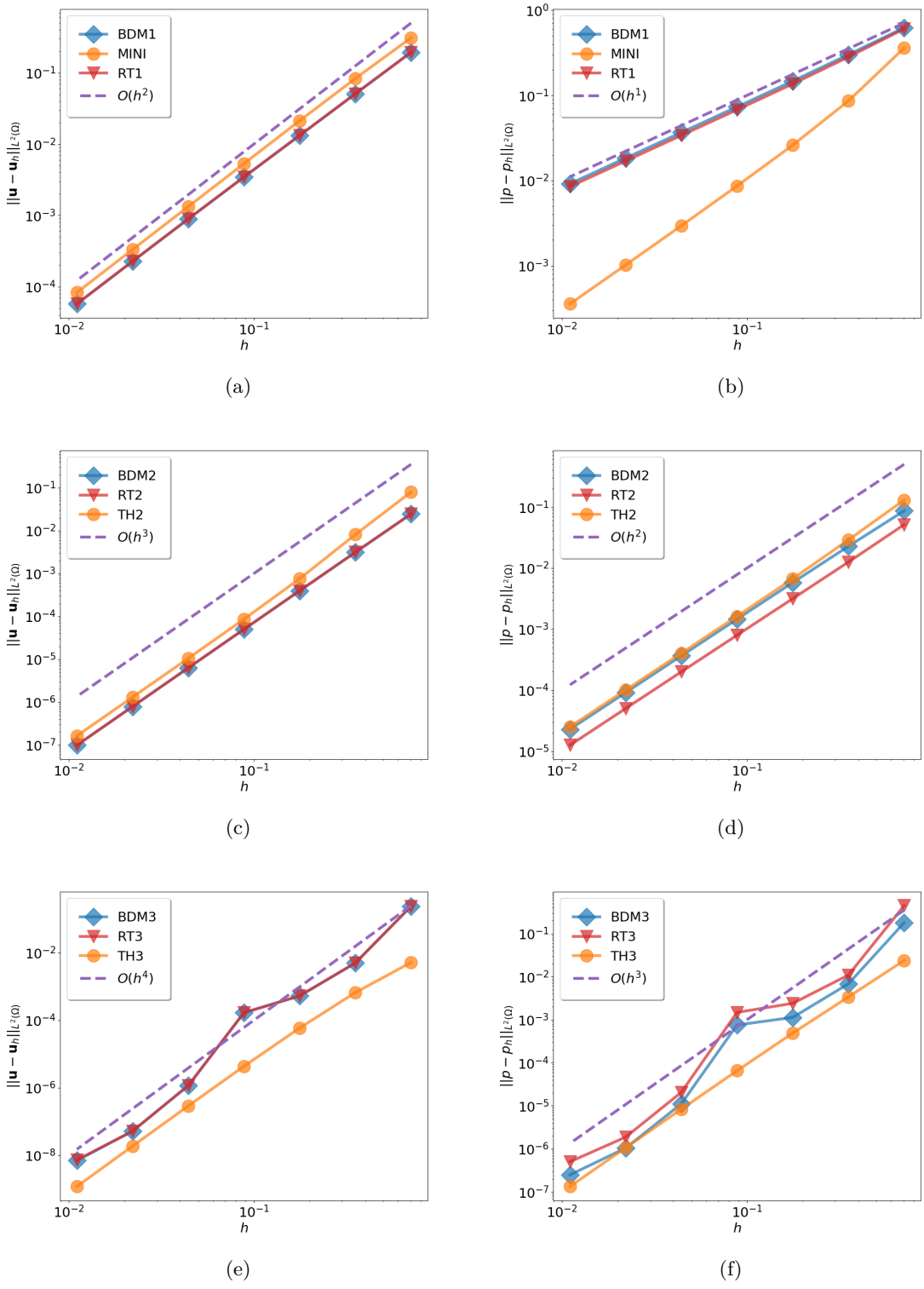

Figure A.1: Convergence histories for the 'Harmonic solution' example

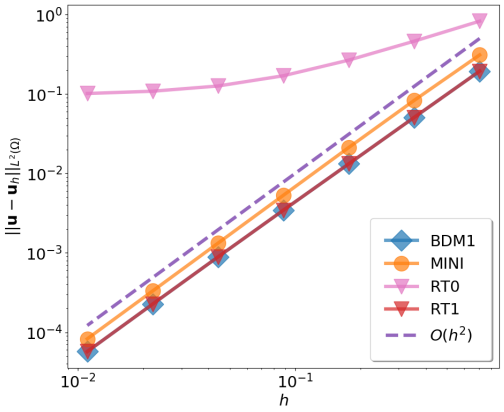

(a) RT_0

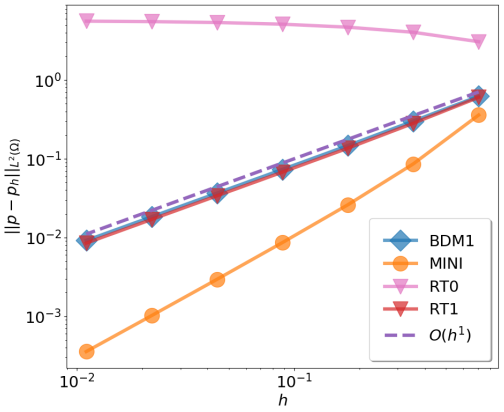

(b) RT_0

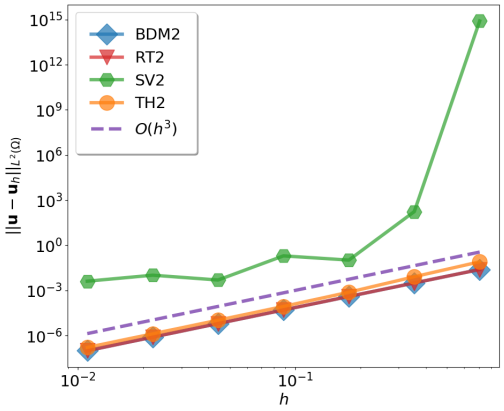

(c) SV_2

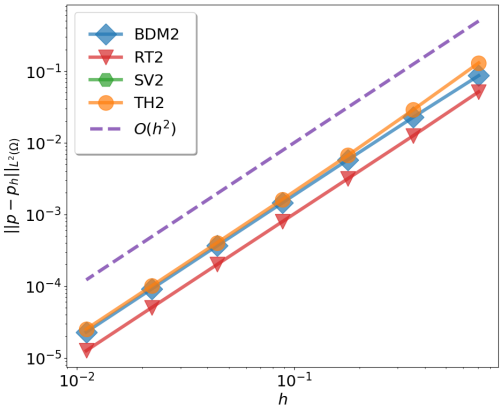

(d) SV_2

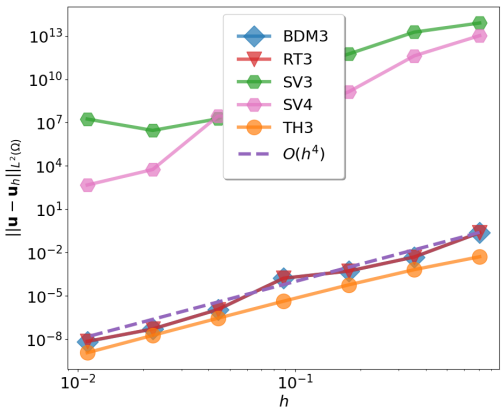

(e) SV_3 and SV_4

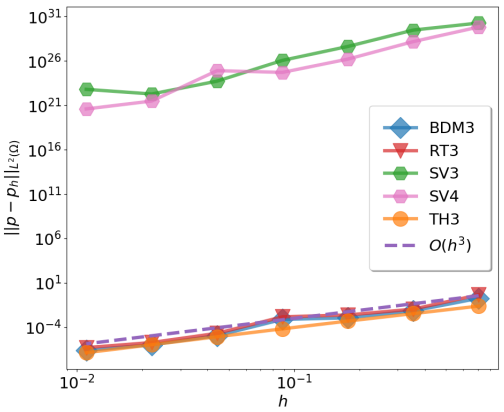

(f) SV_3 and SV_4

Figure A.2: Convergence histories with spaces of non-optimal behavior in comparison to results from figure A.1

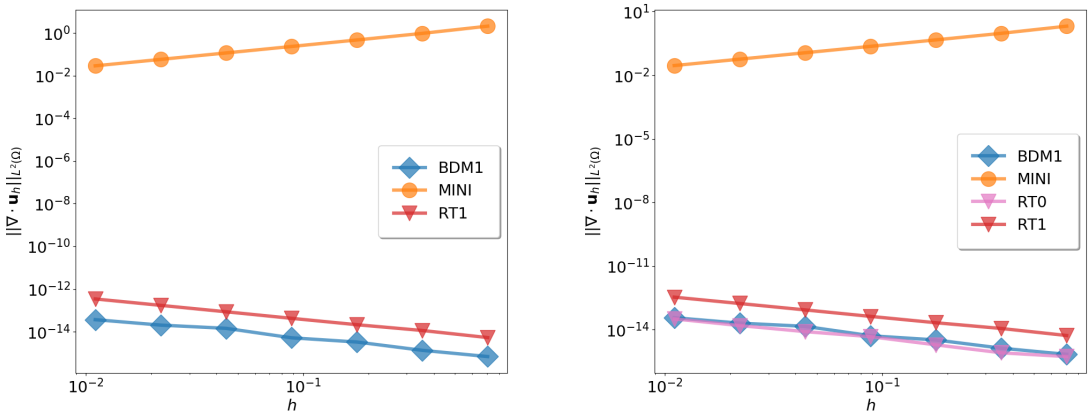

(a)

(b) RT_0

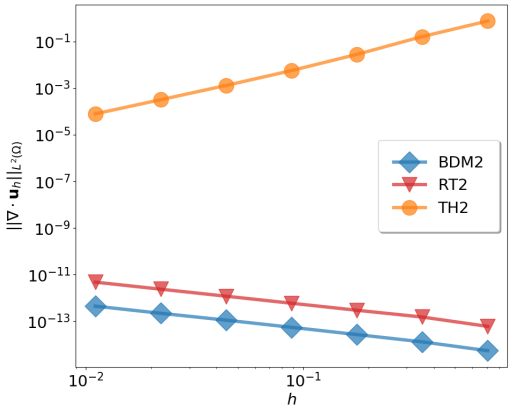

(c)

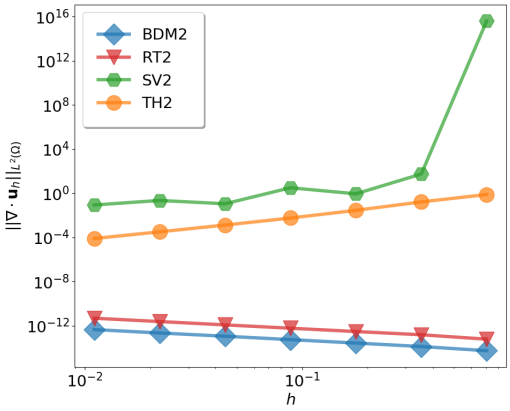

(d) SV_2

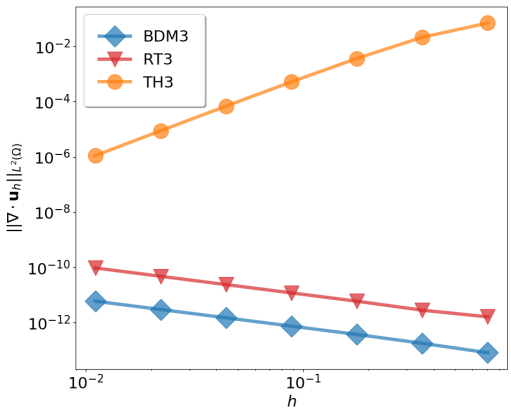

(e)

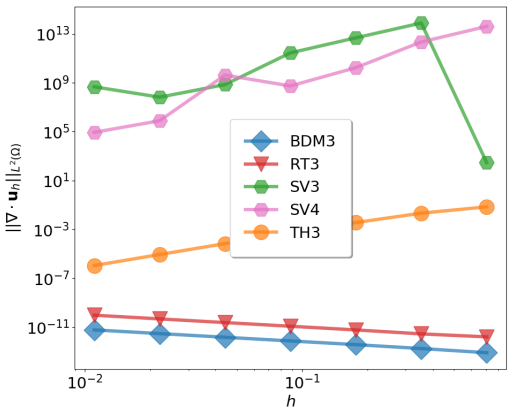

(f) SV_3 and SV_4

Figure A.3: Convergence histories of the divergence of velocity for the 'Harmonic solution' example

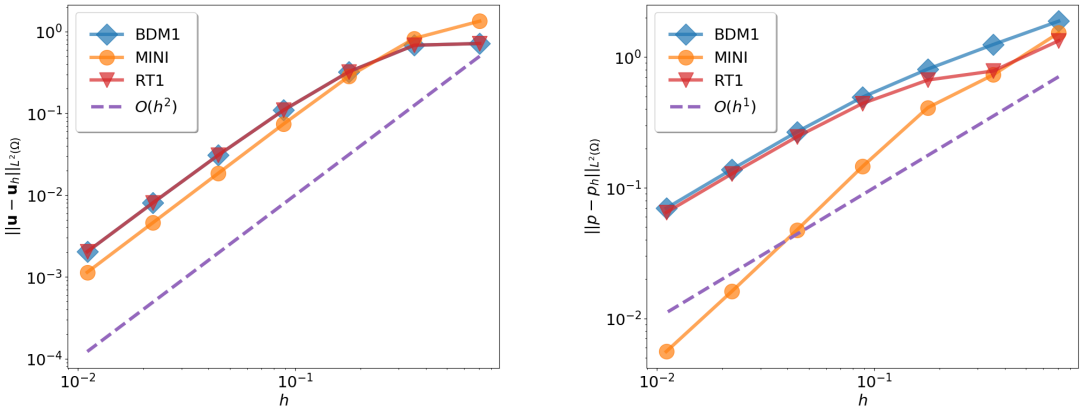

(a)

(b)

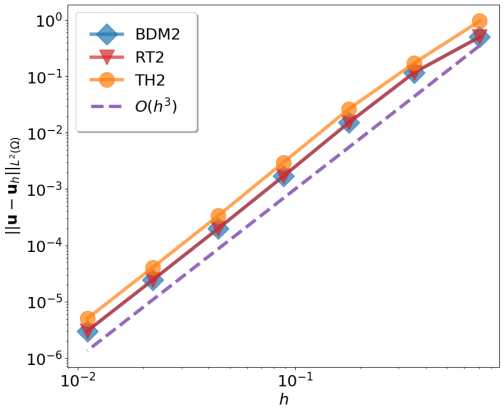

(c)

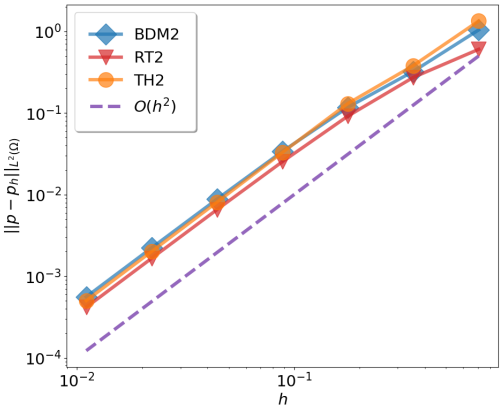

(d)

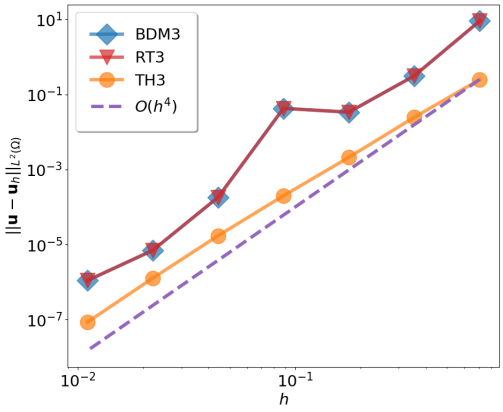

(e)

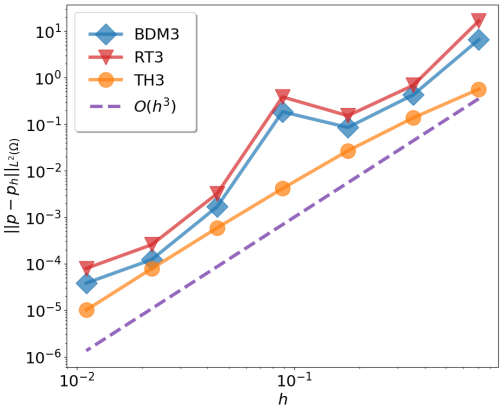

(f)

Figure A.4: Convergence histories for the 'Polynomial solution' example

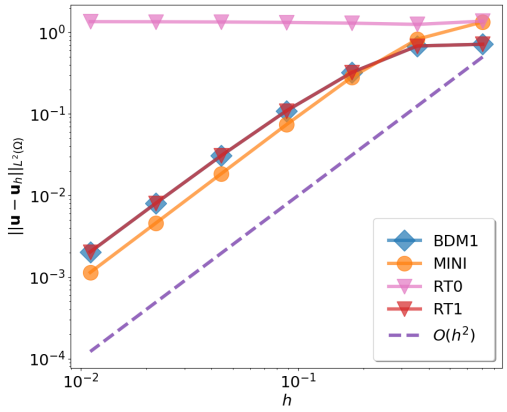

(a) RT_0

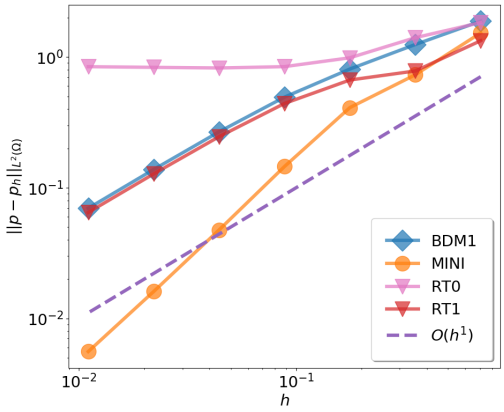

(b) RT_0

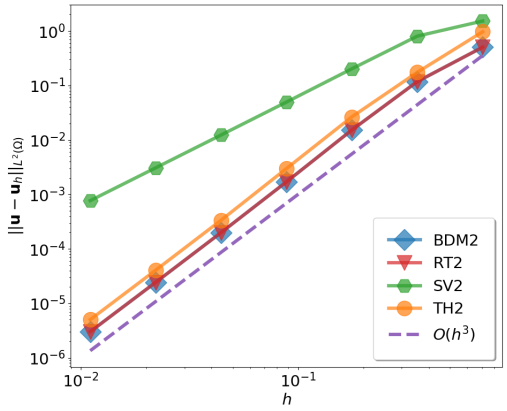

(c) SV_2

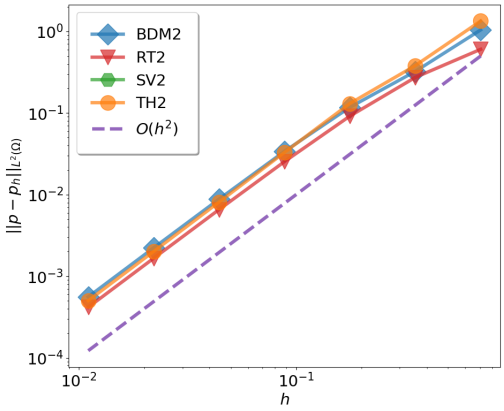

(d) SV_2

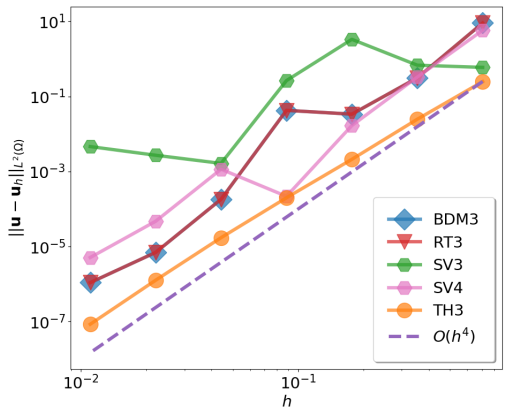

(e) SV_3 and SV_4

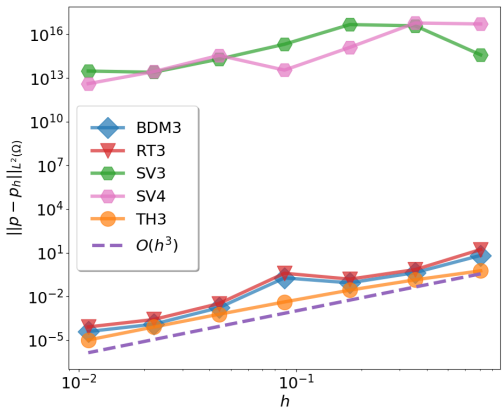

(f) SV_3 and SV_4

Figure A.5: Convergence histories with spaces of non-optimal behavior in comparison to results from figure A.4

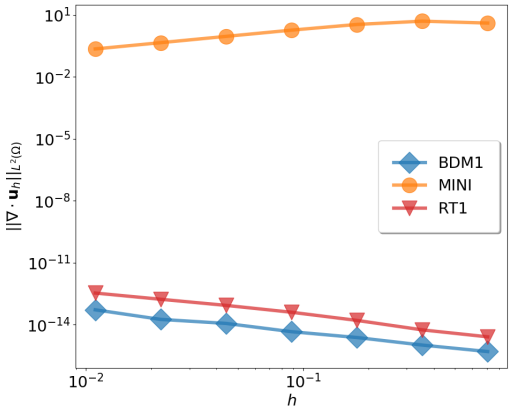

(a)

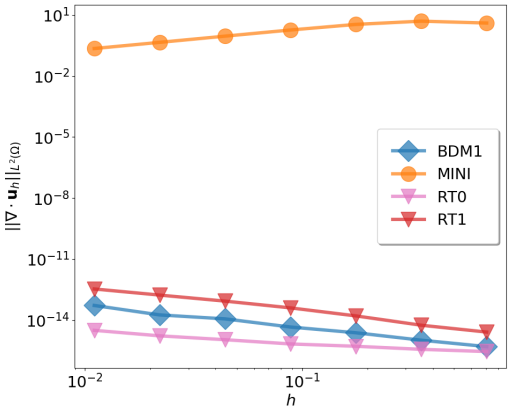

(b) RT_0

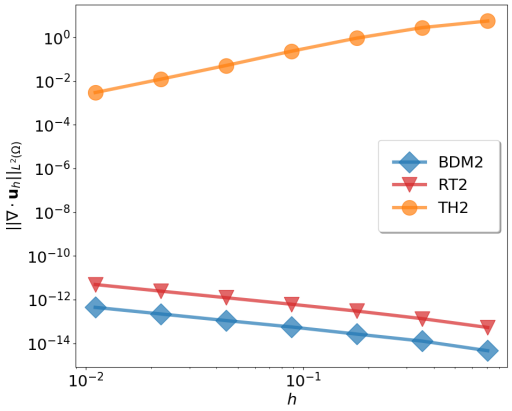

(c)

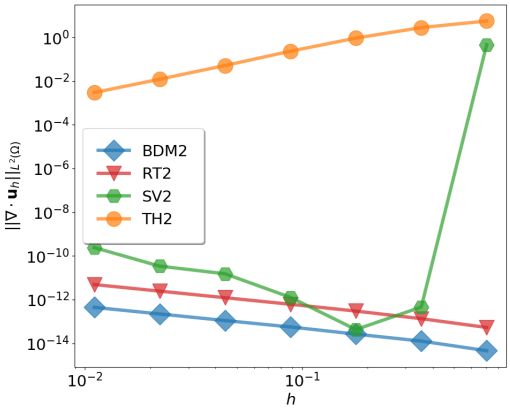

(d) SV_2

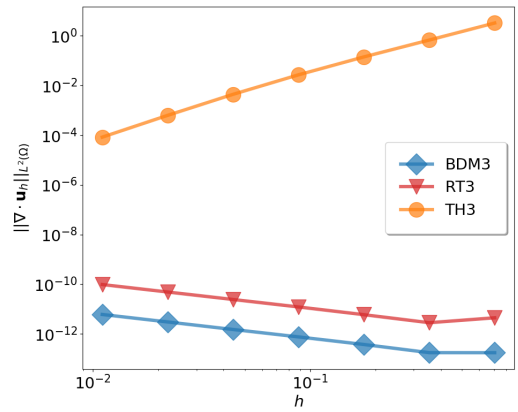

(e)

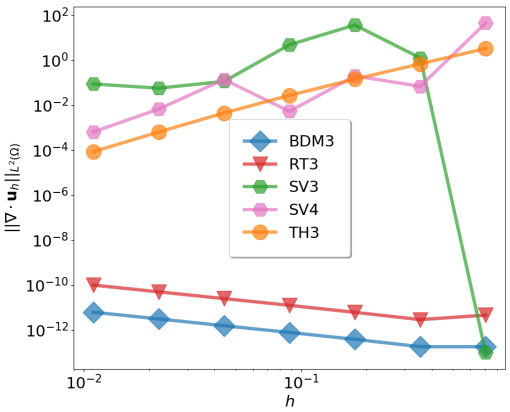

(f) SV_3 and SV_4

Figure A.6: Convergence histories of the divergence of velocity for the 'Polynomial solution' example

A.2 Pressure robustness results

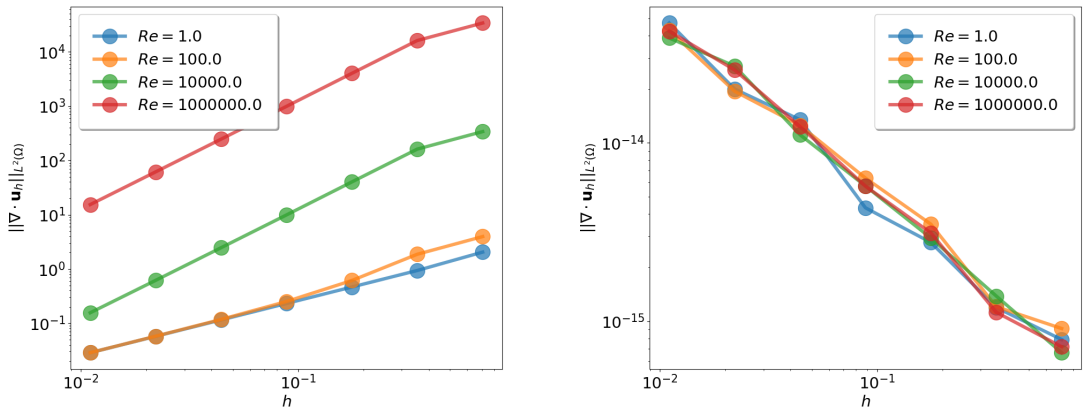

(a) $MINI$ (b) BDM_1

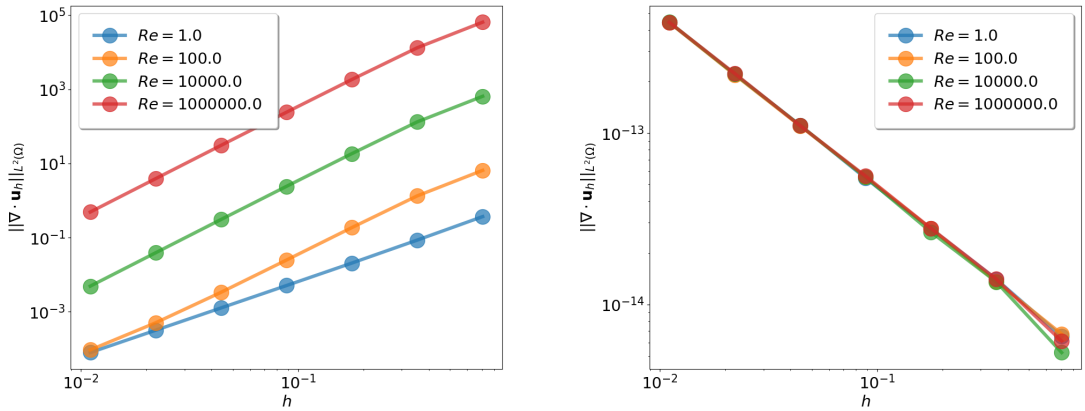

(c) TH_2 (d) BDM_2

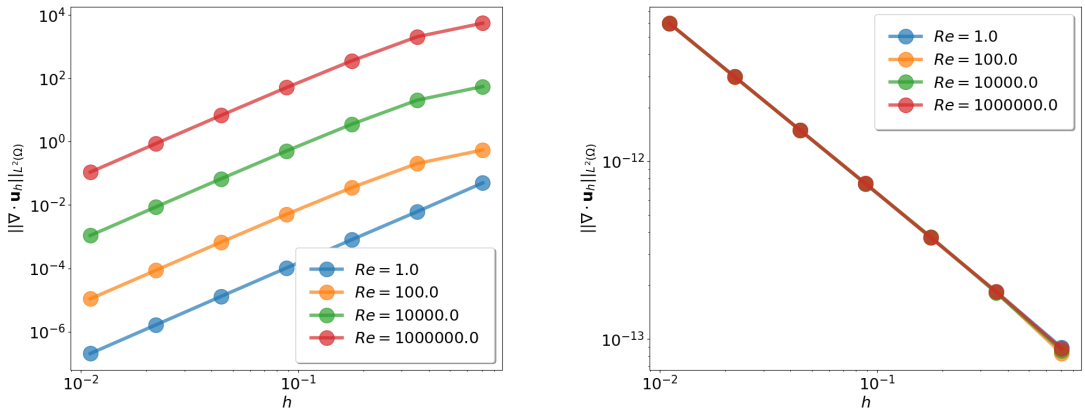

(e) TH_3 (f) BDM_3

Figure A.7: Pressure robustness comparison of H^1-conforming spaces with BDM_k for the 'Harmonic solution' example

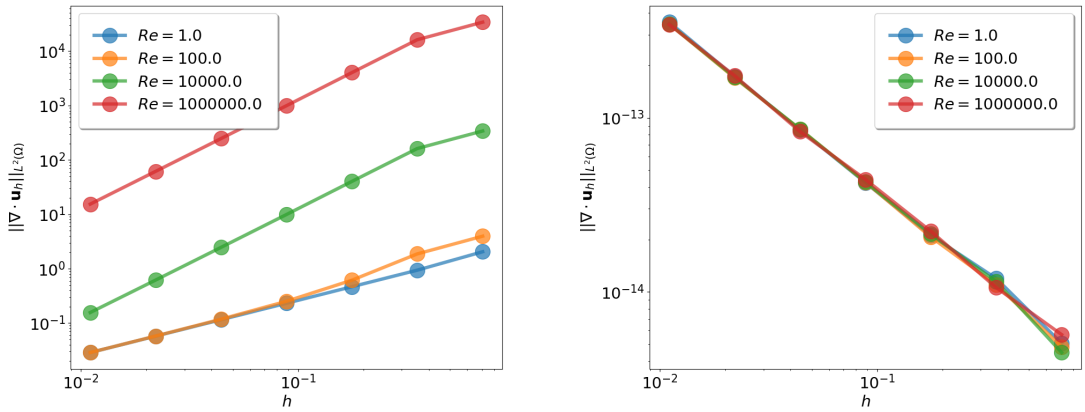

(a) $MINI$ (b) RT_1

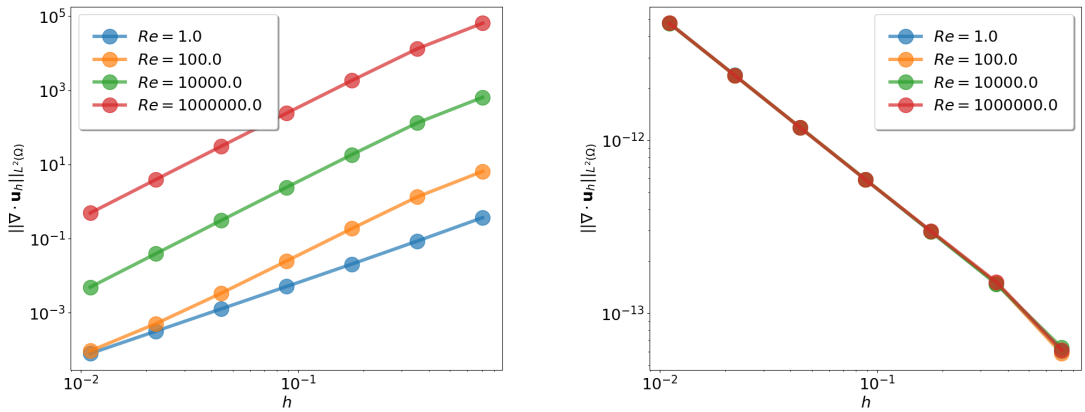

(c) TH_2 (d) RT_2

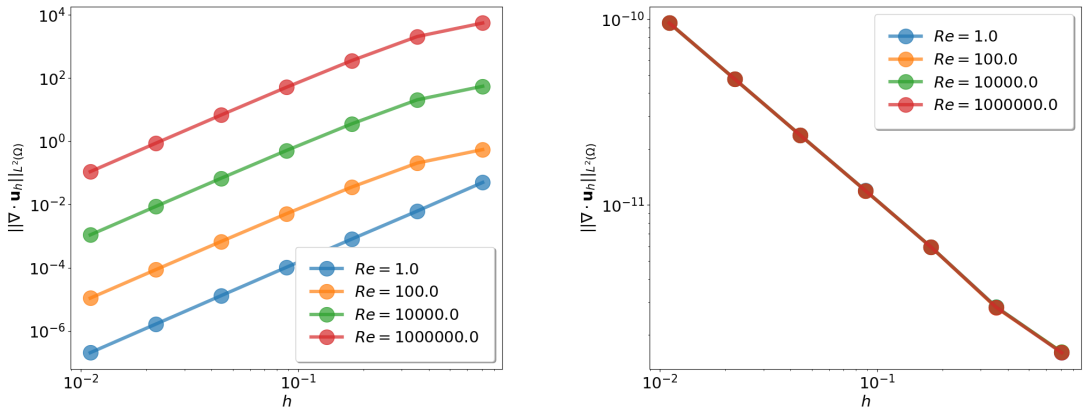

(e) TH_3 (f) RT_3

Figure A.8: Pressure robustness comparison of H^1-conforming spaces with RT_k for the 'Harmonic solution' example

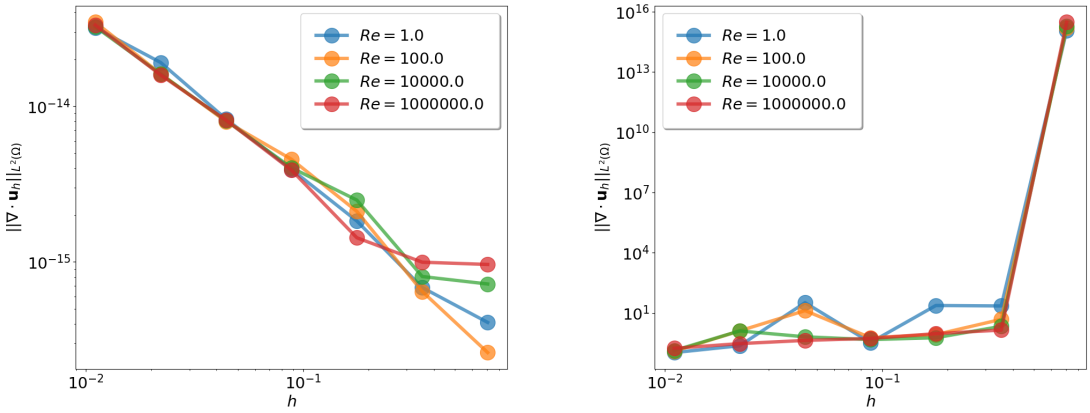

(a) RT_0 (b) SV_2

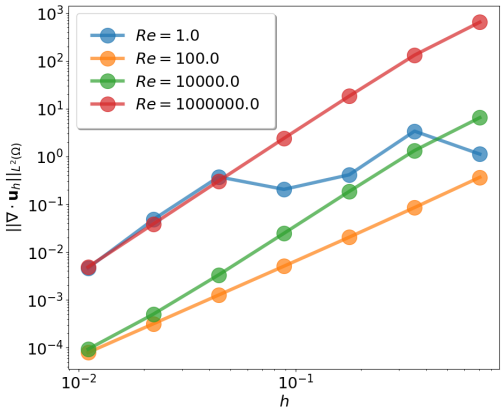

(c) SV_3

Figure A.9: Pressure robustness results with spaces of non-optimal behavior for the 'Harmonic solution' example

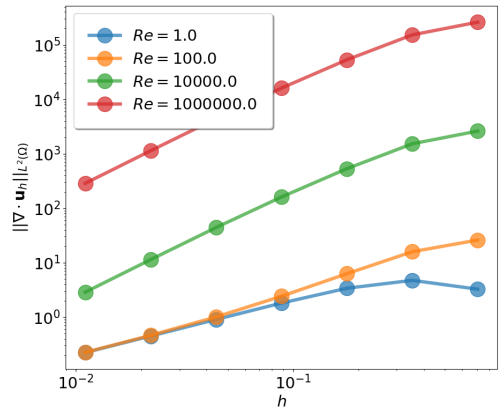

(a) $MINI$

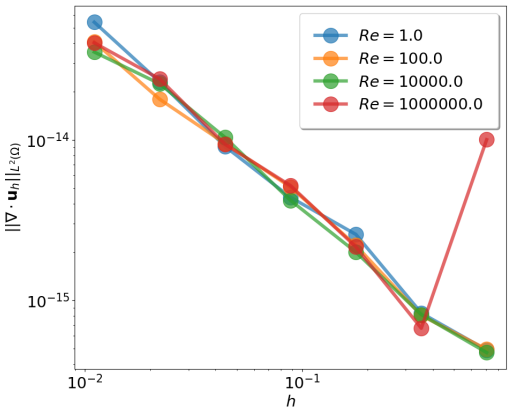

(b) BDM_1

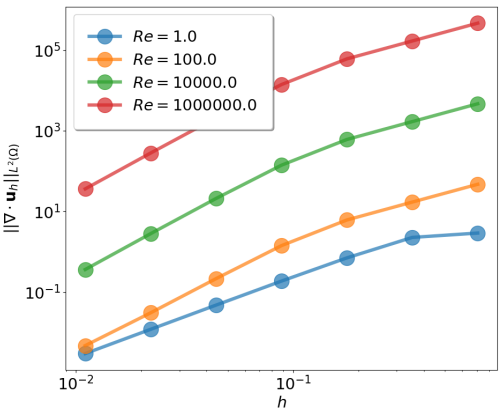

(c) TH_2

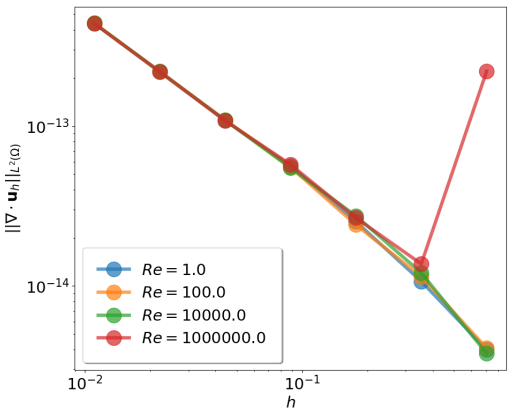

(d) BDM_2

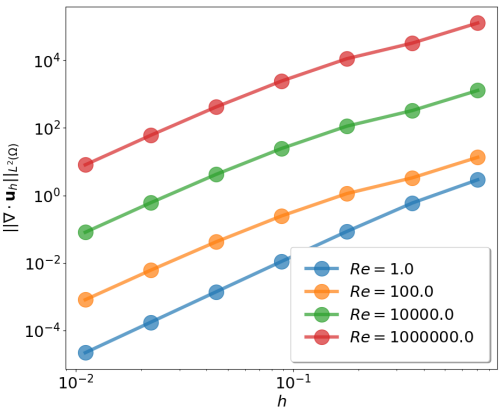

(e) TH_3

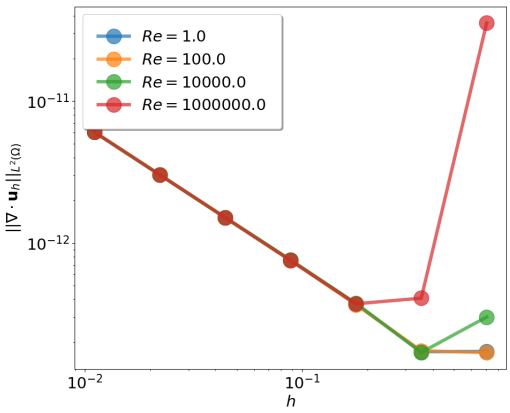

(f) BDM_3

Figure A.10: Pressure robustness comparison of H^1-conforming spaces with BDM_k for the 'Polynomial solution' example

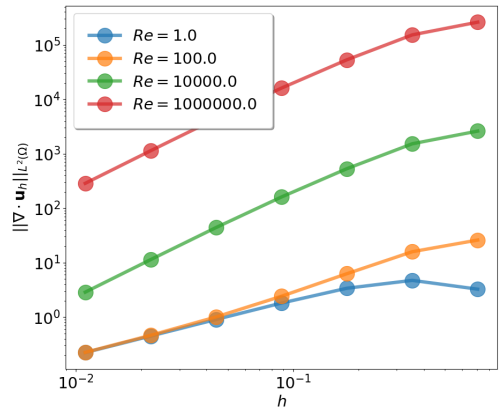

(a) $MINI$

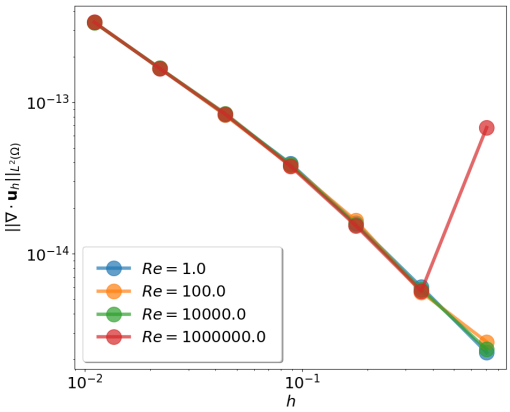

(b) RT_1

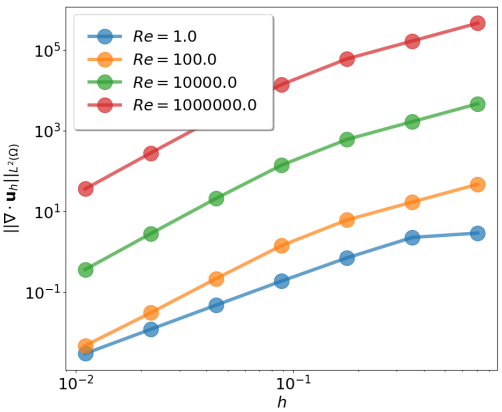

(c) TH_2

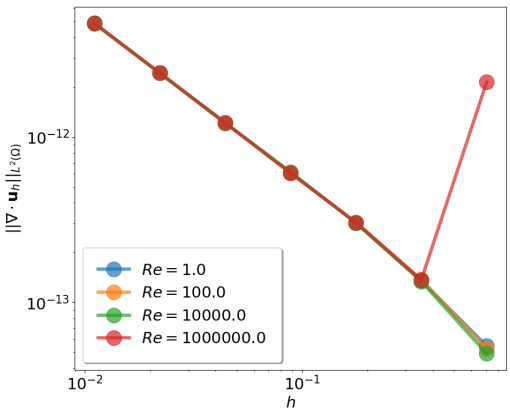

(d) RT_2

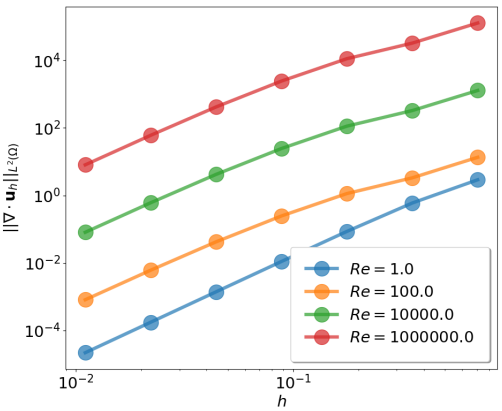

(e) TH_3

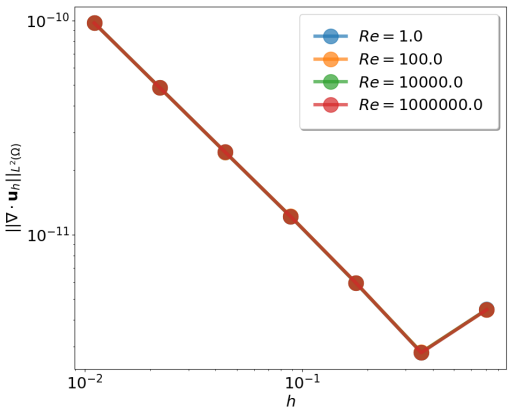

(f) RT_3

Figure A.11: Pressure robustness comparison of H^1-conforming spaces with RT_k for the 'Polynomial solution' example

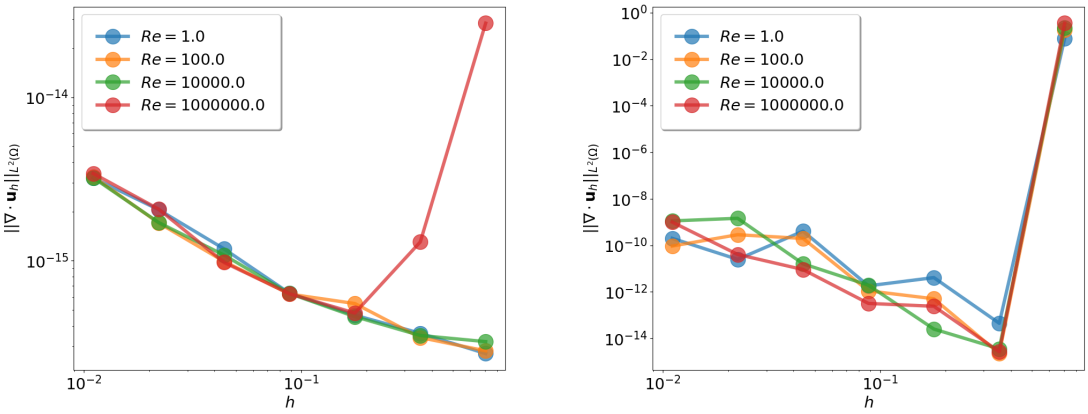

(a) RT_0

(b) SV_2

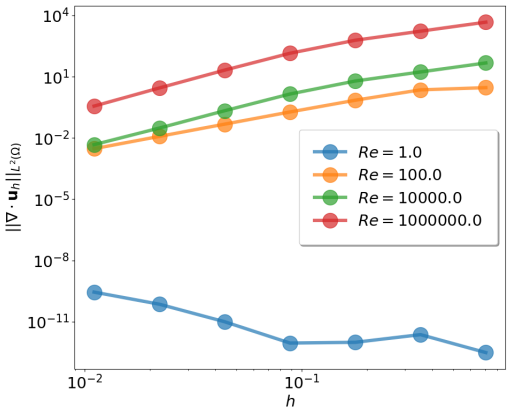

(c) SV_3

Figure A.12: Pressure robustness results with spaces of non-optimal behavior for the 'Polynomial solution' example

Bibliography

[1] L. A. *On the role of the Helmholtz decomposition in mixed methods for incompressible flows and a new variational crime.* 2014.

[2] F. M. Arnold DN, Brezzi F. *A stable finite element for the Stokes equations.* 1984.

[3] R. G. Bernardi C. *Analysis of some finite elements for the Stokes problem.* 1985.

[4] F. M. Boffi D., Brezzi F. *Mixed finite element methods and applications.* 2013.

[5] R. P.-A. Crouzeix M. *Conforming and nonconforming finite element methods for solving the stationary Stokes equations. I.* 1973.

[6] G. P. Galdi. *An Introduction to the Mathematical Theory of the Navier-Stokes Equations, Steady State Problems.* 2011.

[7] R. P.-A. Girault V. *Finite element methods for Navier-Stokes equations. Theory and algorithms.* 1986.

[8] S. R. Gresho P. *Incompressible flow and the finite element method. Vol 1: advection-diffusion. Vol 2: isothermal laminar flow.* 2000.

[9] J. D. Hunter. Matplotlib: A 2d graphics environment. *Computing in Science & Engineering*, 9(3):90–95, 2007.

[10] W. R. Inc. Mathematica, Version 12.3.1. Champaign, IL, 2021.

[11] F. Irgens. *Continuum Mechanics.* 2008.

[12] Q. J. *On the convergence of some low order mixed finite elements for incompressible fluids.* 1994.

[13] V. John. *Finite Element Methods for Incompressible Flow Problems.* 2016.

[14] V. John, A. Linke, C. Merdon, M. Neilan, and L. G. Rebholz. On the divergence constraint in mixed finite element methods for incompressible flows. *SIAM Review*, 59(3):492–544, 2017.

[15] X. Y. Junping Wang, Yanqiu Wang. A robust numerical method for stokes equations based on divergence-free h(div) finite element methods. *SIAM J. Sci. Comput.*, 31(4):2784–2802, 2009.

[16] G. Kanshat. *Lecture Notes: Mixed Finite Element Methods.* 2017.

[17] MATLAB. *version 9.11.0.1769968 (R2021b).* The MathWorks Inc., Natick, Massachusetts, 2021.

[18] T. L. Matthies G. *The inf-sup condition for the mapped Q_k,-$P^{disc.}{}_{,k-1}$, element in arbitrary space dimensions.* 2002.

[19] S. R. *Analysis of mixed finite elements methods for the Stokes problem: a unified approach.* 1984.

[20] S. R. *On some three-dimensional finite elements for incompressible media.* 1987.

[21] B. Rivière. *Discontinuous Galerkin Methods for Solving Elliptic and Parabolic Equations. Theory and Implementation.* 2008.

[22] Z. S. *A new family of stable mixed finite elements for the 3D Stokes equations.* 2005.

[23] V. M. Scott L.R. *Conforming finite element methods for incompressible and nearly incompressible continua. Large-scale computations in fluid mechanics, Part 2 (La Jolla, CA, 1983).* 1985.

[24] E. Sonnendrücker and A. Ratnani. *Lecture Notes: Advanced Finite Element Methods.* 2016.

[25] U. Wilbrandt, C. Bartsch, N. Ahmed, N. Alia, F. Anker, L. Blank, A. Caiazzo, S. Ganesan, S. Giere, G. Matthies, R. Meesala, A. Shamim, J. Venkatesan, and V. John. Parmoon—a modernized program package based on mapped finite elements. *Computers Mathematics with Applications*, 74(1):74–88, 2017. 5th European Seminar on Computing ESCO 2016.